An investigation of extensive air showers in the range 10(^4) to 10(^6) particles

Smith, Alan C.

AN INVESTIGATION OF EXTENSIVE AIR SHOWERS IN THE RANGE 10^4 to 10^6 PARTICLES

by

AIAN C. SMITH, B.Sc.

A Thesis
submitted to the University of Durham
for the degree of
Doctor of Philosophy

January, 1976

Of making many books there is
no end and much study is a
weariness of the flesh.

Ecclesiastes 12:12

ABSTRACT

A small air shower array of radius 60 m is described which will be used initially to study extensive air showers in the range 10^4 to 10^6 particles in size and to supplement existing research programmes into hadron and muon spectroscopy in the Cosmic Ray Laboratory of the University of Durham.

There are fourteen plastic scintillator detecting elements, in the first stage of construction of the array, located in a hexagonal geometry around the Physics Department.

An important feature of this array is in its data handling procedures in which the initial array data are assembled in analogue form, digitised and then transferred to an on-line I.B.M. 1130 computer disc for subsequent analysis. The array has been made as versatile as possible whilst retaining a measure of simplicity. It may be triggered in a variety of ways depending upon the mode chosen and upon the peripheral experiments and may also be added to with the minimum of electronic modification and delay. Because of the digitisation technique used one is able to provide instructions, when the data are being analysed, to compensate for any drift in the electronics automatically.

A preliminary shower size spectrum, based on over 200 hours of operation, has yielded a spectrum in the range

$$8.10^5 \leq N \leq 3.10^6$$

with an integral exponent of $\gamma_I = -2.6 \pm 0.2$.

PREFACE

The work described in this thesis was carried out during the period 1973 to 1975 whilst the author was working under the supervision of Dr. M. G. Thompson in the Cosmic Ray Group of the Physics Department in the University of Durham.

During this time, the author has been responsible for the design and commissioning of the Air Shower Array, the data handling electronics, the analysis of the air shower data and, with his colleagues, in the calibration and running of an experiment to measure the number spectrum of Air Showers in the range 10^4 to 10^6 particles. The deduction of the number spectrum from the observed experimental data has been the responsibility of the author.

The design and operation of the array has been described by Rada et al. in the Proceedings of the XIVth International Conference on Cosmic Rays (Munich, 1975).

CONTENTS

PLATE I

THE DATA HANDLING ELECTRONICS

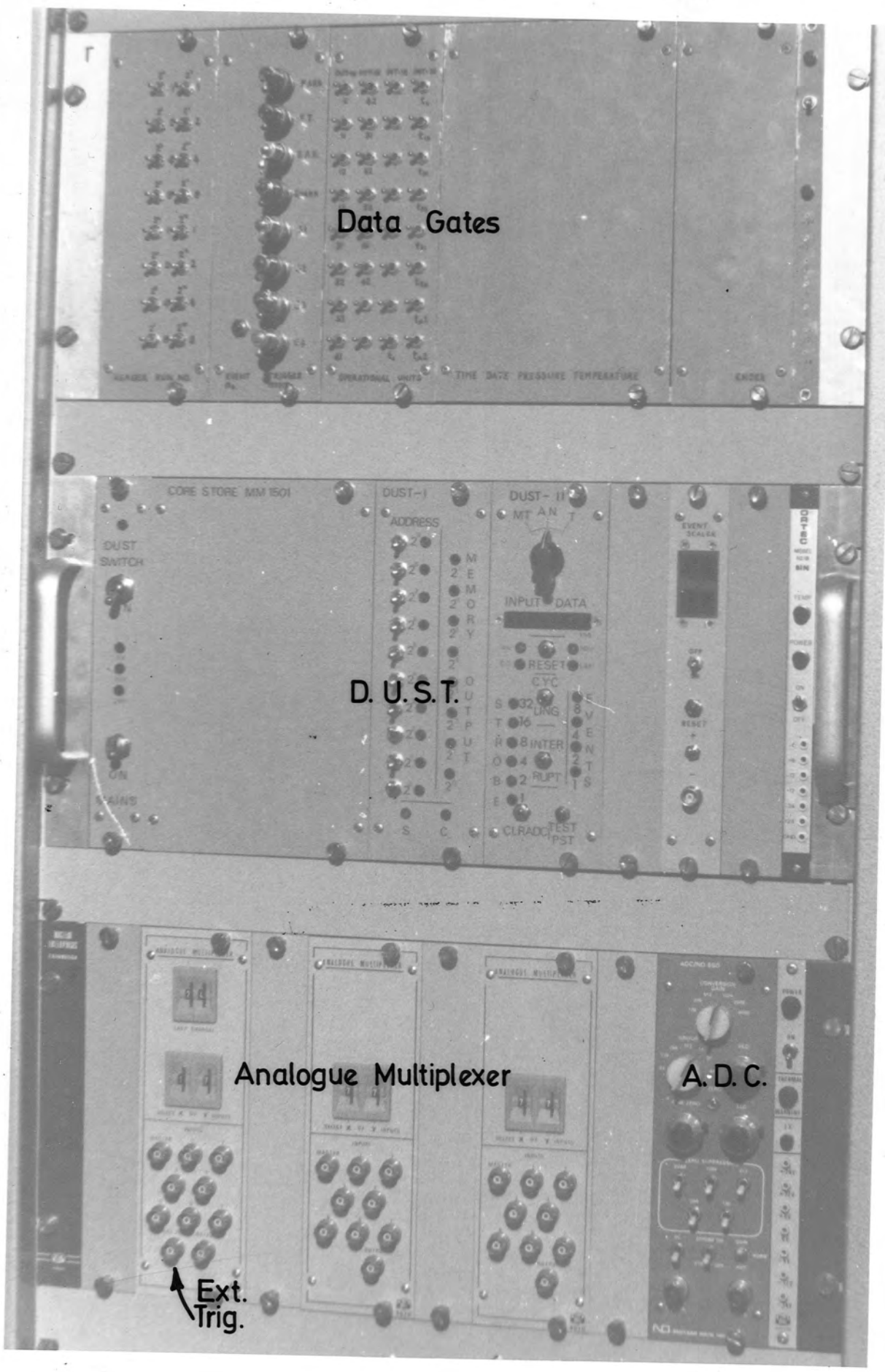
Data Gates
D. U. S. T.
CORE STORE MM 1501
DUST SWITCH
DUST-I
ADDRESS
MEMORY
OUTPUT
DUST- II
MAINT
INPUT DATA
RESET
CYC
LNG
INTER
RUPT
CLR ADC
TEST PST
EVENT SCALER
Analogue Multiplexer
A. D. C.
Ext. Trig.

CHAPTER ONE

COSMIC RADIATION - ITS NATURE AND IMPORTANCE

1.1 Introduction

The intriguing problems of the fundamental processes of nature have commanded the interest of the physicist for a very long time. Measurements of the properties of the Cosmic Radiation, made in the hope of understanding them more clearly, have presented a challenge since their discovery some 60 years ago. The observed energies and isotropy of the radiation have demonstrated that the sun, probably the most obvious source, is not the main contributor.

1.2 The Discovery of the Radiation

For more than 100 years it has been known that air possesses a slight electrical conductivity. In 1899 - 1900 a careful study of this phenomenon was made by Elster and Geitel (1899), Geitel (1900) and Wilson (1900) using elestroscope techniques by observing the rate at which electric charge was lost. The conductivity of the air inside the electroscopes was found to be permanent, despite the continual removal of the ions from it by an electric field. In consequence, it was inferred that the ions were constantly being produced in the air of the electroscopes by some external agency. Rutherford and Cooke (1903) soon found that the ionisation could be reduced by screening the electroscopes with a heavy layer of lead, from which it was concluded that the cause of these effects lay in traces of radioactive material residing in the environment of the apparatus. Thus it was assumed that if this was the cause of the ionisation then the ionisation intensity would fall off with the increasing altitude. In the expectation of this effect Gockel (1910, 1911) ascended in a balloon and made observations at various heights. He found the expected effect to be present, but only weakly.

Between 1911 and 1914 Hess and Kolhörster extended the balloon observations

to greater altitudes and found that above a few hundred metres the conductivity began to increase again. This increase persisted up to an altitude of 9000 metres where measurements were discontinued. To account for the observed facts Hess proposed the hypothesis that the ionisation was produced by a penetrating radiation from outside the earth. Even at this early stage he realised that the radiation could not be coming in a large part from the sun since the ionisation was found to be about the same at all times of the day.

1.3 Observations of Cosmic Rays under Water

Confirmation that the source of the radiation was extraterrestrial came when Millikan and Cameron (1926) lowered sealed electroscopes to various depths below the surface of two Californian lakes - Arrowhead Lake at 1554 m above sea level, and Muir Lake at 3600 m above sea level. The ionisation fell off rapidly within the first metre or so, thereafter decreasing more slowly as the depth increased.

By comparing the ionisation rate of the electroscopes at equal depths under water, a discrepancy was found but when the depths were made equivalent by accounting for the additional 2046 m of air above Arrowhead Lake the observed values of ionisation were found to be in close agreement. On the assumption that the intensity of the rays were the same at both localities the result showed that the intervening air between the two lakes acted only as an absorber and did not contain sources to any noticeable extent.

1.4 The Discovery of the Latitude Effect

A number of workers realised that the nature of the primary particles could be investigated by studying the variation of the Cosmic Radiation intensity with latitude by using the earth's magnetic field. Charged primaries would have their trajectories affected in the magnetic field whereas uncharged particles would be unaffected. Millikan and Cameron looked for such an effect in 1926 but failed to find any systematic change. Clay (1927), on voyages covering a larger range of latitudes than Millikan and Cameron,

found a positive effect. A. H. Compton (1933) concluded that, after a world-wide survey of cosmic ray intensity measurements, his results correlated much better with the geomagnetic latitude than geographical latitude, proving conclusively that at least part of the radiation was charged.

The mathematical theory of the effect of the earth's magnetic field on incoming charged particles had been worked out in considerable detail by Størmer to try to account for the aurora borealis. The theory was suitable for its application to cosmic rays and Le Maitre and Vallarta (1933) calculated the allowed orbits and trajectories of all cosmic particles in the vicinity of the earth.

For particles that enter the earth's atmosphere, as in figure 1.1, vertically and parallel to the geomagnetic lines of force at the poles there is little interaction. At the equator the magnetic field is perpendicular to the direction of the cosmic rays and the interaction is greater resulting in the effect that the less energetic cosmic rays are deflected away from the earth more than at the magnetic poles. Only those particles exceeding a cut off energy are able to reach the earth's surface and this resembles a cut off in the energy spectrum that is latitude dependent and is

$$P_{min} \simeq 14.85 \cos^4 \lambda \text{ GeV/c}$$

where λ is the geomagnetic latitude (Jory, 1956). No particles below this momentum can reach the surface of the earth at a given λ.

Since the main geomagnetic field of the earth is directed from South to North a positive incoming particle would be deflected towards the east. This gives rise to an East-West effect in which the observed intensity of cosmic rays are greater from the West than from the East. This asymmetry has been correctly interpreted and fully demonstrated experimentally as being caused by an excess of positively charged cosmic rays, mainly protons.

1.5 The Origin of Cosmic Rays

Observation of cosmic ray intensities show that the sun must

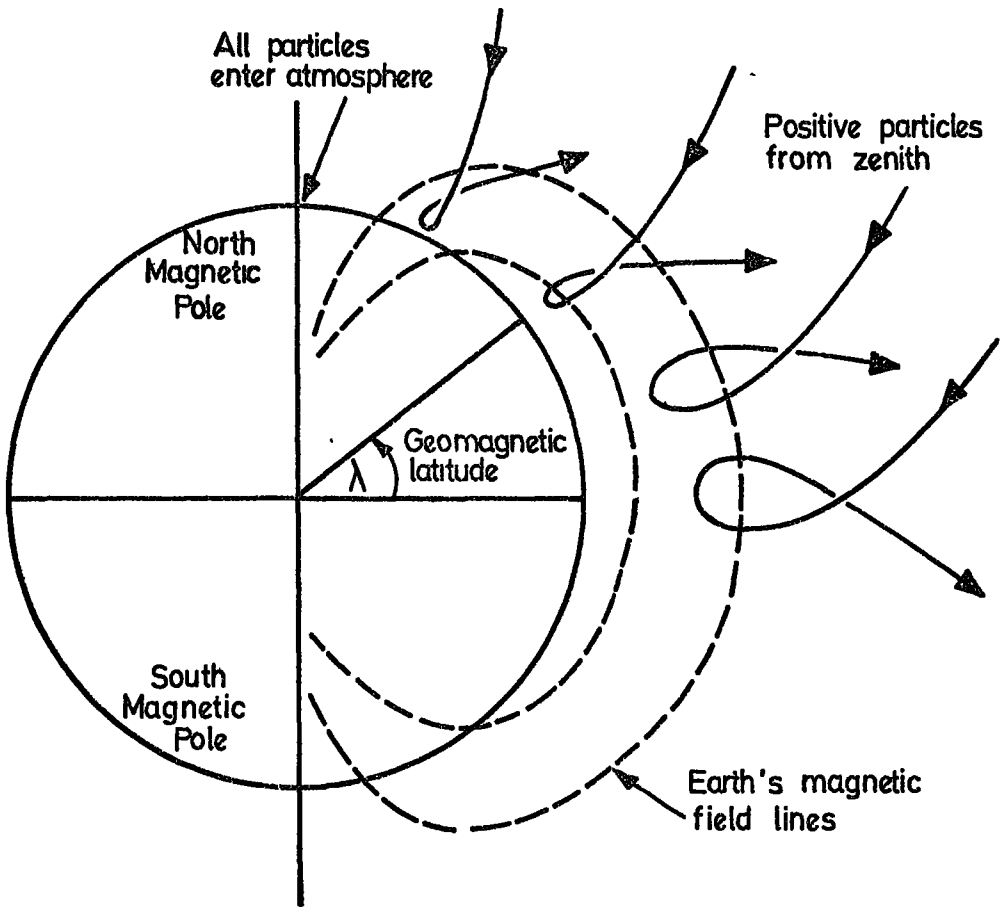

Figure: 1.1. Deflection of cosmic ray particles in the Earth's magnetic field.

actually be the source of at least some of the lower energy ($\lesssim$ 10 GeV) primaries. At times of high solar activity an increase in the cosmic ray intensity is found but the sun can only account for a small fraction of the total. Since the cosmic rays are nearly isotropic around the earth their origin in such a point source as the sun is precluded and one must look for sources and mechanisms that may exist in the deeper regions of space for their production and acceleration.

Following the suggestion of Fermi (1949, 1954) cosmic rays have their origin in interstellar space and are accelerated to high energies by the galactic magnetic fields as they stream through the arms of the galaxy. The cosmic ray particle is ejected from the surface of some stellar body with an appreciable energy and spirals in the local magnetic field. This particle then interacts with another magnetic field moving rapidly towards it whereupon the particle is reflected and gains energy. If this particle is trapped between two fields of this kind then it will steadily gain energy until it is able to leak out. This acceleration mechanism may continue until the particle reaches the earth where it is observed.

On the basis of this theory it is predicted that it would be favourable for particles to be created in the vicinity of magnetically active stars where they will also acquire the bulk of their energy. Supernovae, pulsars, galactic nuclei - all have been suggested as potential sources and all may be correct.

1.6 The Nature of the Cosmic Radiation

Valuable information can be derived from the mass composition of the primary cosmic rays as regards their mean age and possible production mechanisms. It is found that even Z elements are more abundant than odd Z elements and that Li, Be, B are much more common in the cosmic radiation than is estimated for the universal abundances.

Hitherto only direct measurements of the composition have been made

in the energy range from ~10 MeV to ~100 GeV by using balloons and satellites carrying emulsion stacks and ionisation calorimeters. The composition of the primary flux for Ep $\lesssim$ 1000 GeV is given in Table 1.1 after Juliussen (1975), normalised to a percentage of the total. Those figures depart from those of Ginzburg and Syrovatskii (1964) in the respect that the abundances clearly depend on energy. The rise in the abundance of iron with energy is perhaps due partly to interaction and spallation in the interstellar medium, energy losses caused by solar modulation and, most likely, as a consequence of the production mechanisms at source. For higher energies the chemical composition is not certain due to the low flux of cosmic rays rendering direct methods of detection inefficient.

Table 1.1

Composition of Cosmic Rays at High Energies

Z	Elements	Kinetic Energy per Nucleus (eV) 10^{10}	10^{11}	10^{12}	10^{13}
1	Hydrogen	58±5	47±4	42±6	24±6
2	Helium	28±3	25±3	20±3	15±5
3-5	Light nuclei	1.2±0.1	1.1±0.1	0.6±0.2	
6-8	Medium nuclei	7.1±0.4	12.2±0.8	14±2	
10-14	Heavy nuclei	2.8±0.2	6.7±0.5	10±1	
16-24	Very heavy nuclei	1.2±0.2	3.6±0.4	4±1	
26-28	Iron group nuclei	1.2±0.2	4.5±0.5	10±2	24±7
$\geq$ 30	Very, very heavy nuclei		0.007±0.004		

The observation of the L group of nuclei being about 10^6 times more abundant than the universal abundance suggests that these are products of spallation of heavier nuclei from travelling through interstellar matter. Taking this assumption further, one is able to calculate an approximate value

of the amount of matter through which the cosmic rays in this energy range have travelled. Using the ratio of the abundances of the light nuclei to the medium nuclei and the available cross sections for various spallation reactions, Shapiro and Silberberg (1968) have calculated the average amount of matter traversed by cosmic rays required to create the observed L/M ratio. They obtained the value of $\lambda = 4.0 \pm 1.0$ g cm^{-2} which corresponds to an average age for the cosmic radiation of a few million years.

It should be realised that this is a very crude estimate (alternative estimates based on the $^{Be}/_{B}$ and $\frac{^3He}{^3He+^4He}$ ratios give values of this order) but it appears as though the majority of the cosmic radiation has a lifetime of less than 20 million years. This is small when compared to the age of the Universe of about 4.5×10^9 years and the dimensions of the Galaxy.

1.7 The Primary Energy Spectra

The spectra of the primary radiation can be expressed in a variety of ways; the choice usually being determined by the method of measurement. Thus use may be made of energy or momentum effects or magnetic rigidity by using the geomagnetic field as a momentum analyser.

A survey of the data that is at present available is presented in figure 1.2 from the summary of Wolfendale (1973). The various domains in which a particular kind of investigation is most efficient are included. For energies below about 1 GeV direct measurements can be taken, as is the case with satellites. Good data on the spectra of the more abundant elements have been obtained, notably those of Garcia-Munoz et al. (1971) who used cosmic ray telescopes aboard the IMP-5 satellite of 1969 when solar activity was a minimum. Figure 1.3 shows the Garcia-Munoz et al. spectra. The statistical accuracy of the energy spectra of the primary particles becomes increasingly poor as the energy of the primary increases. Beyond about 10^{12} eV per nucleon there is virtually no direct information about particles with Z greater than one and

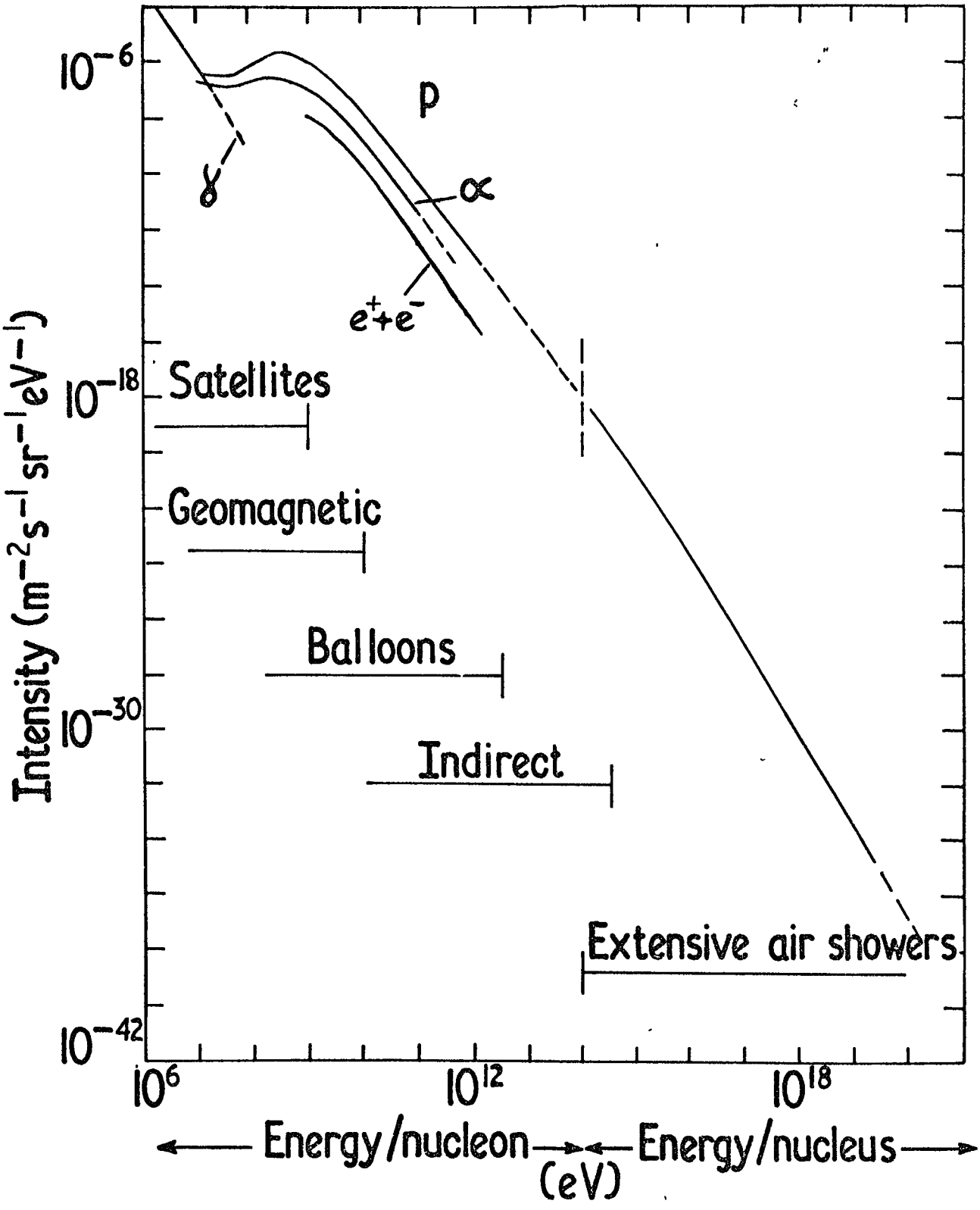

Figure 1.2. Primary cosmic ray spectra.
(After Wolfendale, 1973)

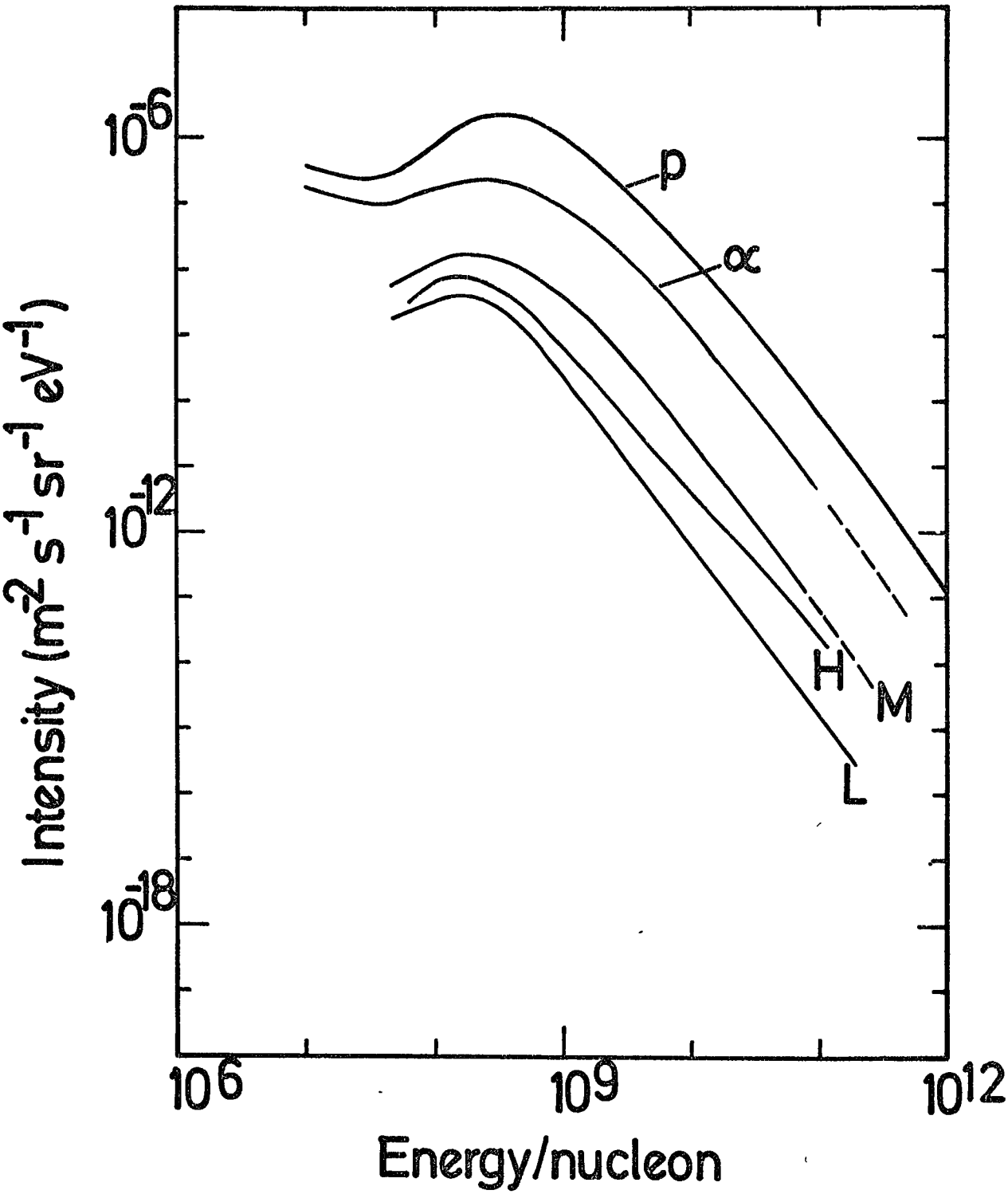

Figure 1.3 Energy spectra for low energy Cosmic Rays. (After Wolfendale, 1973).

the energy spectra must be inferred from ground level observations of the protonic and muonic fluxes via an interaction model. There is a degree of confidence in these calculated spectra because they fit smoothly with the direct observations and the extensive air shower data. For a recent review of cosmic ray composition see Juliusson (1975).

The spectrum measured beyond about 10^{14} eV is investigated by means of the extensive air shower technique in which the atmosphere amplifies the effect of a single high energy primary to such an extent that particle detectors need to be spread over large areas at detection level. The spectrum thus obtained yields data on the energy of the incoming particle and hence the spectrum's energy axis must be labelled 'energy per nucleus'. It is in this energy region that there exists much contemporary interest in the cosmic radiation.

1.8 Summary of the data about Cosmic Rays with Ep > 10^{12} eV

Features which are relevant to the problem of the origin of the cosmic radiation can be summarised as follows:-

(i) Energy: the total energy density is about 1 eV cm^{-3}. That above 10^{12} eV is about 2.10^{-2} eV cm^{-3}.

(ii) Energy Spectrum: extends beyond 10^{20}eV and has a differential slope of -2.6 from 10^{12} eV to 310^{15}eV and -3.2 above this. The transition of the slope changes over a relatively small range of energy.

(iii) Mass composition: above 10^{12}eV very little is known.

(iv) Isotropy: no significant anisotropy has been observed.

Any theory that is formulated in respect of the origin must therefore embody the above observations.

1.9 The Astrophysical Significance of Cosmic Rays

In any attempt to explain the observed features of the primary

spectrum above 10^{12}eV the properties of the galaxy and its environment need to be considered. The shape and magnitude of the spectrum is of direct relevance to the understandingand ascertaining from where the particles originate, how they are accelerated and how they propagate through space. Recent work by Karakula et al. (1974) has suggested that the majority of cosmic rays with energies between $\sim 10^{14}$eV and $\sim 5.10^{15}$eV are of pulsar origin. The nuclear physics of the processes beyond 10^{12}eV can be inferred by relating secondary cosmic ray phenomena (ground level observations) to the primary energy spectrum through an interaction model. This, at present, is the only way in which ultra high energy nuclear physics can be investigated since modern machines are incapable of providing particles of sufficiently high energy to investigate these reactions. It has been discovered that well established rules governing nuclear physical processes below 10^{12} eV are not as successful as expected in the cosmic ray energy domain. In particular the 'scaling hypothesis' of Feynman (1969) appears to be contradictory to experiment beyond 10^{12}eV.

Direct measurements on the primary spectrum beyond 10^{19}eV are of particular interest since it is at about this energy that the Big Bang 2.7°K black body remnant microwave radiation should begin to attenuate the protonic flux by electron pair and pion pair-production.

1.10 The Shape of the Primary Spectrum above 10^{12}eV

The integral primary energy spectrum has recently been surveyed by Kempa et al. (1974) and is summarised in figure 1.4. An interesting feature of this survey is an apparent bump in the region of 10^{14}eV and 10^{15}eV. Above this bump γ_I is -2.1 whilst below it γ_I is -1.6.

Attempts to explain this feature have been undertaken by several authors (Kempa et al. (1974), Karakula et al. (1974)) as being the result of a contribution from pulsars using as a basis the mechanism of Ostriker and Gunn (1969) although the details of the acceleration process are not well understood.

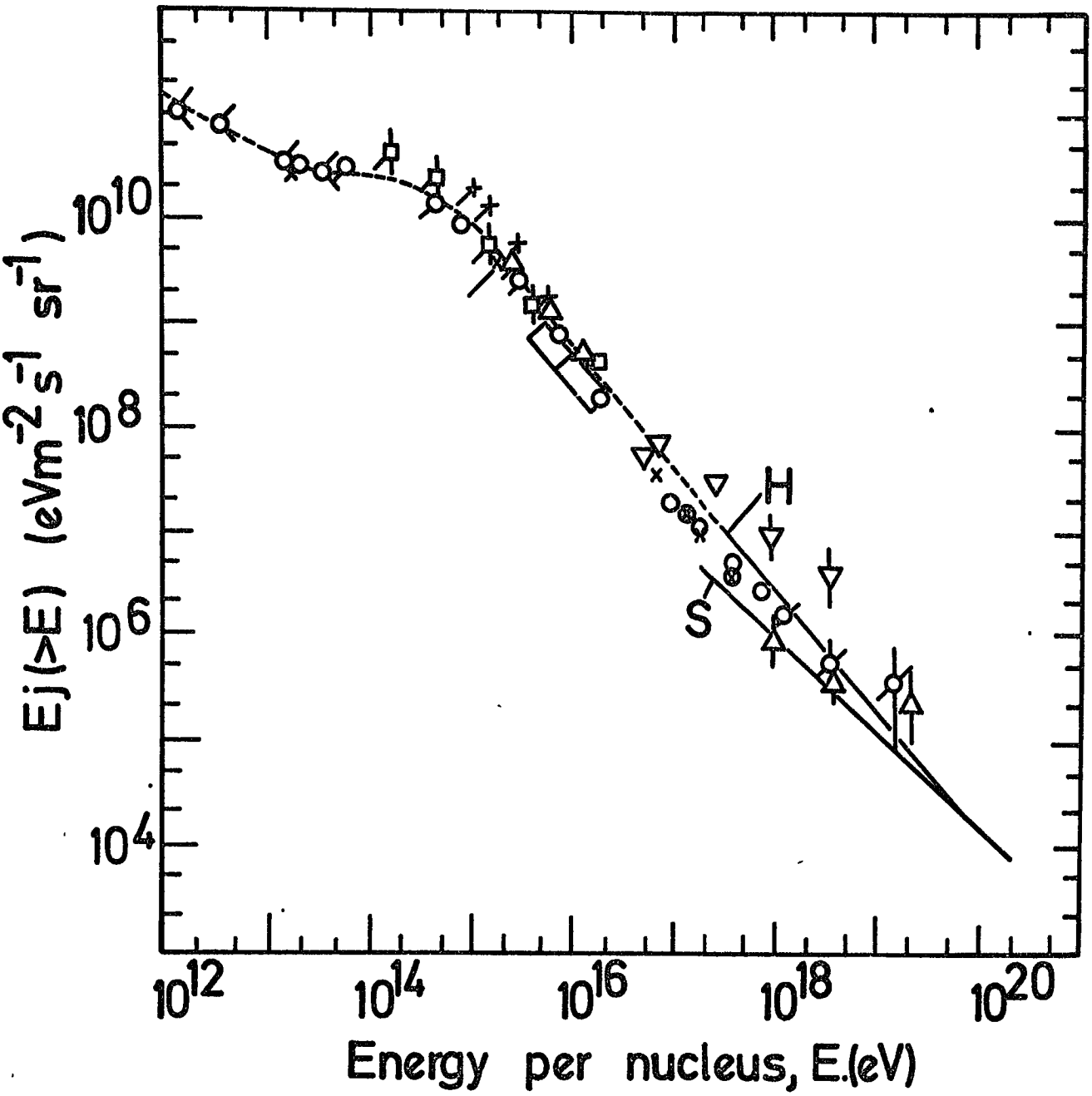

Figure 1.4. The integral primary cosmic ray spectrum. (After Kempa et al. (1974))

The agreement with observation in this region is interesting and perhaps significant. Should the effect be genuine then it would imply a galactic contribution to the integral flux for this energy region. Isotropy measurements and diffusion calculations of cosmic rays within the galaxy support this view.

It has been thought for a long time that the cosmic rays of the highest energy were all extragalactic since galactic magnetic fields would be unable to contain them and because there is no observable anisotropy in this region. Proposals made by Greisen (1966) that there should be a cut-off at about 10^{20}eV in the primary energy spectrum have recently been investigated by Strong et al. (1974) in some detail. This cut-off arises from photonuclear reactions with the 2.7^{o}K Black Body radiation. Figure 1.5 shows the composite primary spectrum of Strong et al. (1974). The line marked Kempa et al. (1974) is the best fit line of Figure 1.4. The figure shows the onset of electron pair production (c.10^{18}eV) and pion production (c.5.10^{19}eV) which are clearly visible. Although there can be no question of exact agreement between the pulsar and extragalactic contributions and experiment, close agreement does warrant further study.

Observations of air showers at the highest energies, notably those of the Haverah Park and Sydney arrays are shown in figure 1.6 from a summary of C. J. Bell et al. (1974). It is evident from the data that no cut-off is seen and this is at variance with the predictions of Strong et al. (1974). Modifications to the existing theory following a suggestion by Brecher and Burbidge (1972) invoking a measure of containment within galactic clusters arising from the presence of magnetic fields which may be present, overcomes the problem to a great extent but a more accurately defined spectrum in this region is undoubtably required.

1.11 The Significance of Cosmic Ray Studies

From what has been said earlier it can be seen that the study of

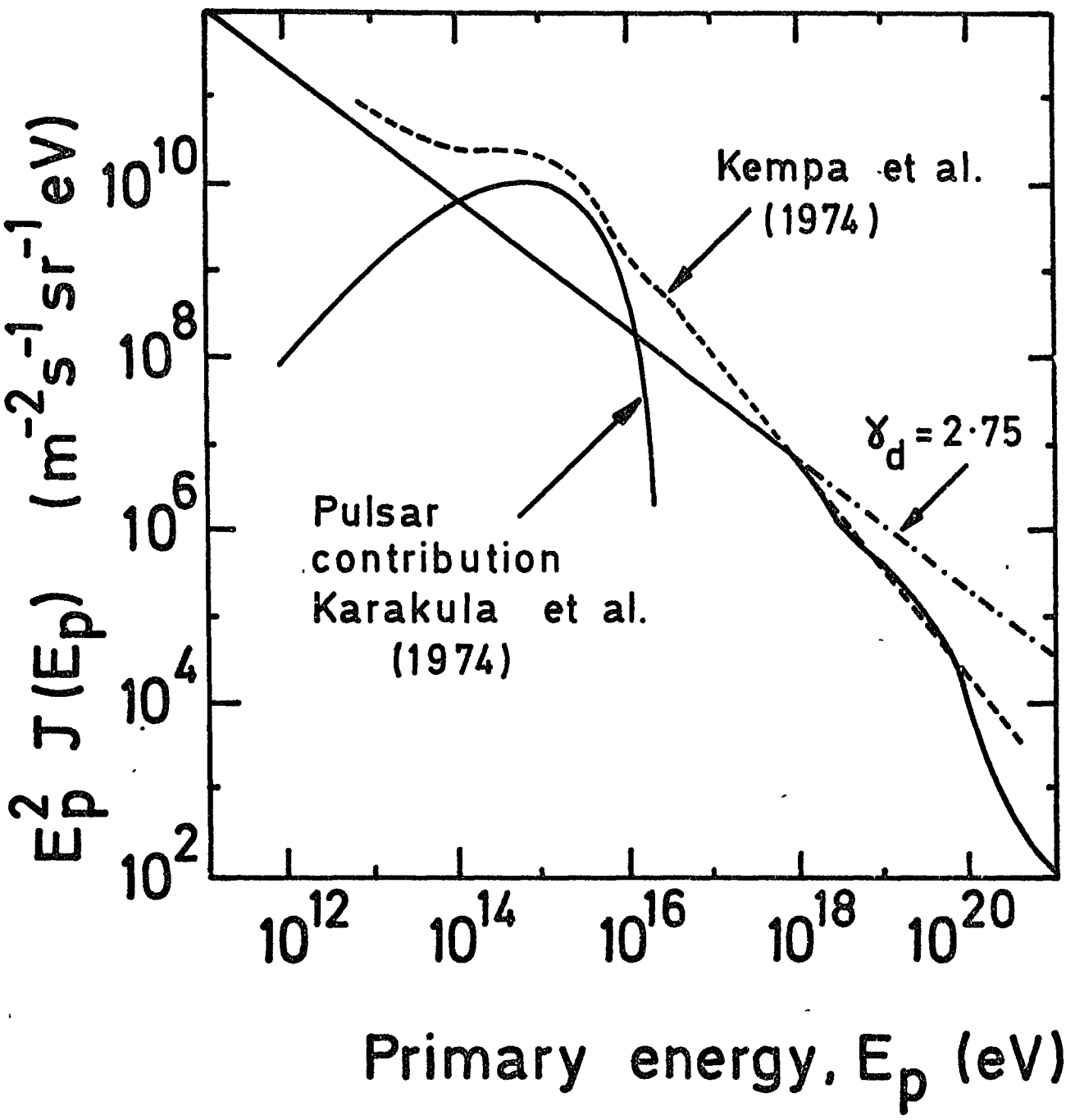

Figure 1.5. Primary cosmic ray energy spectra showing the pulsar contribution of Karakula et al., 1974. (After Strong et al. (1974))

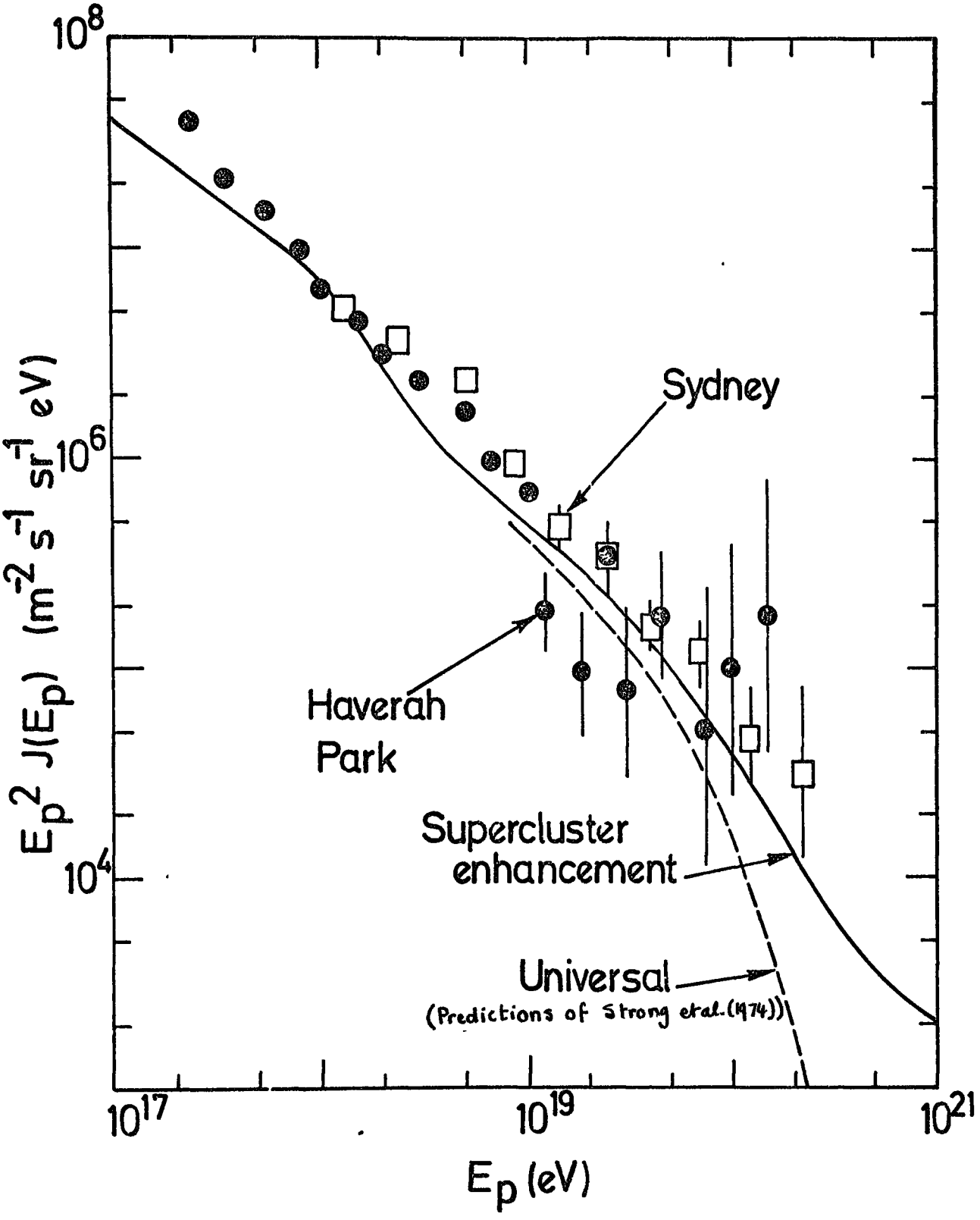

Figure 1.6. The primary cosmic ray spectrum at the highest energies.

the cosmic radiation can yield a wealth of information of phenomena over the extreme ranges of the spatial and temporal scales. In relating these processes a picture of both galactic and nuclear structure can be obtained. Nuclear Physics at the extreme energies encountered in the cosmic radiation cannot, at present, be investigated in a laboratory experiment and it is unlikely that they will be for a very long time. It is for these reasons that there is still much activity in this field.

In an attempt to interpret the ground level observations of secondary effects initiated by a primary particle above the earth's surface, models of nuclear processes must be constructed in order to explain the observations. Many models to describe the general features of interactions have been used and it is regretted that progress is hampered by the poor quality of the information at present obtainable in cosmic ray nuclear physics.

1.12 Nuclear Interactions

There exists a wealth of good data on nuclear physical phenomena up to energies of about 300 GeV that has been provided from particle accelerator experiments. More recently the C.E.R.N. Intersecting Storage Ring facility has enabled a detailed examination of particle physics to about 30 GeV centre-of-mass which has played an important role in establishing a datum for the interpretation of nuclear phenomena at cosmic ray energies. In particular the scaling hypothesis of Feynman (1969), which is a logical extension of these data, predicts an asymptotic behaviour of particle interactions at higher energies.

Implications of the scaling hypothesis as applied to these energies have been suggested by Wdowczyk and Wolfendale (1972,1973a) from which it is derived that scaling is valid if an increase in the primary mass is allowed. As yet very little is known about the primary cosmic ray mass but fluctuations observed in extensive air showers by Khristiansen (1971) suggest that there is at least a significant fraction of the primary particles that are protons. Using the assumption that most of the primaries

are indeed protons then studies of the longitudinal development of extensive air showers can give evidence of which treatment is applicable.

From these measurements the form of the multiplicity distribution can be derived since the position of the shower maximum is related to the length of the electromagnetic cascades resulting from neutral pions. A low multiplicity suggests long electronic cascades with a shower maximum low in the atmosphere whereas a higher multiplicity would result in shorter cascades and a shower maximum higher in the atmosphere. Figure 1.7 shows a distinct inconsistency between the scaling suggestions of Feynman, which predict a logarithmic rise in multiplicity, and that observed at energies greater than c.10^{13}eV. In the énergy range of 10^{12}eV to 10^{14}eV, which is still in the cosmic ray energy region, scaling seems to apply from the approximate constancy of the charge ratio of muons and the slope of the pion production spectrum derived from the observed muon spectrum.

Other features of this hypothesis are the expected constancy of the multiplicity of secondaries that carry a particular fraction of the primary energy and the rapid saturation of the mean transverse momentum p_t of these secondaries at 0.4 GeV/c. From the analysis by Adcock et al. (1970) of the data from the Utah group of Coates et al. (1970) a mean transverse momentum somewhat higher at (0.60 $\pm$ 0.05) GeV/c is found which is again at variance with the Feynman suggestion.

Cosmic ray data above 10^{14}eV imply a multiplicity law proportional to E^{β} where β is about 0.25 (Adcock et al. (1969), Hillas et al. (1971)) which suggests a more thermodynamical treatment of particle production (Hagedorn (1965), Torsti (1975)). Taken together it would seem evident that scaling in its simple form becomes less and less applicable as the energy increases above 10^{12}eV but it seems possible that there could exist two types of treatment of the nuclear physics - that of a scaling and that of a thermodynamic nature.

1.13 The Importance of Extensive Air Showers

The rôle of extensive air showers in an effort to understand the

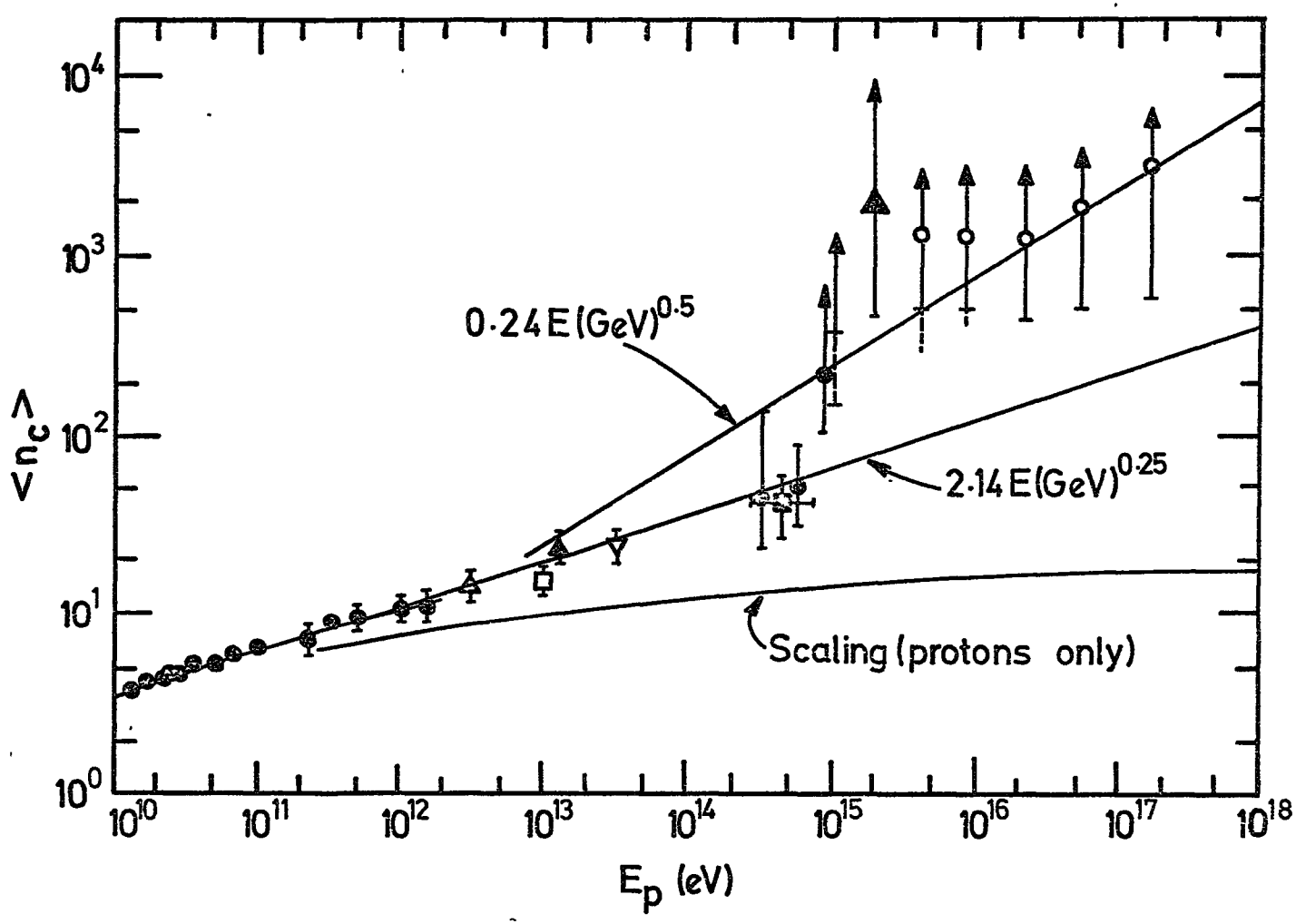

Figure: 1·7. The mean multiplicity of charged secondaries in high energy collisions. Data are from surveys by Wdowczyk and Wolfendale (1973b) and Gaisser et al. (1973).

nature of nuclear processes at the highest energies cannot be denied. As yet they provide the only means of investigating the properties of what occurs at energies in excess of 10^{12}eV and it appears as though they will be the main contributor to this sector for a long while. The study of extensive air showers also provides a valuable tool for investigating the conditions of the galaxy and beyond and it is to these two ends that the extensive air shower needs to be pursued.

CHAPTER TWO

EXTENSIVE AIR SHOWERS

2.1 Introduction

Extensive air showers have been widely studied since their discovery in 1938. Their existence implied that the energies of the particles causing the effect were far greater than those previously studied by geomagnetic means.

At the time of their discovery the most energetic radiations known were gamma-rays and so it was natural to assume that the originators of these showers were of the same character but with energies several orders of magnitude above those previously encountered. Theoretical work by Bhabha and Heitler (1937) successfully accounted for the observations made in cloud chambers (Auger et al., 1939) and thus the gamma-ray origin propagated and became a widely accepted model for many years. Other experiments (Froman and Stearns, 1938) showed the existence of a 'penetrating' component, capable of traversing several centimetres of lead, and on the basis of the electron-photon cascade model were difficult to interpret. Since 1946 the activity in extensive air showers has been considerable and from the results of balloon borne experiments it became clear that many of the high energy primaries were atomic nuclei, mainly protons and helium. The discovery of the π^- mesons in the cosmic radiation gave a clearer picture of air shower development and added impetus to the quest to understand the phenomenon more clearly. Soon the focus of attention turned towards the origin of the particles and their interaction with matter and these form the main problems in cosmic ray physics at the present time. With the progress of high energy particle accelerators, activity in air showers has increased considerably. With the energies now available at which the cross section for multiple particle production predominates, detailed information that is necessary in interpreting the characteristics of air shower development may be obtained.

This present chapter is devoted to the study and interpretation of air shower phenomena in which the characteristics of the observed features are discussed. Individual aspects will be considered in some detail and the theoretical implications necessary for their understanding in terms of the nuclear processes will also be presented.

2.2 General Description of the Extensive Air Shower

For an observable effect at sea level the energy of the initiating primary particle must be in excess of about 10^{13}eV. The collision of this primary with the nuclei of the constituents of air produce many secondary particles, mostly pions; the π^{o} decaying in less than 10^{-15}S into two gamma quanta and the $\pi^{\pm}$ decaying into muons and neutrinos. With the mean free path of the proton primary being 70 - 80 g cm^{-2} it implies that its first interaction takes place between 10 and 30 km above sea-level. Direct information regarding this initial interaction has been obtained only at the relatively low energies of less than 10^{13}eV with the aid of photographic emulsions. Reviews of this work have been done by several authors (see, for example, Fowler and Perkins, 1964). In general one of the nucleons in this interaction takes off about 50% of the primary energy (at least at 10^{13}eV) and it is natural to associate the primary particle with it. This, the pions and surviving nucleons from the interaction continue further down into the atmosphere and interact again producing many more particles in the ensuing collisions. The electromagnetic cascade is constantly rejuvinated by the π^{o} decay gammas through pair-production and bremsstrahlung and contributes by far the most numerous component at the observation level. The particles in such a cascade can reach out to large distances from the shower axis and this is mainly due to the coulomb scattering in the atmosphere. As the available energy, provided by the nuclear cascade, gets divided amongst the increasing number of shower particles, the mean energy per particle decreases until the energy that is lost by ionisation becomes greater than the energy lost by bremsstrahlung.

For an electron this occurs at its critical energy of 84 MeV and beyond this point the number of shower particles decreases.

The rôle of the charged pion in the generation of an air shower is in rejuvenating the nucleon cascade and in producing muons. The mean life of charged pions is such that they have a finite probability of interacting with the nuclei of air molecules before decaying. Due to the relativistic time dilation, the pions with energies in excess of about 10 GeV tend to interact before they decay whilst those with lower energies tend to decay rather than interact. The muons that are the progeny of the decay pions have the very much longer lifetime of $2\mu S$ and this, combined with the time dilation factor, give large mean free paths indicating that, in general, all muons can survive to sea level. The muon has a larger mass than the electron and consequently is not scattered to the same extent, but because of their greater penetrating power muons can be found at great distances from the shower core. This feature is also due to the muons created in the initial interactions of the primary and surviving to observation level whereas other particles are not able to do so.

This general picture of air shower development has been built up over the last three decades, based upon observations from emulsions and small extensive air shower data and it is thought that this broad picture will not change appreciably for its application to showers of the highest energies which are currently being investigated. A schematic diagram of air shower development is given in figure 2.1 in which the appropriate numbers and total energies of each component are included.

Effects due to the passage of shower particles in their journey to the observation level that are produced by mechanisms other than the type discussed include Cerenkov light emission and radio frequency radiation. The radio frequency emission is created by the transverse current of the shower particles, mainly electrons, being deflected by the geomagnetic

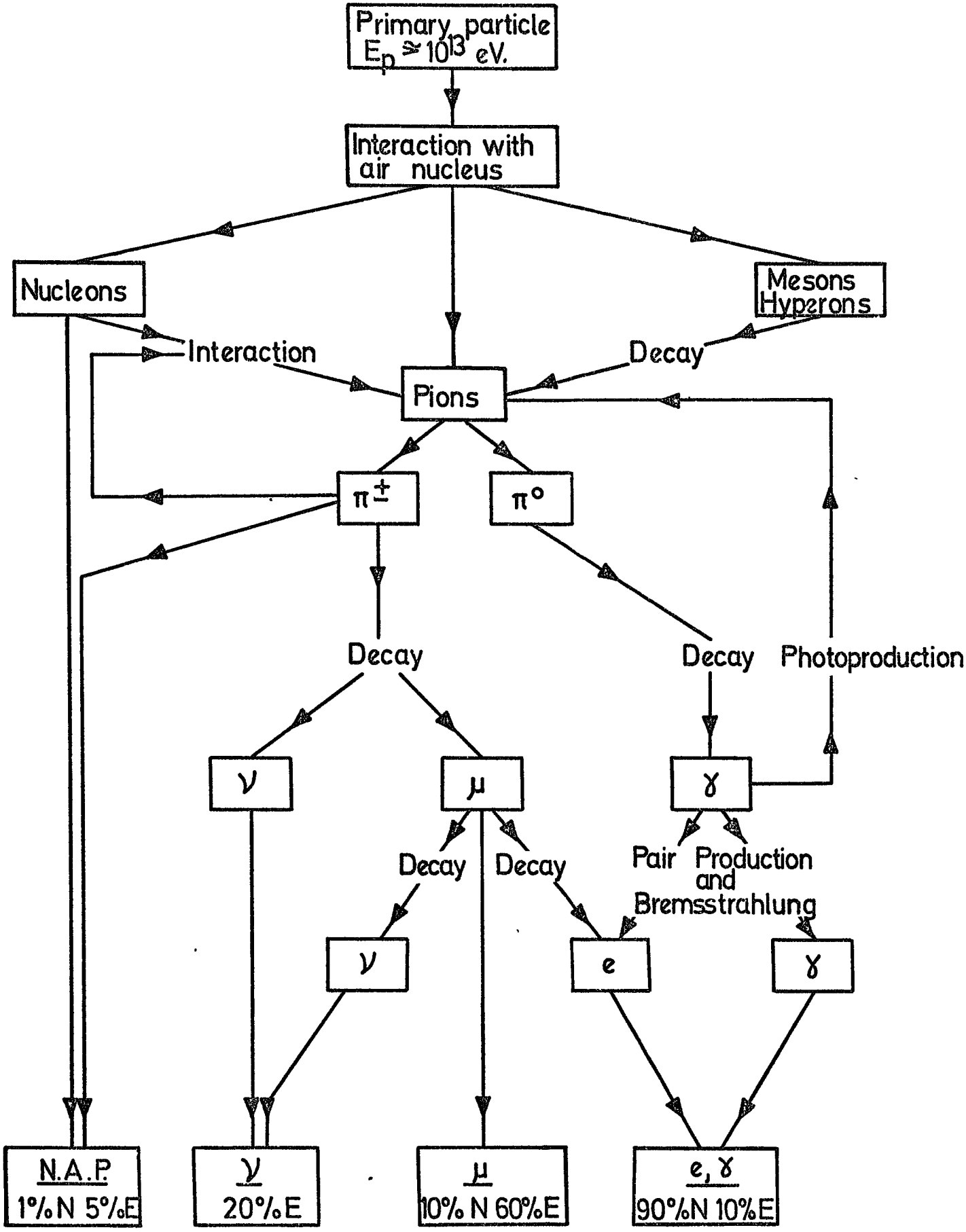

Figure: 2·1. The development of a high energy shower. (E is total energy of a shower containing N particles at ground level.)

field. This phenomenon has been extensively studied in recent years and continues to be so at the Yakutsk and Haverah Park arrays. It is thought by some workers (Allan et al., 1973) that the pattern of the radio lateral distribution can give information about the longitudinal development of a shower and in particular about the height of shower maximum. The extent to which this height is found to vary can give a clue as to the nature of the initiating primaries. Cerenkov light, produced in the atmosphere as a result of the passage of highly relativistic air shower particles, is a feature that is being investigated for detection of very large extensive air showers and will be discussed in a later section.

2.3 Nuclear Physics and the Air Shower

Because of the very nature of the air shower and its complexity of formation detailed calculations must be undertaken to interpret the phenomenon. In general it is only through the models of the high energy interactions, which are not clearly understood, that a consistent picture can emerge of the processes involved. Any deviation from what is experimentally observed from that predicted by theory entails a modification to the model until satisfactory agreement is achieved. On this basis, it is apparent that the nuclear physical models are an important feature for the understanding of the air shower. The standard model employed in this situation, which is most usually regarded as the datum to refer other models, can be summarised as follows (after de Beer et al., 1966).

(i) High energy nucleons lose, on average, 50% of their energy in each collision. Their interaction mean free path is 80 g cm^{-2}. Both of these quantities are energy independent.

(ii) The secondary particles are mainly pions and are created in equal numbers of π^+, π^- and π^o.

(iii) The energy distribution of the pions in the laboratory reference frame is given by the empirical relation of Cocconi, Koester and Perkins (1961) and is

$$S(E,E_o) = \tfrac{1}{2}\left\{\frac{n(E_o)}{\Gamma}\exp\left(-\frac{E}{\Gamma}\right) + \frac{n(E_o)}{G}\exp\left(-\frac{E}{G}\right)\right\},$$

where $n(E_o)$ is the multiplicity of the produced pions, E_o the transferred energy, G the average energy of the pions in the backward cone and

$$\Gamma = 2(KE_o - \tfrac{1}{2}n(E_o)G) / n(E_o)$$

is the average energy in the forward cone.

(iv) The fraction of energy lost by a nucleon which does not appear as pions is assumed to be negligible.

(v) The secondary pion multiplicity, n_s, is given by

$$n_s = 2.7\, E_p^{\frac{1}{4}},$$

with E_p in GeV, for the coefficient of inelasticity, K, at 0.5 and

$$n_s = 2.7.\ 2^{\frac{1}{4}}.\ (KE_p)^{\frac{1}{4}} \quad \text{for all K.}$$

(vi) The distribution in transverse momentum, p_t, of the produced pions is that given by Cocconi, Koester and Perkins

$$f(p_t) = p_t/p_o^2 \exp(-p_t/p_o)$$

where the mean transverse momentum, $2p_o$ is energy independent 0.4 GeV/c.

(vii) The pion interactions are catastrophic and the energy spectrum and multiplicity relations of pions produced in pion interactions are taken to be that given by the same function as for protons with K = 1. Pions have an interaction length of 120 g cm^{-2}.

(viii) The form of the inelasticity distribution is

$$f(K) = -(1+\alpha)^2 (1-K)^{\alpha} \ln(1-K) \text{ with } \alpha = 1.414.$$

2.4 Review of Extensive Air Shower Components

The various components found in air showers fall under three broad headings: the electron, the muon and the nucleon components. Each will be treated separately and features of special interest will be discussed.

2.4.1 The Photo-Electron Component

The main component that characterises an air shower is the photo-electron component which is by far the most numerous but not the most energetic fraction. The lateral distribution of the density of the electronic component is commonly referred to as the structure function and it has been measured by many groups at sea level and mountain altitudes. The results prior to 1960 have been summarised by Greisen (1960) who has combined the results from a large number of experiments to obtain a single experimental relation. This equation has stood up remarkably well throughout the years and it is still believed to give a good representation of the true structure. It is claimed to be indistinguishable from the average experimental distribution for showers with sizes varying between 10^3 and 10^9 particles, atmospheric depths varying from 537 g cm^{-2} to 1800 g cm^{-2} and radial distances of 5 cm to 1500 m from the shower axis. This function is

$$\rho(N,r) = \frac{0.4N}{r_1^2} \left(\frac{r_1}{r}\right)^{0.75} \left(\frac{r_1}{r+r_1}\right)^{3.25} \left(1 + \frac{r}{11.4r_1}\right) \qquad (2.1)$$

where ρ is the density of particles per square metre for a shower of size N at radial distance r metres. r_1 is the characteristic scattering length for electrons in air and is frequently called the Moliere unit. It has the value of 79 m at sea level and about 120 m at mountain altitudes. At distances less than 100 m from the axis this expression becomes a close approximation to the theoretical function of Nishimura and Kamata (1952, 1958) for a pure electromagnetic cascade with an age parameter, s , of 1.25. This is perhaps due to the major electronic contribution in this range. A simplified version of this formula has been suggested by Greisen (1956) as

$$f\left(\frac{r}{r_1}\right) = C(s) \left(\frac{r}{r_1}\right)^{s-2} \left(\frac{r}{r_1} + 1\right)^{s-4.5} \qquad (2.2)$$

where C(s) is a normalisation factor such that

$$\int_0^\infty 2\pi\, f(x)x\,dx = 1, \qquad \text{where} \quad x = \frac{r}{r_1}.$$

Some values of C(s) against s are given in Table 2.1.

Table 2.1

s	0.5	0.75	1.0	1.25	1.50	1.75
C(s)	0.16	0.29	0.40	0.45	0.41	0.28

Assuming that the lateral distribution is independent of shower size, the electron density at the radial distance r from the shower axis may be given as

$$\rho(N,r) = \frac{N}{r_1^2} \cdot f(r) \qquad (2.3)$$

It has been found by some workers (Hasegawa et al., 1962) that the electronic structure function depends upon the method employed in detection. Geiger-Mueller counters represent well the actual density distribution whilst that measured with plastic scintillators is slightly steeper due to the dependence of the scintillator response on the energy spectrum of the electromagnetic component. This is illustrated in figure 2.2 using the structure function of Hasegawa et al., and the Greisen structure function for s = 1.25. The Hasegawa function is:-

$$\rho(N,r) = \frac{N}{2\pi(120\pi)^{\frac{1}{2}}} \cdot \frac{\exp(-r/120)}{r^{1.5}} \qquad (2.4)$$

Measurements of the Sydney group at sea level (Hillas, 1970) give a much flatter distribution function than that of Greisen and is due to the observation of a large proportion of multi-core events for showers induced by primaries of energies approximately greater than 10^{15} eV. It is expressed by:

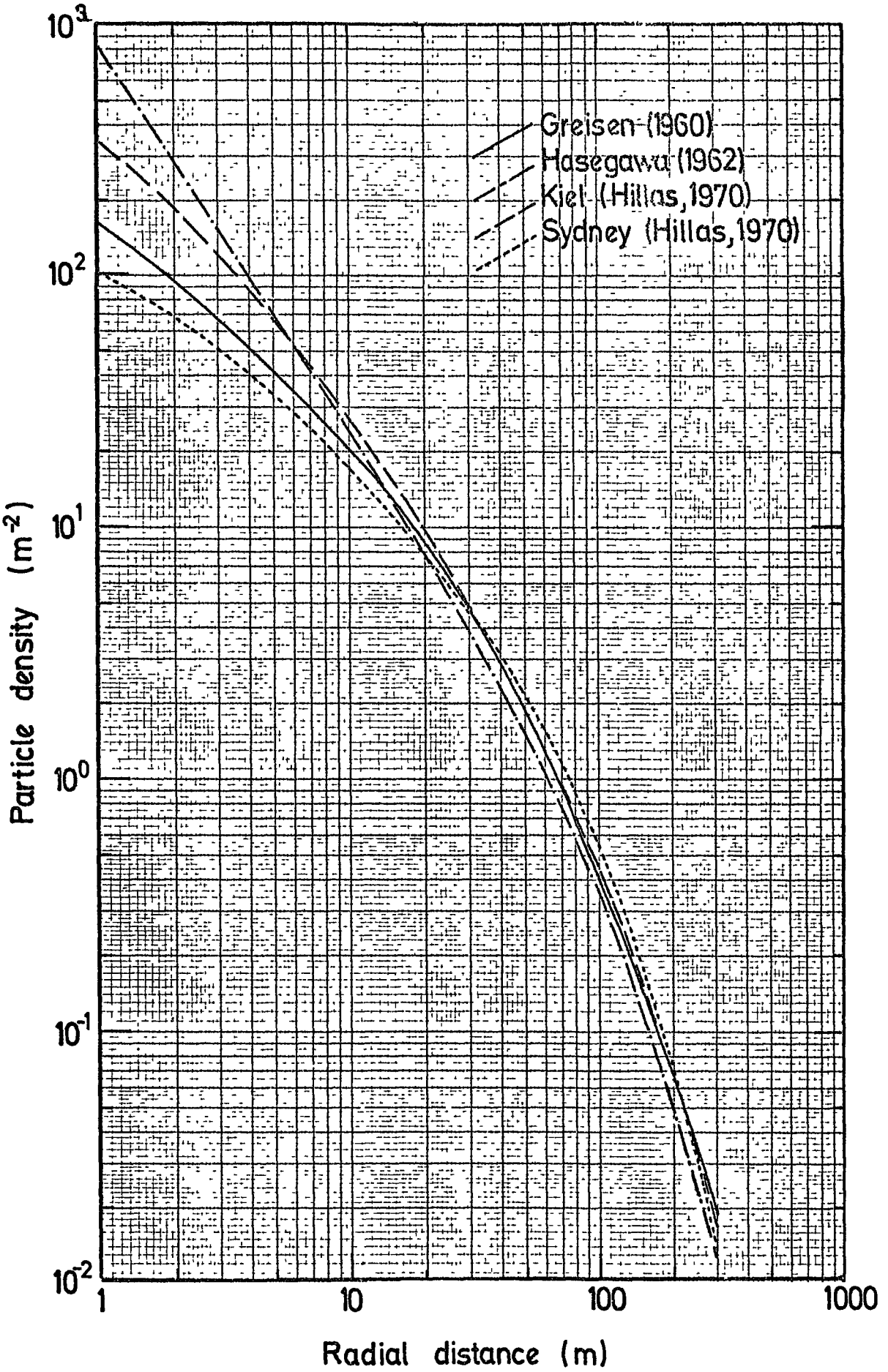

Figure 2·2. Comparison between the air shower lateral structure due to several authors, normalised to $N = 10^5$.

$$\rho(N,r) = 2.1210^{-3} \frac{N}{(r+1)} \exp(^{-r}/75) \qquad (2.5)$$

From measurements of the lateral structure by the use of a neon hodoscope, the Keil group (Hillas, 1970) find that the relation

$$\rho(N,r) = 1.08 \times 10^{-2} \frac{N}{(r+1.1)^{1.5}} \exp(^{-r}/_{120}) \qquad (2.6)$$

fits their data satisfactorily. A comparison of these functions is illustrated in figure 2.2. For all cases there is good agreement in the range

$$10 \text{ m} < r < 300 \text{ m}$$

and the observed discrepancy is partly due to the experimental errors in the core location of the individual experiments.

2.4.1.2 The Longitudinal Development of an Air Shower

The electron component, although representing only a small fraction of the total energy of an air shower, is an important measure of the stage of development of the air shower and has featured in many theoretical treatments and experimental measurements. Although it has not yet been possible to measure the total shower size at different depths in the atmosphere for a vertical shower, this information has been obtained from many showers by making equi-intensity cuts in the size spectra recorded at different zenith angles (Linsley et al., 1962, La Pointe et al., 1968). Data derived from the Chacaltaya experiment by Bradt et al., (1965) are shown in figure 2.3 plotted with the aerial data of Antonov et al., (1971) obtained at a height of 10 km. The curves so obtained show that the electromagnetic cascades initiated by individual interactions of nuclear active particles are relatively short and that they are subject to large fluctuations. The shortness of these cascades indicate a rapid division of the energy of the nuclear active particles; that is a high multiplicity of the secondary particles. The growth and decay of the shower in the atmosphere is typified by the depth at shower maximum. Figure 2.4 shows the variations in the depth of maximum development and electron shower size

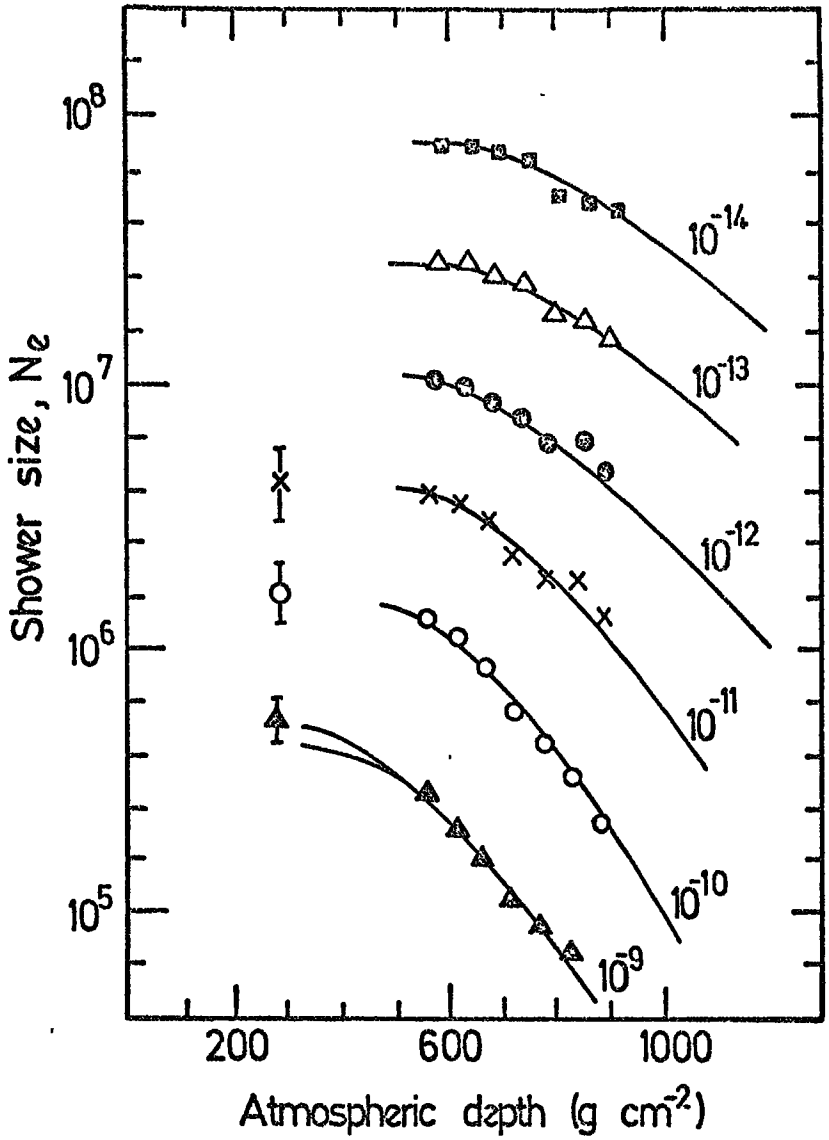

Figure 2.3. Equi-Intensity cuts of air showers. (After Wdowczyk, 1973)

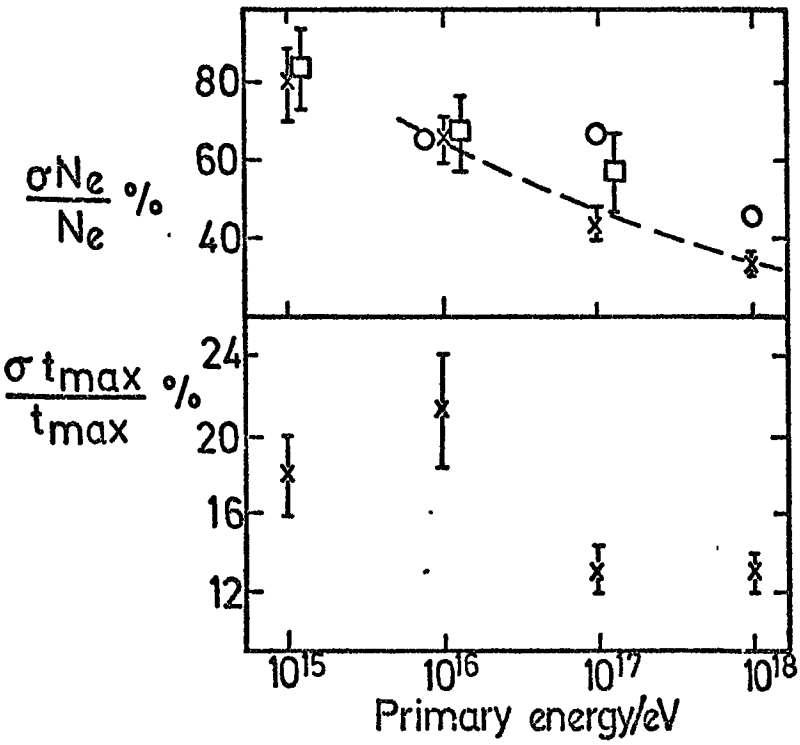

Figure 2.4. The relative standard deviation of the electron shower size and depth of maximum development for proton initiated showers. ✕ Dixon and Turver (1974b), O Marsden (1971), ⊡ Khristiansen et al. (1966). The curve is due to de Beer et al. (1968).

at sea level with primary protonic energy (after Dixon and Turver, 1974). Results from various theoretical treatments are included. It appears as though there is satisfactory agreement between the data from these theoretical studies; slight differences being due to the differences in the models adopted. Shower longitudinal development can be further specified by the variation in the absorption length with electron size. From the work of Dixon et al., (1974a) the shower attenuation length can be given, from computer simulations, by

$$\lambda_A = 47.7 \ln N_e + 32.0 \text{ g cm}^{-2}$$

and

$$\lambda_B = 25.0 \ln N_e + 95.0 \text{ g cm}^{-2}$$

where λ_A and λ_B refer to the attenuation lengths under the Greisen (1956) electron cascade approximations A and B which, under approximation A, take into account the radiation loss of electrons and the gain in electron number from pair-production from gamma-rays. Under approximation B, there is included an additional term allowing for ionisation loss.

Contemporary interest in the longitudinal development has focussed on the possibility of the mean height of maximum development, linked with the individual fluctuations of this quantity, being related to the rate of development which reflects the nature of the primary cosmic ray particle and the details of their high energy interactions (Turver, 1973). It is expected that protonic or light nuclei initiated showers will show greater fluctuations in the longitudinal development than is the case for heavier primaries. A consequence of 'heavy' initiated showers would be a decrease in the average depth of maximum development and a lack of large fluctuations in observed showers. Figure 2.5 illustrates the average development of computer simulated vertical showers of Dixon et al., (1974b) for superposition and partial fragmentation assumptions of the heavy nucleus break-up. The difference between showers induced by assuming a superposition or partial fragmentation hypothesis becomes important as the primary energy increases. The choice of fragmentation model makes little difference to the electron

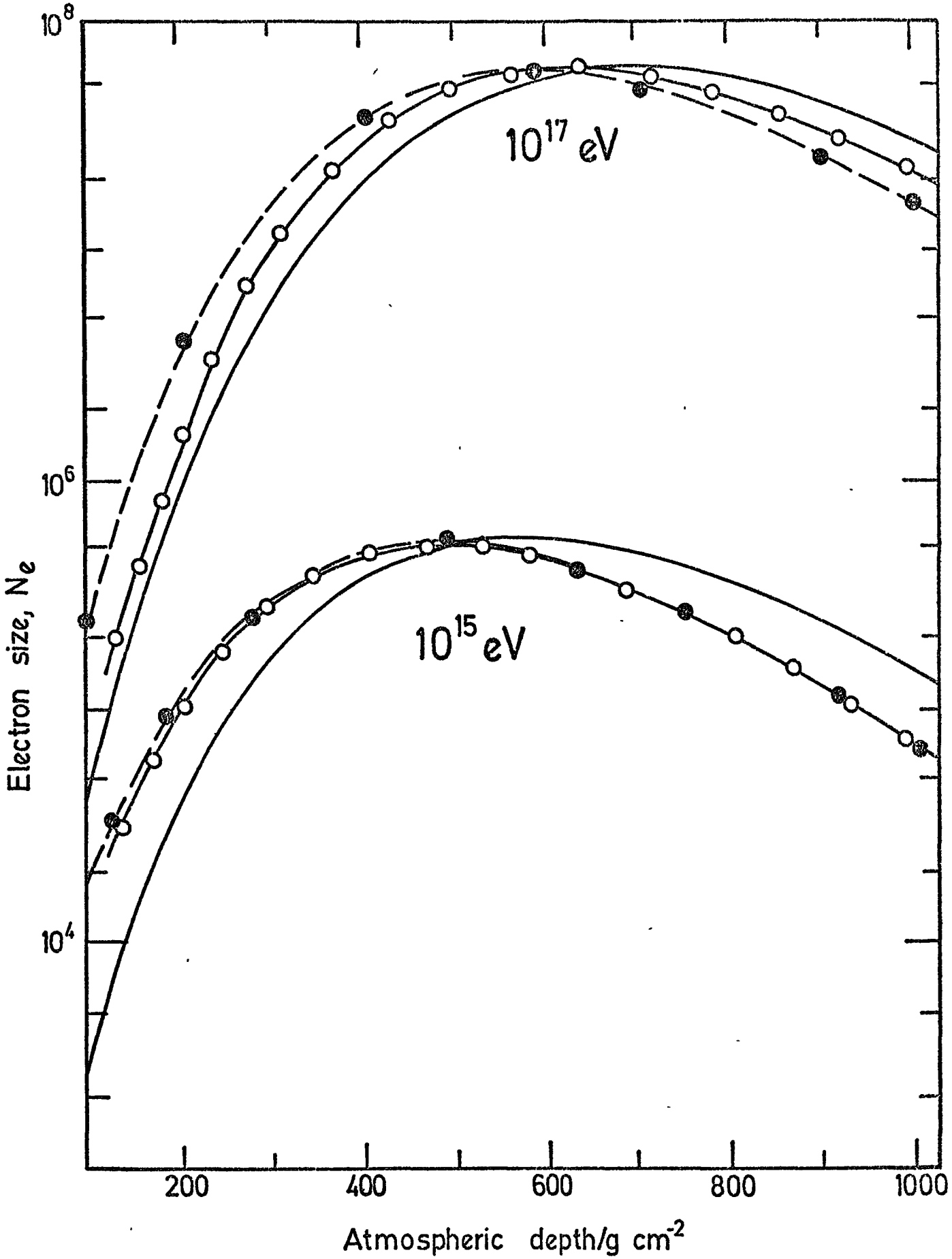

FIGURE 2.5 The average longitudinal development of the electron cascade in vertical showers initiated by primaries of energy 10^{15} eV and 10^{17} eV/nucleus. Models for the fragmentation of heavy nuclei are the partial fragmentation model based upon measurements made in emulsion and the superposition principle. ——, proton; O, iron nucleus (partial fragmentation); ●, iron nucleus (superposition model). (After Dixon et al. 1974 (b)).

cascade at 10^{15}eV but it has some effect on the muon component.

2.4.1.3 The Age Parameter

The age parameter is a quantity that characterises the stage of development of an air shower. For s less than one the shower is 'young' and is capable of further development. For s greater than one the shower is 'old' and its size is decreasing and for s equal to one the shower is at its maximum development whilst for s greater than two the particles remaining in the shower have become less than one. Nishimura and Kamata, (1950), in their treatment of the longitudinal development of an air shower define s to be the solution of

$$\lambda_1'(s)t + \ln\left(\frac{E_o}{E_c}\right) + \ln\left(\frac{\epsilon_c r}{E_s r_1}\right) \approx 0$$

where t is the atmospheric depth in radiation lengths, E_o the primary electron energy, ϵ_c the critical electron energy (84 MeV), E_s is 21 MeV and $\lambda_1'(s)$ given by

$$\lambda_1'(s) \approx \frac{1}{2}\left(1 - \frac{3}{s}\right)$$

(Greisen, 1956). This equation gives s to be a function of the radial distance from the core and can be replaced by

$$s \approx 3t/(t + 2\ln(E_o/\epsilon_c) + 2\ln(r/r_1))$$

Theoretical predictions of the age parameter using the standard model of de Beer et al., by Karakula (1968) for various shower sizes, are given in figure 2.6. The variation appears to be larger than that observed experimentally by Vernov et al. (1970) whose observed values are shown. Monte Carlo simulations of showers by Dixon and Turver (1974) show a decrease in the age parameter with increasing shower size but the increase of Vernov et al. could be interpreted as arising from a flatter distribution function than that given by equations 2.1. and 2.2. It is found, however, that the structure function is flatter at large radial distances from the core and steeper at smaller radial distances. Since large showers are measured at

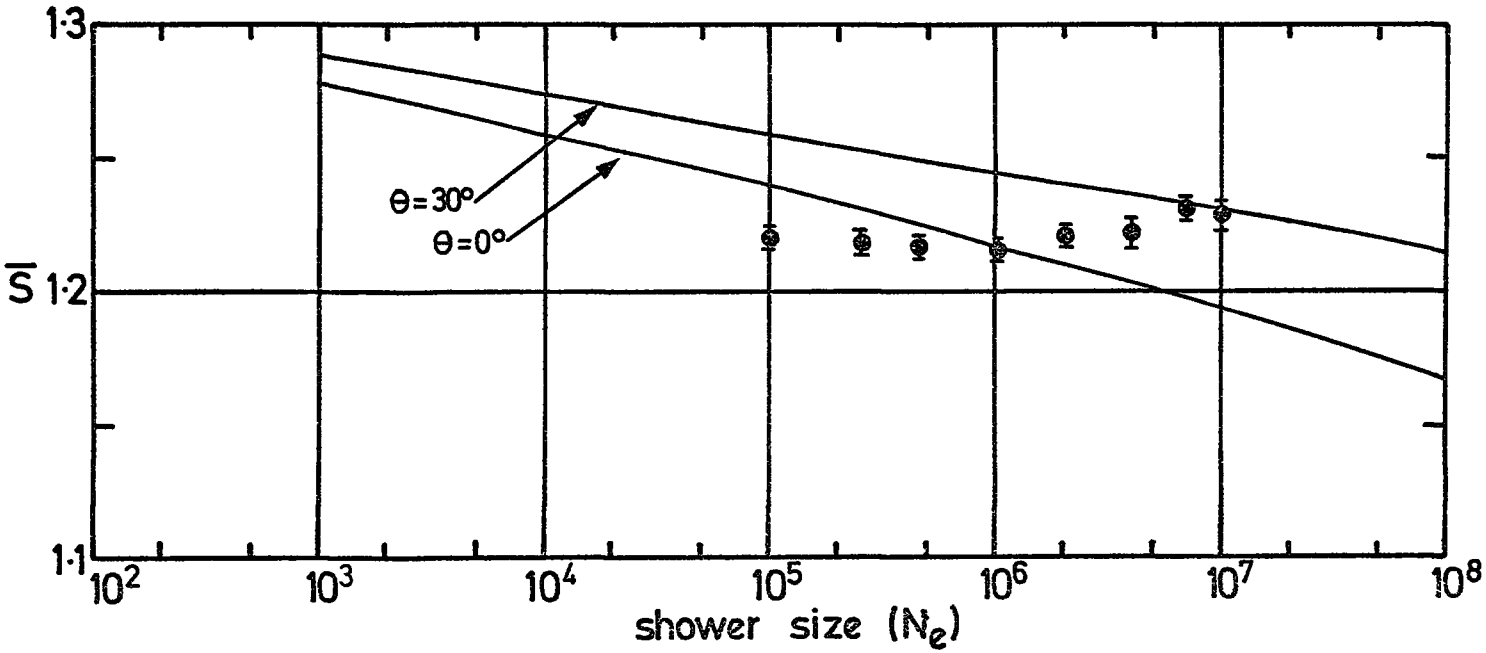

Figure: 2·6. The age parameter as a function of electron shower size. The experimental points are from Vernov et al. (1970).

generally larger radial distances, the age parameter should be larger than average. This is indeed found to be the case: the average age parameter at small ($\lesssim$20m) distances being about 1.15. The observation of the near constancy of the age parameter suggests a high degree of equilibrium between regeneration by the nuclear active component of the electromagnetic cascade and its absorption in the atmosphere.

The effect of the age parameter on the structure of a shower is illustrated in figure 2.7, after Galbraith (1958).

2.4.1.4 Fluctuations in Air Showers

Fluctuations in air shower parameters are linked with primary mass and can be obtained only if there is a large proportion of protons in the primary beam. Possible sources of fluctuations in proton initiated showers are the depths of the first interaction in the atmosphere of the nucleons and the variation in the coefficient of inelasticity in each interaction. Variations in the distribution of number (multiplicity) and energy of the secondaries may also give rise to fluctuations in shower development. The amount of fluctuation expected for the age parameter in proton initiated showers, at ground level, is about 4% - 8% and depends upon the model of the nuclear physics employed to deduce this value. The fluctuations expected for heavier nuclei should be negligible because it is generally assumed that a heavy nucleus initiated shower may be considered as a superposition of several smaller showers, thus averaging out any strong variation in individual cascades.

Simulation studies by Ueda and Ogita (1957) suggest the depth of the first interaction of the primary nucleon with an air 'nucleus' as a dominant parameter in a shower's development and the simulation studies of Dixon and Turver (1974) between the depth of the first interaction, shower size at sea level and depth of shower maximum are shown in figure 2.8 for an E_p of 10^{15}eV proton initiated shower. These data indicate that a large degree of variation does exist in the observed shower size

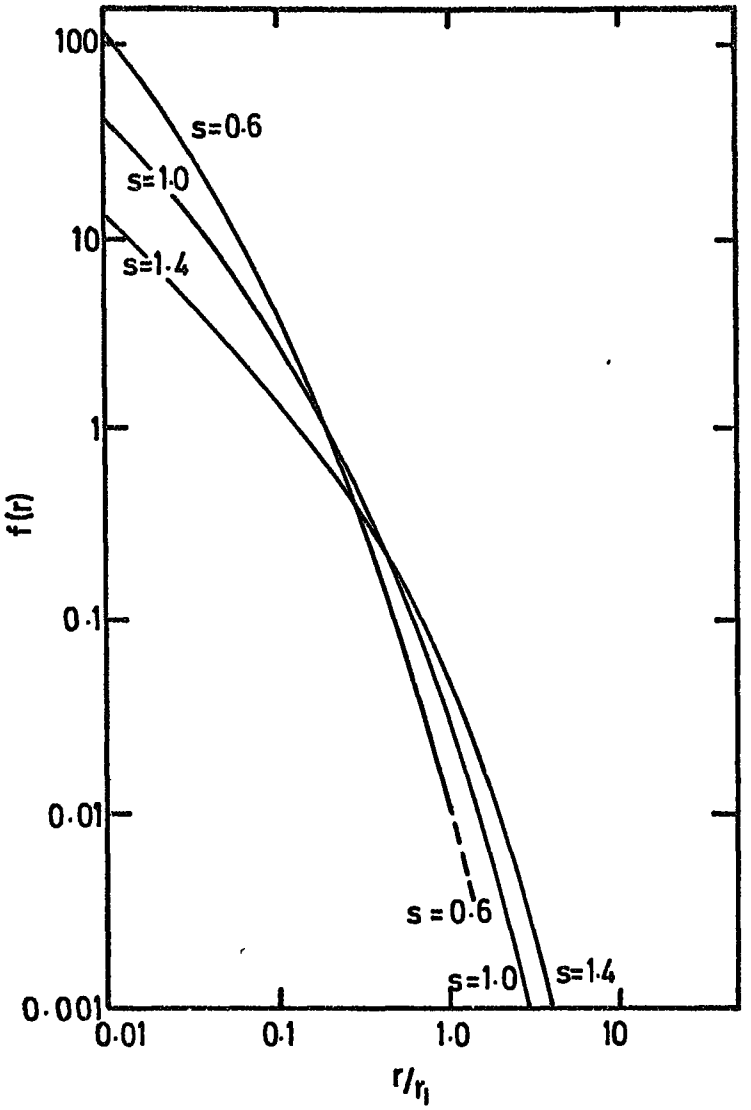

Figure 2·7. The lateral distribution of electrons about the axis of an air shower. (After Galbraith, 1958).

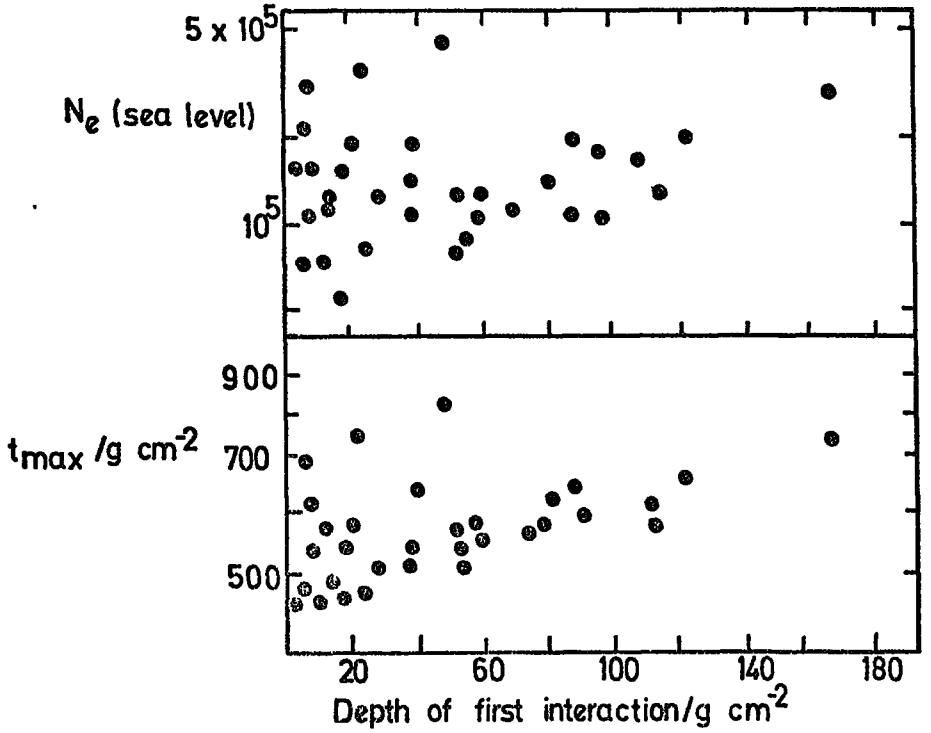

Figure 2·8. The correlations of electron size and depth of cascade maximum with the depth of initial interaction for vertical showers initiated by primary protons of energy 10^{15} eV. (After Dixon & Turver 1974)

from a primary of fixed energy. Observations of fluctuations in shower size by Vernov et al. (1968a)of 5% - 6% in the age parameter can be taken as a strong indication of a predominantly protonic flux at about 10^{15}eV. Greater variations in the age parameter determined by scintillation counters is probably due to fluctuations in scintillator response. Fluctuations in other air shower parameters have been treated in detail by means of computer simulations by Dixon and Turver (1974) to which the reader is referred.

Another useful parameter, sensitive to the primary mass composition, is the ratio of the central electron density to the total number of particles in the shower. This is due to the rough proportionality of the central electron density to the energy per nucleon whereas the shower size is indicative of the energy per nucleus. The results of Samorski et al. (1971) are in agreement with predominantly protonic primaries.

2.4.2 The Muon Component

Muons carry rather more precise data relating to a shower than do electrons. This is because of their relatively weak interactions and also because they represent the directions of emission of their parent particle. Thus, studies of the lateral distributions of muons yield valuable information on their parents' transverse momenta and longitudinal development of air showers. The lateral and energy distributions of muons in air showers as a whole are connected with the characteristics of the nuclear interactions at these high energies. In general, measurements of the muon number spectrum at ground level enables one to calculate a rather more accurate primary spectrum. This follows from the long shower attenuation length of muons in the atmosphere. Detection of the muon component is much more difficult than that of the electrons because of their much reduced density. The construction of large and well shielded detectors is required which tend to be much more expensive due to their large area and large amount of absorbing material. Muons in extensive air showers provide, in general, less detailed information than do unassociated muons. Magnetic spectrographs

are capable of extracting good quality data on individual muons but suffer from their high cost and small area and thus are unable to give a complete picture of muons in air showers. Their use in air shower experiments does, however, yield data relevant to the nuclear interactions in which π-mesons are produced.

2.4.2.1 The Lateral Distribution of Muons

A quantity that is much more readily obtained than the total muon number is the density of muons above a particular energy threshold at various radial distances from the shower core. Early work on the detailed form of the muon lateral distribution function was done by Clark et al. (1958) in which muons with energies greater than 1.2 GeV in showers, whose size was in the range 2.10^5 to 2.10^8, were studied. Their experimental data was reduced by Greisen (1960) to the form

$$\rho_\mu(N,r) = 18\left(\frac{N}{10^6}\right)^{0.75} r^{-0.75}\left(1+\frac{r}{320}\right)^{-2.5} \qquad (2.7)$$

where $\rho_\mu(N,r)$ is the density of muons per square metre falling at a core distance r metres in a shower of size N. Investigations of the variation in structure with energy threshold by the Cornell group (Bennett et al., 1962) give the relation

$$\rho_\mu(N,r,>E_\mu) = 14.4\left(\frac{N}{10^6}\right)^{0.75} r^{-0.75}\left(1+\frac{r}{320}\right)\left(\frac{51}{E_\mu+50}\right)\left(\frac{3}{E_\mu+2}\right)^{0.14r^{0.37}} \qquad (2.8)$$

in which E_μ is in GeV and for which the equation holds valid in the range 1 GeV - 10 GeV. Subsequent measurements of the lateral density of muons in this low energy (< 10GeV) region do not show any marked deviation from these equations for r approximately greater than 20 metres. Typical data are summarised in figure 2.9. The solid curve is equation 2.8 and the data have been normalised to a shower size of 2.10^7 particles. From data such as these it may be said that no serious deviation from this relation is observed. The flattening of the observed data at small radial distances has been ascribed partly to errors in the shower core location (Wdowczyk, 1973).

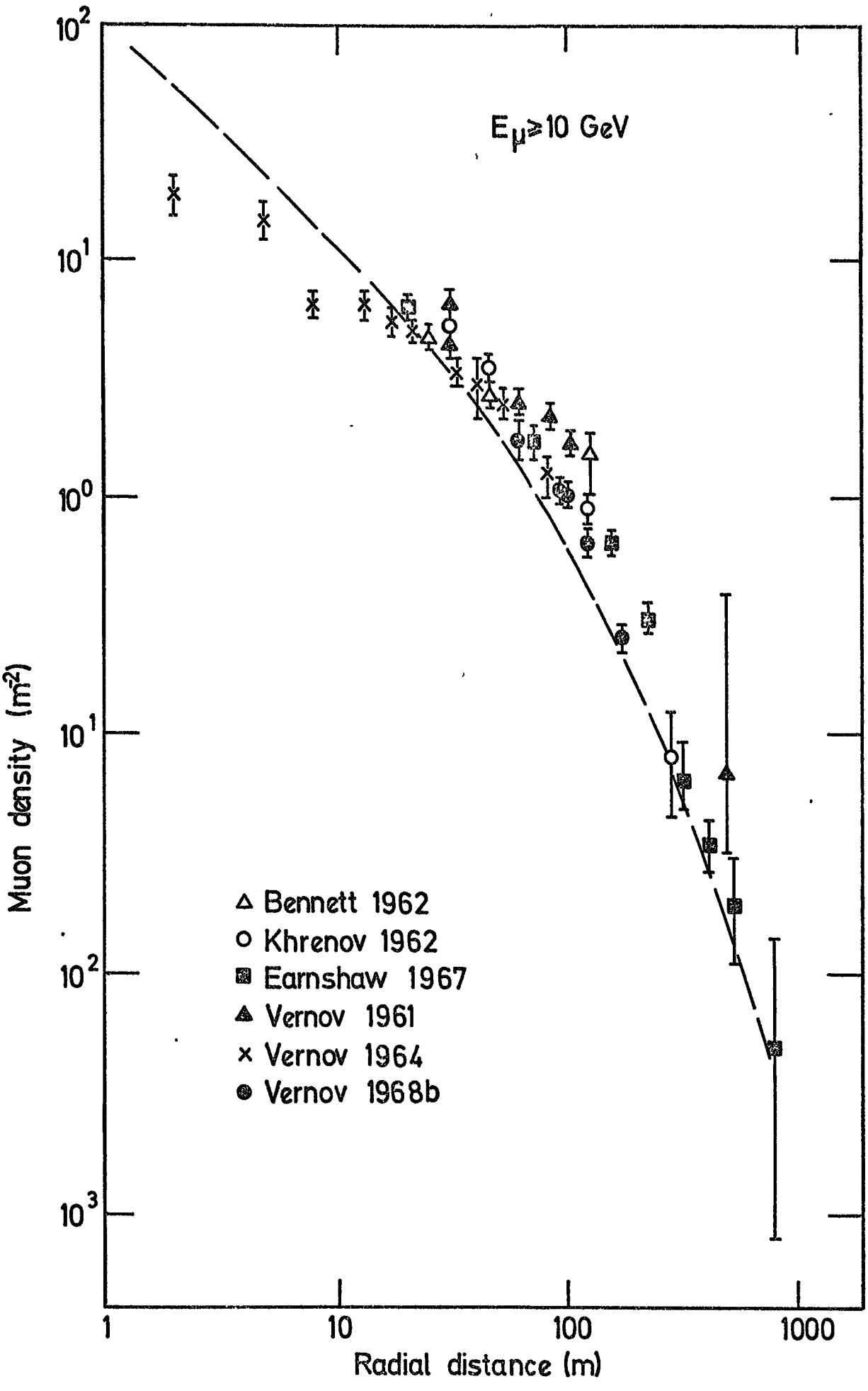

Figure 2.9. The muon lateral distribution for a 10 GeV energy threshold. Data are normalised to 2.10^7. (After Wdowczyk, 1973).

Murthy et al. (1968) have compared the predicted lateral distribution for $E_\mu > 1$ GeV and a shower size of 3.10^7 particles with equation 2.8, using a number of different models, for core distances between 1 m and 1000 m. In all cases it is found that the models predict steeper distribution functions than have been observed. Computer simulations of the muon density show a steepening also as both the muon energy and radial distance increase. A comparison between the observed muon lateral distributions and theoretical predictions, based on the standard model, show that the model predicts narrower distributions than are observed. Wider distributions would require larger pion transverse momenta or the production of muons higher up in the atmosphere. Interpretation of the lateral distribution suggests, then, that its width relates to the transverse momenta of the particles, the height of origin and the multiplicities in the first interactions, all of which are crucial parameters in interpreting the development of the air shower.

2.4.2.2 The Total Number of Muons

Integration of the lateral muon density over r gives the total number of muons, N_μ, with energies exceeding E_μ in a shower of size N. This number, N_μ, is approximately proportional to the number of electrons N_e raised to the power $\frac{3}{4}$. This proportionality is found to hold over a relatively wide range and the index is not very sensitive to the muon energy threshold. That there is a slight variation of the index with energy may be explained by the deviation of muon number from proportionality to primary energies but it is small for all threshold energies.

2.4.2.3 Fluctuations in the Muon Component

It is well established that muon parameters fluctuate by much smaller amounts than do the corresponding electron parameters although similar trends are present. Studies of the fluctuations of the muon number to the electron number, in particular the ratio of the width of the size fluctuations against size have been investigated by many groups; for example

Gawin et al. (1968), Hasegawa et al. (1962), Vernov et al. (1968a) and Pidcock (1967) and comparison with the expected distributions based on the de Beer standard model show good agreement. The observed greater degree of the fluctuations in the corresponding electron/muon ratio are mainly caused by the greater fluctuations in the total electron number.

2.4.2.4 High Energy Muons

There exists much contemporary interest in high energy muons - from the point of view of their energy spectrum and charge ratio-in deducing characteristics of high energy interactions. High energy muons come directly from the initial interactions and because of their weakly interacting nature are easily observed. By studying the muons' parameters a picture of the processes of muon production and hence nuclear physics may be deduced. The sea level muon spectrum is related to the primary cosmic ray spectrum via the nuclear interactions in the atmosphere. The muons are produced, in general, as a result of the decay of π's and K's. From the point of view of interpretation of muon phenomena one starts with the diffusion equations that govern π- and μ- spectra and develop these according to the assumptions and approximations that may be considered appropriate. A complete review of the general method of solution of those equations has been given by Fowler and Wolfendale (1961). A recent review of high energy muons has been given by Thompson (1973).

2.4.3 The Nuclear Active Component

The role of the nuclear active component is in the development and sustenance of an air shower. It is this component that, in terms of energy dominates the shower and is responsible for creating the mesons and other

strongly interacting particles that will rejuvenate the muon and electron fractions (figure 2.1). The hadrons are far less numerous than other shower particles and are really only distinguished from electrons by their large energies.

A sensitive parameter to the assumed model of high energy interactions is the total number and energy spectrum of hadrons in a shower of fixed primary energy (Greider, 1973) and which may be deduced from the lateral distribution of hadrons. The lateral distribution has been measured by a number of authors for various energies and shower sizes and at various altitudes. For showers within the electron size range of 4.10^4 to 4.10^6 particles at sea level, Kameda et al. (1965) gives the differential lateral density distribution as:

$$\rho(E,r,N)\ dEdr = 0.35N^{0.35}E^{-1.2}e^{-r/r_o}\ dEdr$$

where $$r_o = 2.4N^{0.32}\ E^{-0.25}$$

and N and E are measured in units of 10^5 particles and 100 GeV respectively. Results from other groups are shown in figure 2.10 and correspond to shower sizes between $\sim 10^5$ and $\sim 3 10^6$ particles. Calculations of the hadronic energy spectrum based on the predictions of the de Beer (1966) standard model agree well with the observed data if allowance is made for a small increase in the mean transverse momentum from 0.4 GeV/c to 0.6GeV/c. The transverse momenta of hadrons in nuclear interactions is one of the most directly observed quantities that can be obtained from the study of hadrons in showers. From observations of multicore structure in air showers (Dake et al., 1971) it was concluded that there existed, in the nuclear active component particles with transverse momenta of about 10 GeV/c. However, these conclusions are doubtful since there is inconsistency between similar experiments (Miyake et al.,1970, Samorski et al., 1971). Recent work by Aseikin et al. (1975a)suggest an increasing transverse momenta with energies above 100 TeV.

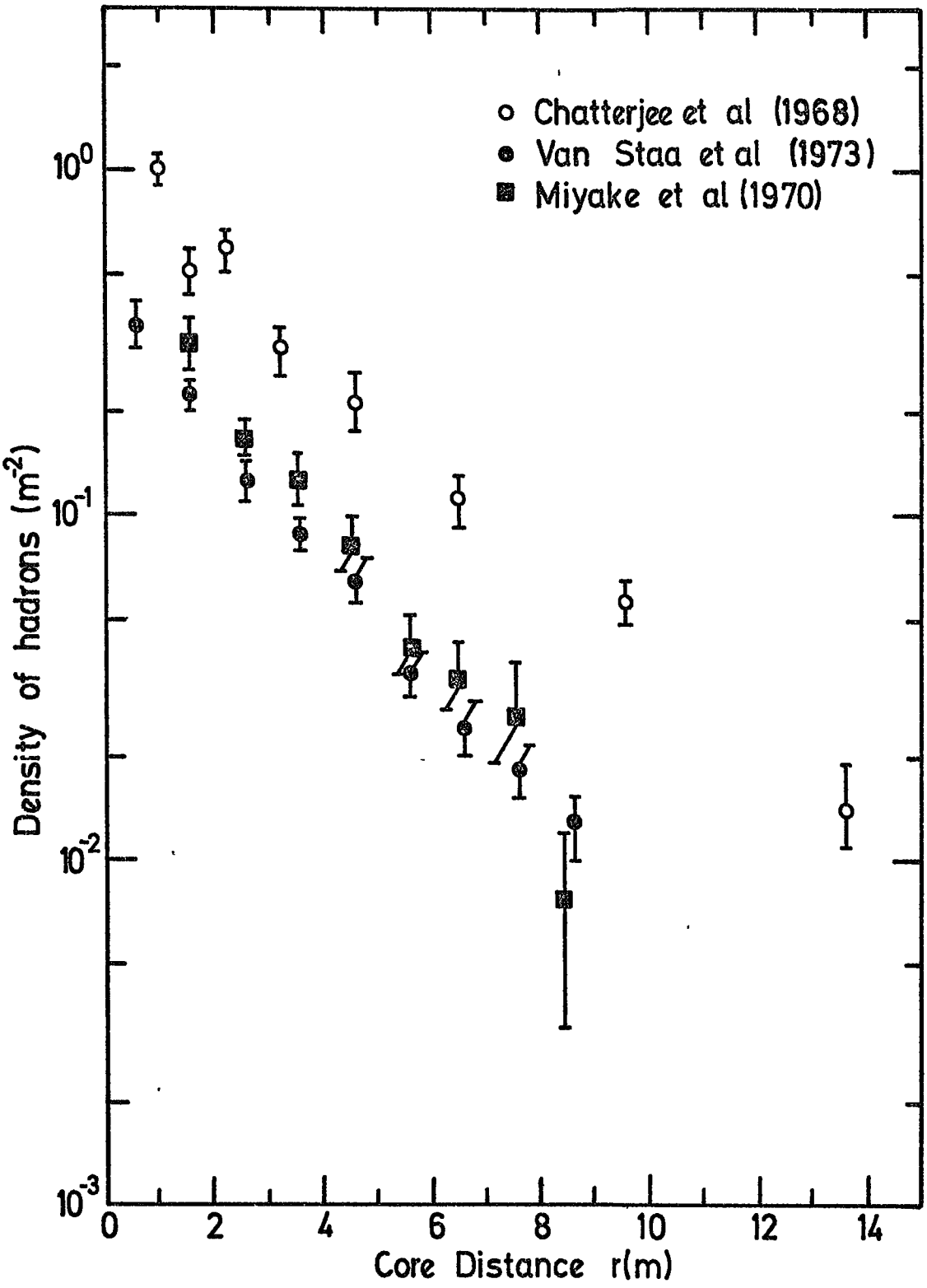

Figure 2.10. The lateral distribution of hadrons in air showers. (See Table 2.2.)

Table 2.2

References for the data used in figure 2.10

Reference	Energy Threshold of hadrons (GeV)	Range of shower size	Altitude of observation (gcm^{-2})
Chatterjee et al. (1968)	200	$1.8.10^5$ -$3.2.10^5$	800
Miyake et al. (1970)	200	3.10^5 - 10^6	550
Van Staa et al. (1973)	200	$1.3.10^5$ - $3.2.10^6$	730

2.5 Cerenkov Radiation in Air Showers

Following the pioneer work of Galbraith and Jelley (1953) into Cerenkov radiation from air showers, there has been much activity into its experimental and theoretical aspects in the hope of using the effect to detect very large ($>10^{17}$eV)air showers (Protheroe, 1975). Arrays, constructed from simple Cerenkov detecting elements, could be made relatively cheaply and extremely large with possible detecting areas of 1000 km^2 since wide separations of the detectors would be possible. An array of 1000 km^2 could detect about 10 air shower events with energies exceeding 5 x 10^{19} eV per year and thus would improve the bleak statistics in this energy region by a considerable degree. It has been suggested by Efimov et al. (1973) that the Cerenkov pulse shape can be directly related to the shower development as a consequence of the delaying effect of the air on the produced light and the temporal spread of the electron shower disc. This would enable data from extensive air showers at various stages of their development, from observations at one level, to be accumulated. Experimental results from Bosia et al. (1972) have shown that structure to the Cerenkov pulse, if observed with nano-second sensitivity can show up multiple cores in showers whilst Orford et al. (1975) have taken this idea further to extract other parameters as shower front curvature and core distance.

CHAPTER THREE

THE AIR SHOWER EXPERIMENT

3.1 Introduction

We have seen in Chapter 2 how a primary cosmic ray, incident upon the upper layers of the earth's atmosphere, creates the seed of an air shower and with the multiplicative properties of the atmosphere amplifies the primary event into a cascade of many types of particle that may be observed covering a large area at observation level. Because of the very nature of the air shower being spread over many square metres the detecting elements of an air shower array must be spread over a similar area. The energy of the primary particle dictates the size of the shower both in the number of particles and the area of its shower front. Consequently, the size of an air shower array will limit the maximum shower size that can be successfully analysed.

The general design of an air shower array takes the form of several particle detectors spaced at intervals over a large area: each detector being able to measure the flux of particles that pass through it and by some means convert this flux into a quantity that is capable of being stored or recorded and subsequently used in the analysis of the air shower event. To determine when an air shower event has occurred, and therefore initiate a data storage sequence of operations, depends upon the experiment but as a rule a combination of detectors in a coincidence mode furnish this signal.

3.2 The Ground Parameters

Prior to the design of the Durham array account was taken of what parameters were to be measured by it. Essentially these are the shower electron size, the shower core location and the direction of arrival of the shower front. Quantities such as multiple cores and shower front radius of curvature could not be measured easily because of experimental difficulties which will be described in later sections. In order to determine these

former quantities the parameters to measure are the electron density at each detector and the relative times between detectors when the shower front passes through them. Thus, with these basic data the shower size, direction of arrival and point of impact of the shower core can be calculated; the accuracy of which depends upon the accuracy in measuring the observed quantities.

3.3 Air Shower Arrays

There have been a great many air shower arrays built in the last twenty years, many of which have operated in the shower range of 10^3 to 10^7 particles, yet there still exists a great deal of uncertainty about the detailed shape of the shower size spectrum. Only a few large arrays have been built (Haverah Park, Volcano Ranch, Sydney and Tokyo - Turver, (1973)) which have contributed to the identification of large air showers initiated by primaries of the highest energies. Table 3.1 summarises the pertinent features of important arrays that have recently been reported or are still in operation. No attempt has been made to make the table exhaustive. Major differences between arrays are those of their detecting elements and in their geometries. Figure 3.1 illustrates the geometries of several arrays in Table 3.1 from which it is seen that a large variation exists.

3.4 The Durham Air Shower Array

Preliminary work on the Durham Array began in January, 1973 when calculations were performed in order to deduce the most suitable geometry and detector locations. It was found that the detector sites did not severely effect the response of the array to showers of various sizes and, after some consideration; the most suitable sites on which to put the detectors suggested an equilateral triangle geometry. Figure 3.2 shows the arrangement that is used at present. It can be seen that use is made of the strong symmetry of the Physics Department roof in providing two arms of the array. In order to maintain a symmetrical arrangement extra detectors

Table 3.1

Air Shower Arrays recently reported

Array	Atmospheric depth (g cm^{-2})	Detectors	~Area (m^2)	~E_p range	Reference
Agaziz	1040	P.S.	10^5	3.10^{15} - 3.10^{18}	Turver, 1973
Chacaltaya	540	P.S.	2.10^5	8.10^{14} - 3.10^{17}	Kaneko et al. P.I.C.C.R.(1971), 7,2720
El Alto	630	P.S.	4.10^5	8.10^{14} - 3.10^{17}	Turver, 1973
Haverah Park	1016	W.C.	$1.2.10^7$	2.10^{17} - 5.10^{19}	Andrews et al. P.I.C.C.R.(1971),3,995
INS (Tokyo)	1020	P.S., S.C.	6.10^3	2.10^{13} - 10^{16}	Kawaguchi et al. (1975) P.I.C.C.R.,8,28
Kiel	1030	P.S., C.C.	$5.6.10^3$	2.10^{13} - 10^{16}	Bagge et al.(1965) P.I.C.C.R.,2, 738
K.G.F.	920	P.S., W.C.	$3.2.10^4$	10^{14} - 10^{17}	Chatterjee et al.(1965) P.I.C.C.R.,2,62
Lodz	1020	P.S., G.M.	10^3	10^{14} - 10^{16}	Firowski et al(1973) P.I.C.C.R.,4, 2605
Moscow	1020	P.S., G.M., I.C.	3.10^2	10^{14} - 10^{16}	Grigorov et al.(1965) P.I.C.C.R.,2,649
Mt. Norikura	738	P.S., S.C.	$2.4.10^4$	10^{14} - 10^{17}	Kino et al. (1975) P.I.C.C.R.,8, 2837
Ooty	800	P.S., C.C., L.S.	3.10^3	2.10^{13} - 10^{16}	Chatterjee et al.(1965),P.I.C.C.R., 2, 802
Osaka	750	P.S., W.C.	8.10^3	10^{14} - 10^{16}	Miyake et al. (1965),P.I.C.C.R.,2,762
Pic du Midi	700	P.S., G.M.	2.10^3	10^{13} - 10^{15}	Van Staa et al. (1973),P.I.C.C.R.,4,267
Sydney (i)	1016	L.S., S.C.	8.10^2	c.10^{15}	Bray et al.(1965),P.I.C.C.R.,2,685
Sydney (ii)	1016	P.S., G.M.	4.10^7	10^{17} - 10^{20}	Wilson et al.(1971),P.I.C.C.R.,3,1025
Tien Shan	680	P.S., I.C.	3.10^4	10^{14} - 10^{16}	Aseikin et al.(1975),P.I.C.C.R.,8,2726
Tokyo	1020	P.S., S.C.	10^6	10^{17} - 10^{19}	Kawaguchi et al.(1973),P.I.C.C.R.,4,256
Verrieres	1020	P.S., G.M.	$1.2.10^3$	2.10^{14} - 10^{15}	Catz et al.,(1971),P.I.C.C.R., 3,1035
Volcano Ranch	820	P.S.	$1.2.10^6$	10^{16} - 5.10^{18}	Turver, 1973
Yakutsk	1020	P.S., G.M.	$3.3.10^6$	10^{17} - 10^{19}	Egorov et al. (1971), P.I.C.C.R.,6,2059

P.S. Plastic Scintillator W.C. Water Cerenkov G.M. Geiger-Mueller L.S. Liquid Scintillator
S.C. Spark Chamber I.C. Ionisation Calorimeter C.C. Cloud Chamber

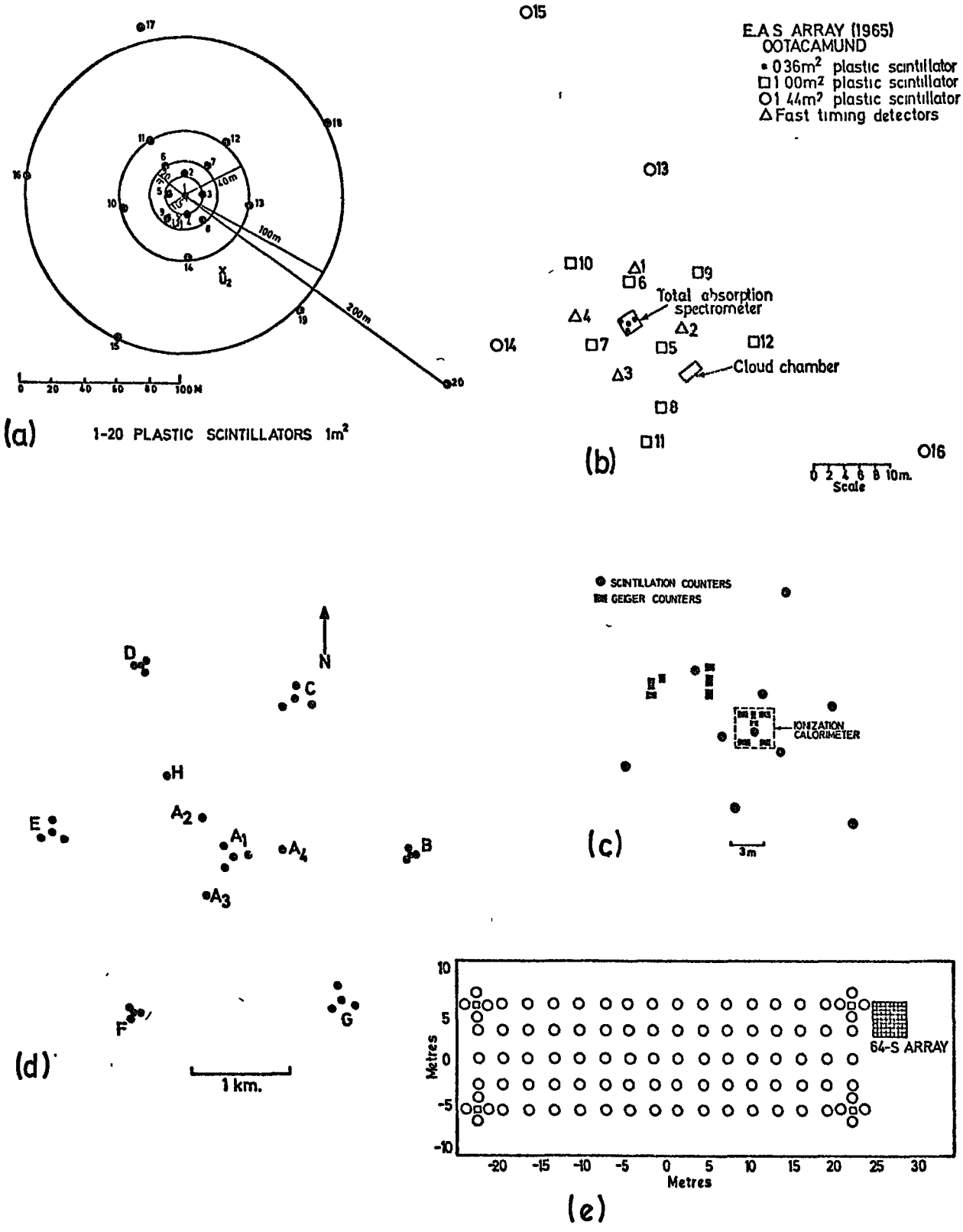

Figure 3·1 The geometries of five air shower arrays listed in Table 3·1.
(a) Kolar Gold Fields, (b) Ootacamund (Ooty),
(c) Moscow (1965), (d) Haverah Park,
(e) Sydney (i).

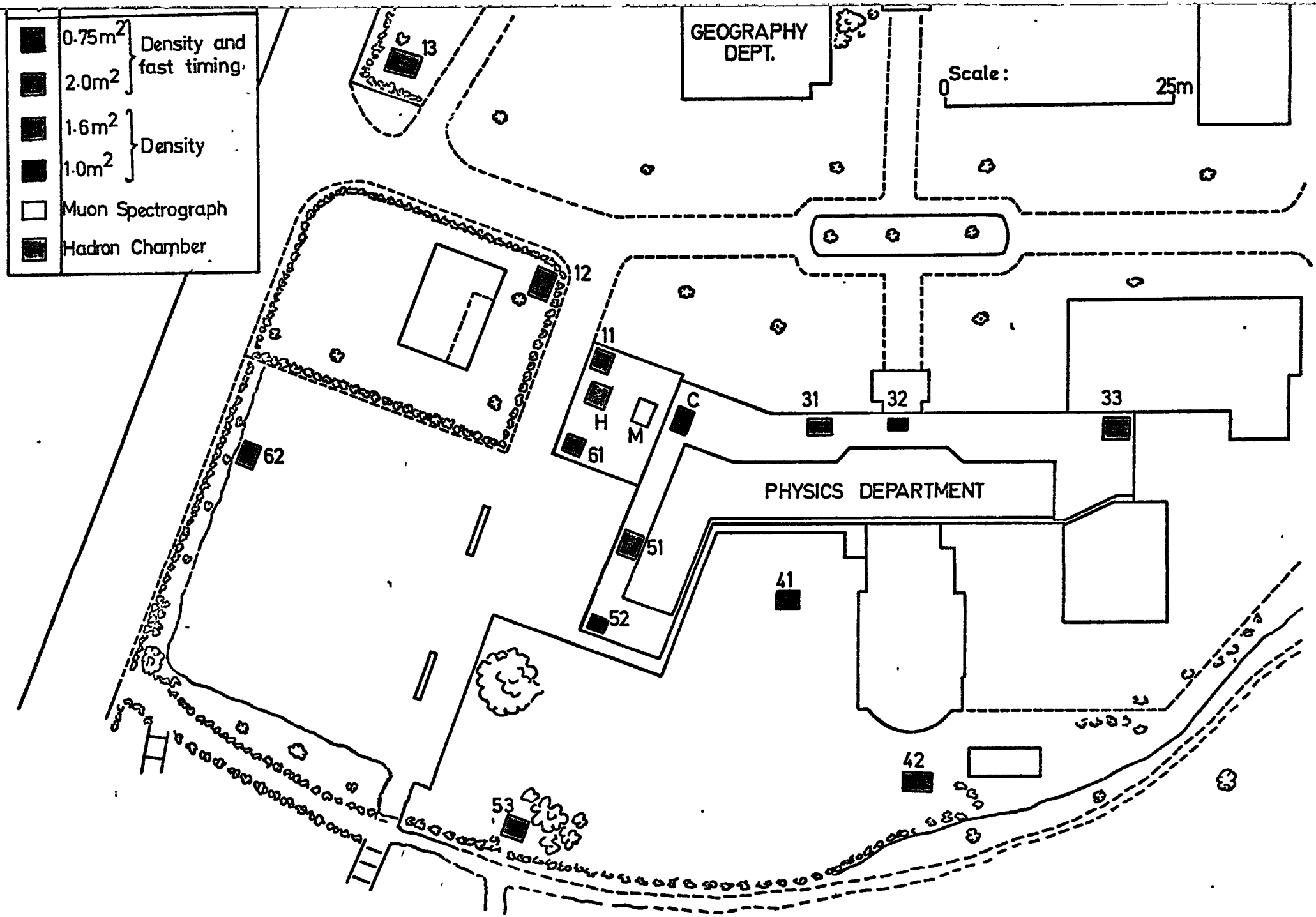

Figure: 3·2. The Durham Extensive Air Shower Automated Research Array.

were located in positions that made a hexagonal geometry in which similar types of detectors in similar positions should behave in similar ways.

All of the array detectors in figure 3.2 are plastic scintillators. There are fourteen in all. Each detector is viewed by a number of photomultiplier tubes to record the particle density and, in addition to these, on seven of the detectors is a photomultiplier tube that is used in measuring the time of arrival of an air shower front. Four sizes of scintillator are used, mainly because of their availability in the laboratory, but the $2m^2$ scintillators were specially manufactured for the array by Nuclear Enterprises of Edinburgh. Of all these detectors the central and $2m^2$ detectors are the most important. This is because they furnish the fast timing as well as density measurements. The central detector is also used to define the spatial and temporal origin of the array.

The presence of walls and buildings near to some of the detectors naturally restricts the zenith angle acceptance for showers that will be accepted for final analysis. However, all showers collected are analysed but only those whose cores fall within the array and whose zenith angles are less than 30° will be used to produce final spectra. In the near future up to ten 0.3 m^2 liquid scintillators will be located within the array to improve the accuracy of the estimation of the showers' parameters whose axes fall within it.

3.4.1 The Response of the Durham Array

In order to understand and interpret the results produced by any experiment it is necessary to know how it responds to the phenomena being observed for without this knowledge the results will be of limited usefulness. One can estimate very simply the expected response of an air shower array if its dimensions and detector areas are known. Figure 3.3 illustrates the method used, taking the simplified structure function of Rozhdestvensky et al. (1975),

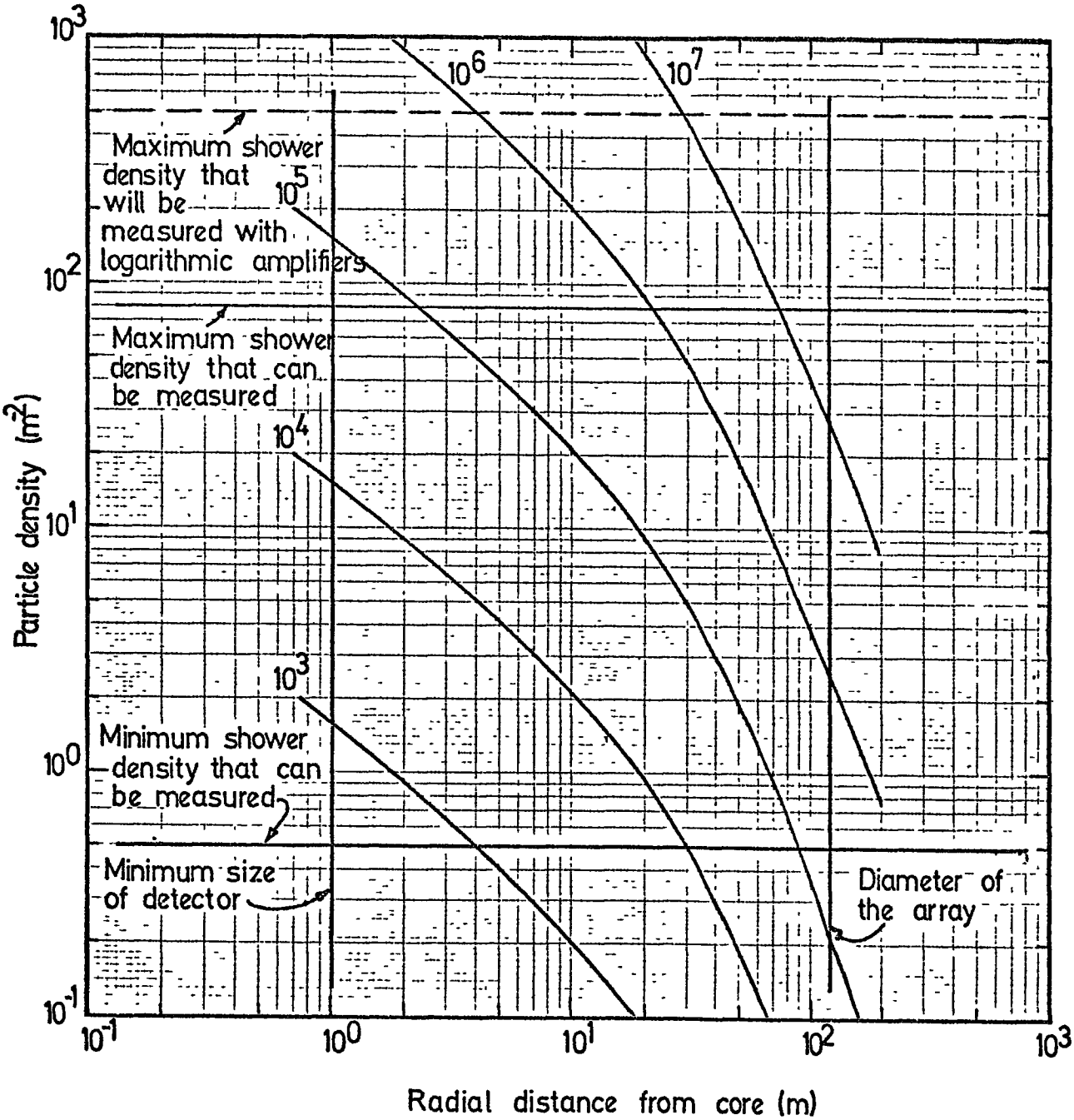

Figure: 3·3. The general response of the air shower array.

$$\rho(N, r) = 2.10^{-3} N \frac{e^{-r/60}}{r}$$

and drawing curves for various shower sizes. In the case of the Durham array the smallest detector is 1m x 1m and thus no information on shower structure is obtainable below 1 metre. The vertical line at 1 metre limits, then, the minimum radial distance to which useful data may be obtained. The diameter of the array is 120 metres and although showers falling outside the array may trigger the experiment they will not be used in the final analyses because of the increased inaccuracy of the showers' parameter measurements. Thus, a vertical line at 120 m provides an upper limit on the maximum radial distance that is useable.

In considering the dynamic range of particle density measurements it is clear that the smallest density that can be measured is one particle in the largest detector. This corresponds to 0.5 m^{-2} for this array since the area of the largest scintillator is 2 m^2. The largest density that can be measured is largely governed by the saturation limit of the particle density measuring electronics and at present this corresponds to 80 particles per square metre. With the introduction of logarithmic amplifiers this upper limit will be increased to over 500 particles per square metre. These four boundaries therefore limit the magnitude of some of the parameters which are measured. In this case the shower size response is about 10^3 to about 10^7 particles and these represent the upper and lower limits of successful shower analysis. By imposing triggering requirements these values will change and result in a smaller area than that defined in figure 3.3.

In a more detailed treatment of the array's response one needs to take into account those parameters that will influence the detection of an event. In particular these are the detectors coordinates (x_i, y_i, z_i), their areas and their efficiencies. Those parameters that are more easily varied, such as the triggering criteria - these are the trigger density threshold and the detector coincidence combination - are allowed to vary

to find the most suitable combination that gives the response that is required. In these calculations only the central and 2 m^2 detectors were considered. This was because these detectors possess the fast timing facility and it is necessary to have an estimation of the shower arrival direction before a full event analysis is possible.

Having decided on the positions of the detectors and their areas, various combinations of triggering criteria and density threshold were selected for investigation. This would lead to a much more thorough understanding of the array's response and capabilities. To do this an electron structure function needs to be assumed and it was taken to be the Greisen (1960) function:

$$\rho(N, r) = \frac{0.4N}{r_1^2}\left(\frac{r_1}{r}\right)^{0.75}\left(\frac{r_1}{r+r_1}\right)^{3.25}\left(1+\frac{r}{11.4r_1}\right) \qquad (2.1)$$

The procedure involved to calculate the air shower array's response was to calculate the array's Effective Collecting Area, A_e. This area represents an area that may be considered as being totally efficient in detecting showers and is naturally shower size dependent. What was done was to simulate the air shower array on a computer and fire showers of a particular size at the array at random zenith and azimuthal angles and random core locations (the random zenith angles were modulated by a $\cos^7\theta$ distribution) within the restrictions of the array acceptance criteria. For each shower, the particle densities, ρ_i , at each of the triggering detectors were calculated from which the detection probability, p_i , for a given particle threshold, m, could be determined. These probabilities, when multiplied together, give the array triggering probability for recording a shower with the same size, core location and arrival direction. By firing in many such showers the average array triggering probability can be deduced and this, multiplied by the geometrical area of the array in which shower axes are accepted, Ag, gives the array effective collecting area, A_e . In effect what is calculated is

$$A_e = \int_o^{A_g} \prod_{i=1}^{j} p_i (X_c, Y_c)\, dA \qquad (3.1)$$

with the product extending over all triggering detectors and with the p_i's being averaged over many (θ,ϕ)at the same (X_c, Y_c). Defining

$$P = \prod_{i=1}^{j} p_i (X_c, Y_c) \qquad (3.2)$$

equation 3.1 can be re-written as

$$\frac{A_e}{A_g} = \frac{\int_o^{A_g} P\,dA}{\int_o^{A_g} dA} = \bar{P}$$

Hence, $A_e = \bar{P} \cdot A_g$. (3.3)

3.4.2 Calculation of the Average Triggering Probability

For detectors with 100% efficiency, p_i may be given by the poissonian probability of a particular density, ρ_i , on a detector of area s_i exceeding a particle threshold of m as

$$p_i (\rho_i s_i, \geq m) = e^{-\rho_i s_i} \sum_{n=m}^{\infty} \frac{(\rho_i s_i)^n}{n!} \qquad (3.4)$$

This is generally true and applicable to geiger tube arrays, but with scintillators the detecting elements tend to have efficiencies that depend both on the number of particles incident on them and on their particle threshold. If the efficiency is defined as $\xi_i(n,m)$, where n is the number of particles and m is the particle threshold, equation 3.4 becomes

$$p_i(\rho_i s_i, \geq m) = e^{-\rho_i s_i} \sum_{n=0}^{\infty} \frac{(\rho_i s_i)^n}{n!} \xi_i(n,m) \qquad (3.5)$$

The function ξ_i is a function of the detecting elements and has to

be determined empirically. Figure 3.4 illustrates what is meant by the efficiency for scintillators. The curves n = 1, 2, 3.... are the scintillator response curves to 1,2,3..... particles incident upon the detector. The vertical line at m indicates a particle threshold and is generally set and adjusted by an electronic disciminator in the laboratory (§ 5.21). The efficiency for two particles on the detector is the ratio of the area under the curve n = 2 to the right of the vertical line to the total area beneath the curve. Similarly for n = 3,4,5..... it is seen that the efficiency quickly approaches unity in this case. For 100% efficient detectors the efficiency function is a step function with the efficiency becoming unity at m.

Scintillator response curves cannot be produced easily for greater than about two particles. This is because of experimental difficulties, especially in the extended acquiring times, with many particle telescopes (§ 4.7), due to the low cosmic ray flux of multiparticle events. To overcome this problem multiparticle spectra can be derived from a single particle's response by folding it upon itself as many times as one requires. Thus, a two particle spectrum is obtained by folding a single particle's with itself and normalising the area beneath the curve to be equal to that beneath the single particle's. A three particle distribution may then be obtained as a result of folding a two particle distribution with a one particle spectrum, and so on. In this way many multiple particle distributions can be deduced and the efficiency for detecting n particles with a detector threshold of m can be quickly obtained. Briefly, to produce an empirical single particle distribution for a detector, a telescope technique is usually preferred in which the response of the entire detector is included. This technique suffers from the disadvantage that the particle distribution thus obtained corresponds to a distribution of ≥ 1 particles and so to create a pure single particle spectrum the multiple particle spectra must be removed from it. Calculations based on the density spectrum of Hayakawa (1969) gave a contamination of

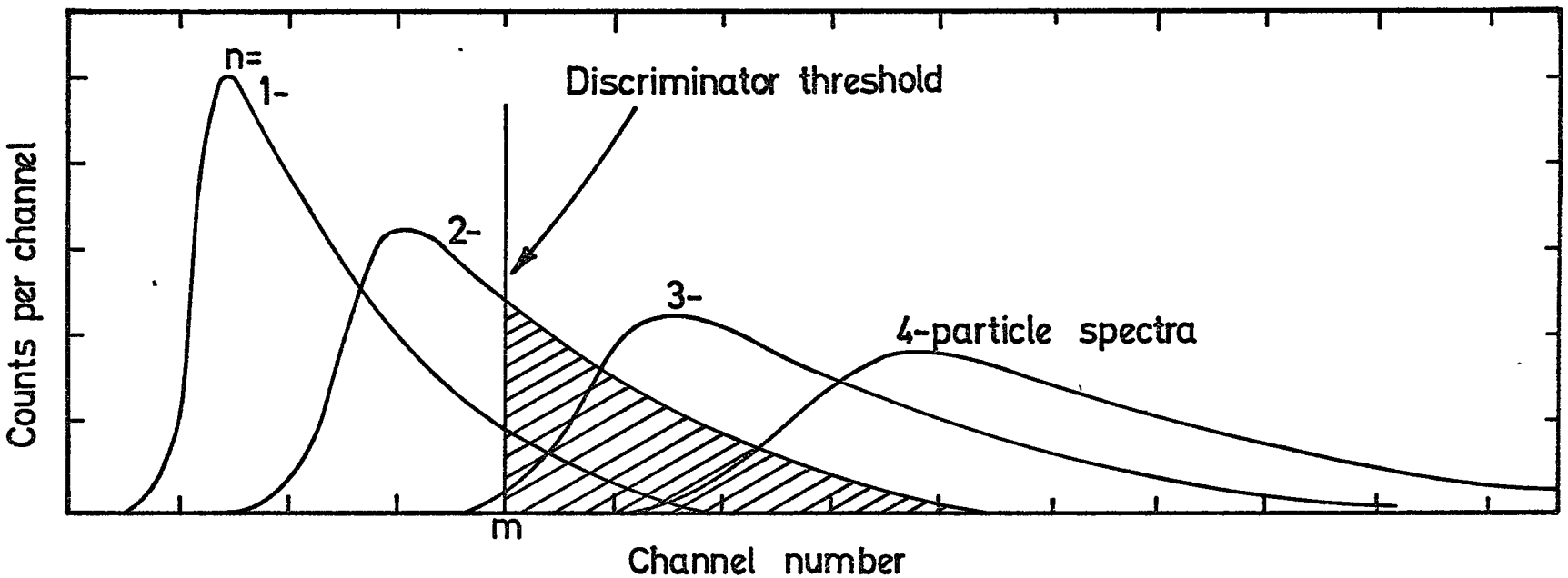

Figure 3.4. Schematic of the method used in calculating the detector efficiencies.

~3 % for ≥ 2 particles in the ≥ 1 particle distribution as experimentally observed. This is a small contribution but could introduce significant error in the production of multi-particle spectra if it were not removed. Starting with the ≥ 1 distribution, which in itself is a good approximation to a pure 'one', a better approximation can be obtained by folding the ≥ 1 with itself and then normalising the area beneath the new distribution to be 3% of the original and subtracting this from the ≥ 1 . It was with this almost pure single particle distribution that the efficiency terms were calculated.

Using equations 3.2, 3.3 and 3.5 the array effective collecting area as a function of N was calculated. As would be expected as the shower size increases so does A_e until a shower size where A_e is equal to A_g. For the Durham array this corresponds to a shower size of about 10^6 particles. Figure 3.5(a) illustrates how $A_e\Omega$ varies for several triggering criteria and figure 3.5(b) shows, for comparison, the effect of calculating $A_e\Omega$ with and without efficient detectors; here Ω is the array solid angle.

3.5 The Response of External Devices and the Array in a coincidence mode.

It is the case with some experiments that there is the need to investigate associated events with showers. This imposes additional restrictions and limitations on the response of the array as determined above. What needs to be done in calculating the response of the combined experiment is to fold the external devices differential shower response (as a probability) into the array response for whatever selection criterion is in operation at that time. Thus, if $\overline{P}_e$ is the triggering probability of the external experiment for a shower of size N then the array and external experiment effective collecting area will be:

$$A_e = \overline{P}_{array} \cdot \overline{P}_e \cdot A_g$$

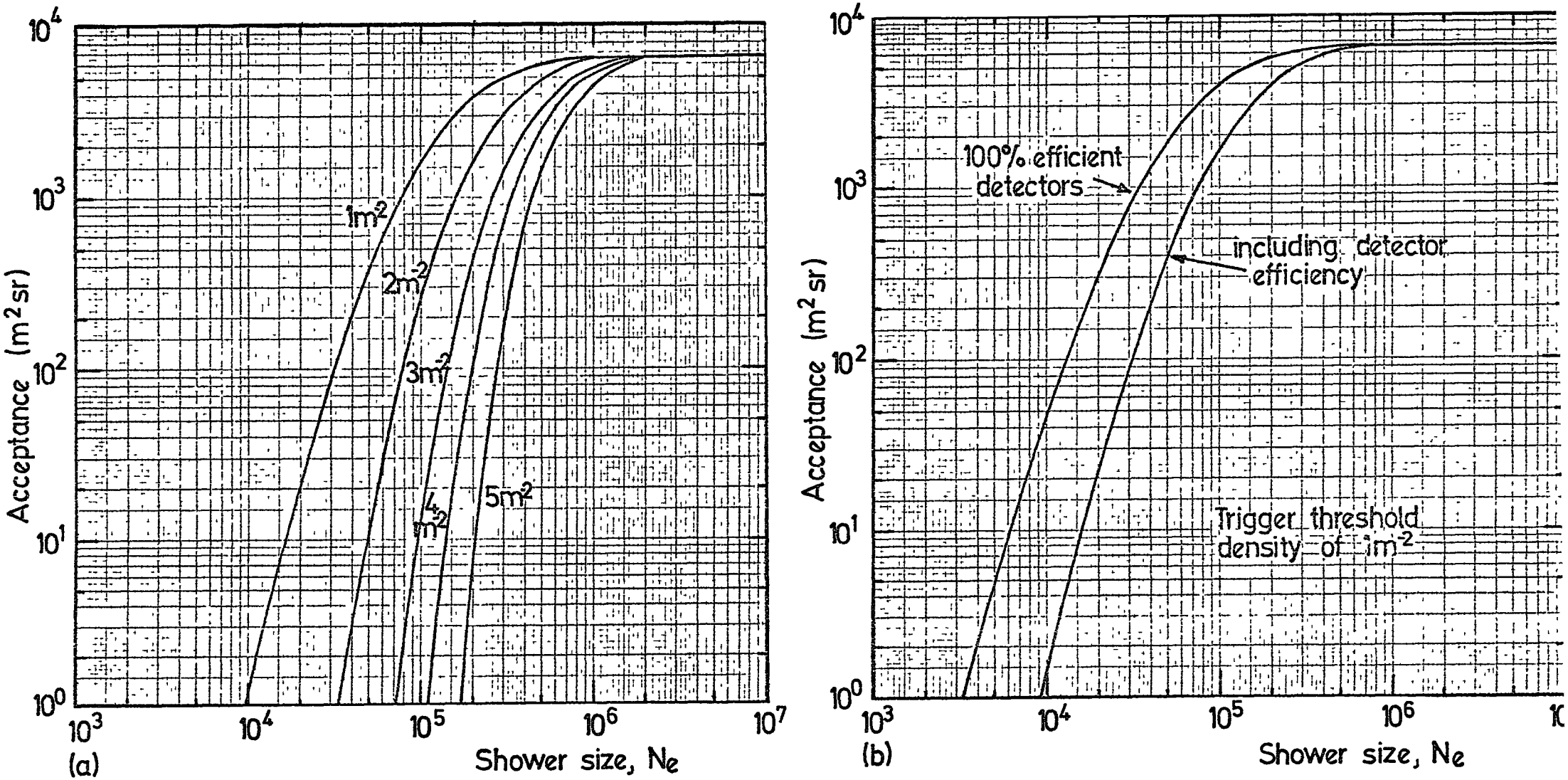

Figure 3·5. The acceptance of the air shower array, to showers falling within a radius of 50m of the central detector and with $\theta \leq 30°$, for a C+13+33+53 coincidence. (a) with detector efficiencies included, (b) comparison with 100% efficient detectors. Ω is 0·8418 sr. in these figures.

It is a feature of this array that it can be externally triggered when the other experiment registers an event. In this case the triggering probability of the array is unity in the above expression for A_e since triggering by this method does not require the array to have satisfied its own trigger requirement.

3.5.1 The Rate of High Energy Muons in Air Showers

Using the external trigger without satisfying the array event acceptance criteria is useful if the external device triggers frequently on events associated with very small ($\sim 10^4$) showers since the array response to those showers of less than this size for certain trigger requirements is small. It is not recommended to trigger in this way for rare shower associated events since many useless showers' data will be stored. This is the case for high energy associated muon events which are much rarer than either unassociated muons or unassociated shower events. For these associated events the array and muon detector must be in a coincidence mode in order to reduce or eliminate useless data from being stored. With this in mind, calculations on the expected rates of high energy muons in showers were performed considering the muon spectrograph, M.A.R.S., already in existence in the laboratory.

3.6 The Muon Automated Research Spectrograph (M.A.R.S.)

M.A.R.S. has been described in detail elsewhere (Ayre, 1971; Whalley, 1974) and so only a brief description of the experiment and those features relevant to the calculation of associated muon rates will be discussed.

The spectrograph (M.A.R.S.) built and in operation in the Cosmic Ray Laboratory in Durham was constructed to study the momentum spectrum and charge ratio of muons in the vertical direction and has been providing data since 1971. Its design enables the spectrum to be obtained up to and in excess of 5000 GeV/c and allows data to be collected and stored automatically on

an on-line I.B.M. 1130. The form of this instrument is shown in figure 3.6. It can be seen to consist of four magnet blocks, in which a field of approximately 16 kG is present. Between each of the blocks are scintillation counters and trays of neon flash tubes which are used to detect the particles travelling through the spectrograph and to determine their trajectory. The spectrograph has a minimum detectable momentum of 6.9 GeV/c, a maximum detectable momentum of 5850 GeV/c and an acceptance of 408 cm^2 s_r for muons of infinite momenta through one side of the spectrograph.

3.6.1 The Acceptance of M.A.R.S.

The acceptance of the spectrograph has been defined by Whalley (1974) as "that amount by which the vertical intensity has to be multiplied in order to give the rate of passage of muons through the three scintillation counters." Because of the bending of the particle's trajectory in the magnetic field this acceptance is momentum dependent. The acceptance is also a function of the angles of incidence of the muon striking the spectrograph in both the front (bending) plane and side plane of the spectrograph. Following the method of Whalley (1974), for the infinite momentum case, and representing the scintillation detectors as planes as in figure 3.7(a) the acceptance at infinite momentum may be calculated. Consider the figure in which AB is the trajectory of the muon. The upper plane represents the top scintillator and the lower plane represents the bottom scintillator. For the purpose of calculating the acceptance the problem may be divided into two parts:

(1) the acceptance in the bending plane of the muon's trajectory

(2) the acceptance in the side plane of the muon's trajectory.

The bending plane being defined as the plane in which the trajectory deviates from a straight line due to the magnetic field.

Using the notation described in figure 3.7(b) the acceptance in one

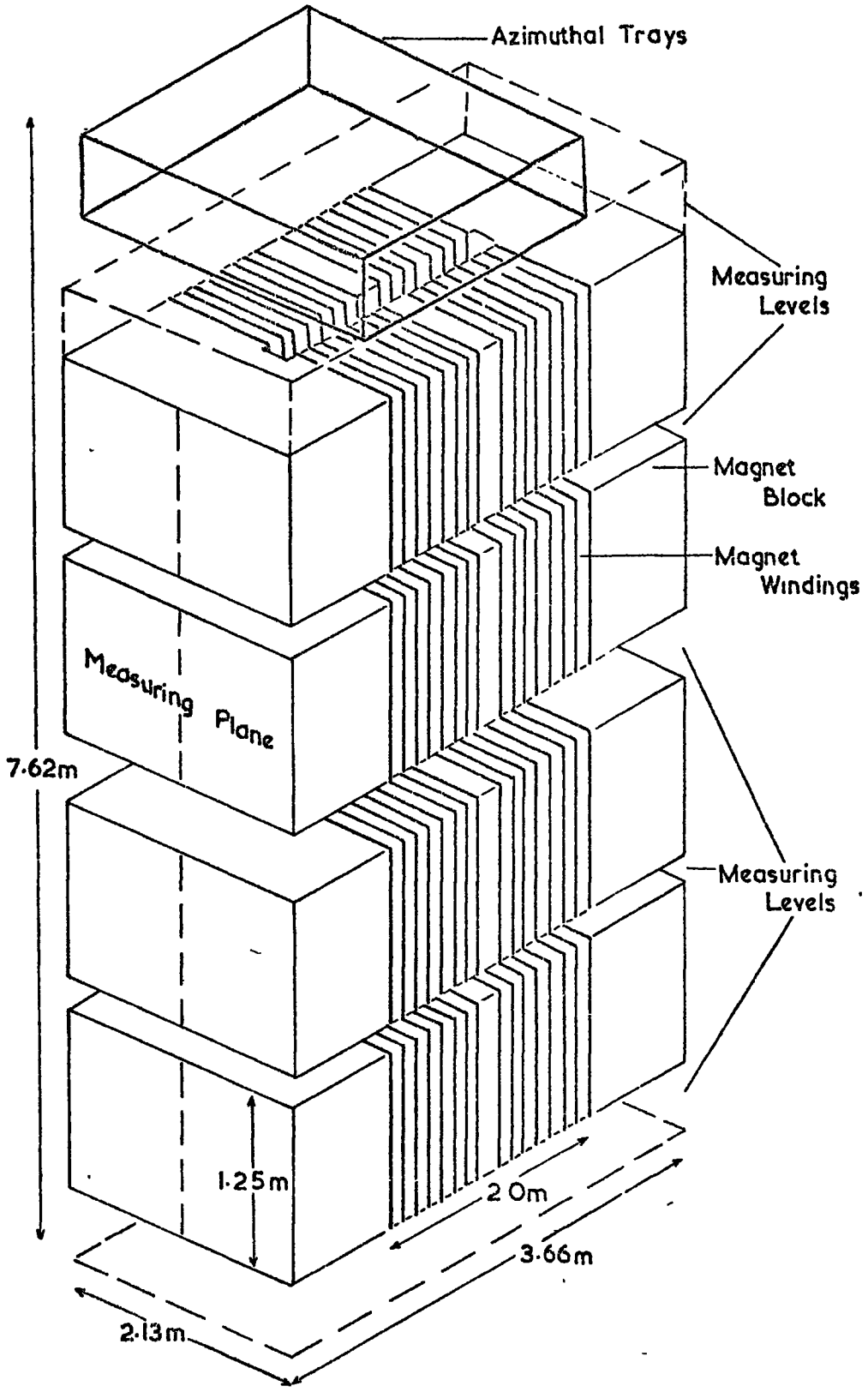

Figure 3·6. The General Features of MARS (after Wells, 1972)

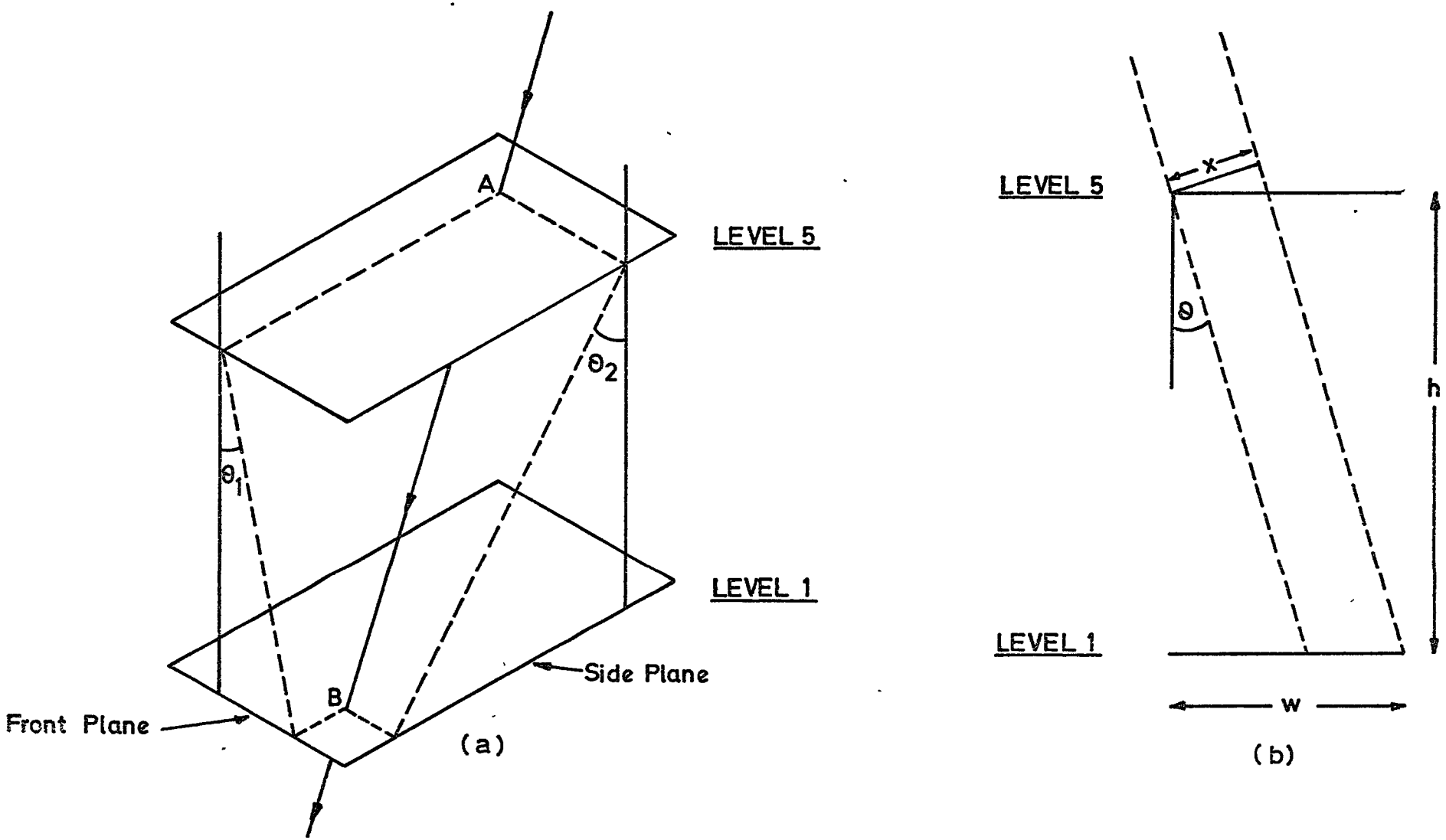

Figure 3.7. Illustrating the notation used in calculating the infinite momentum acceptance. (After Whalley, 1974).

plane is given by

$$A_{cc} = \int_{-\theta_{max}}^{+\theta_{max}} (w\cos\theta - h\sin\theta)\, d\theta$$

where $\theta_{max} = \tan^{-1}\left(\frac{w}{h}\right)$

and represents the maximum angle that a muon may have in order to penetrate the two planes.

Evaluating this integral for both the bending and side planes gives

$$A_{cc}(\infty) = 4\left\{(h^2 + w_1^2)^{\frac{1}{2}} - h\right\} \cdot \left\{(h^2 + w_2^2)^{\frac{1}{2}} - h\right\}$$

Due to the uncertainty in the knowledge of h, resulting from the finite thickness of the scintillators, a small error is present on this acceptance. The acceptance for infinite momenta muons for one side of M.A.R.S. is

$$A_{cc}(\infty) = 408 \pm 2\,cm^2\,sr.$$

The acceptance for other momenta is not as straight forward due to factors such as the trajectory deviation and energy loss. The acceptance for the side plane is uninfluenced by the magnetic field and is thus only a function of incidence angle. The calculation is similar to the above treatment for infinite momentum. In the general case the procedure is to find the acceptance for a given momentum averaged over all possible angles of incidence and to do this one naturally needs the use of computing facilities. Figure 3.8 shows how the acceptance of M.A.R.S. varies for muons in air showers with $P_\mu \geq 10$ GeV/c and shower size N. In this figure the array triggering probability is unity. The muon lateral distribution in air showers was taken to be that due to Greisen (1960) and a "four-tray-acceptance" of the spectrograph was applied since for muon associated events the top measuring flash tube tray probably contains contamination from the electronic component.

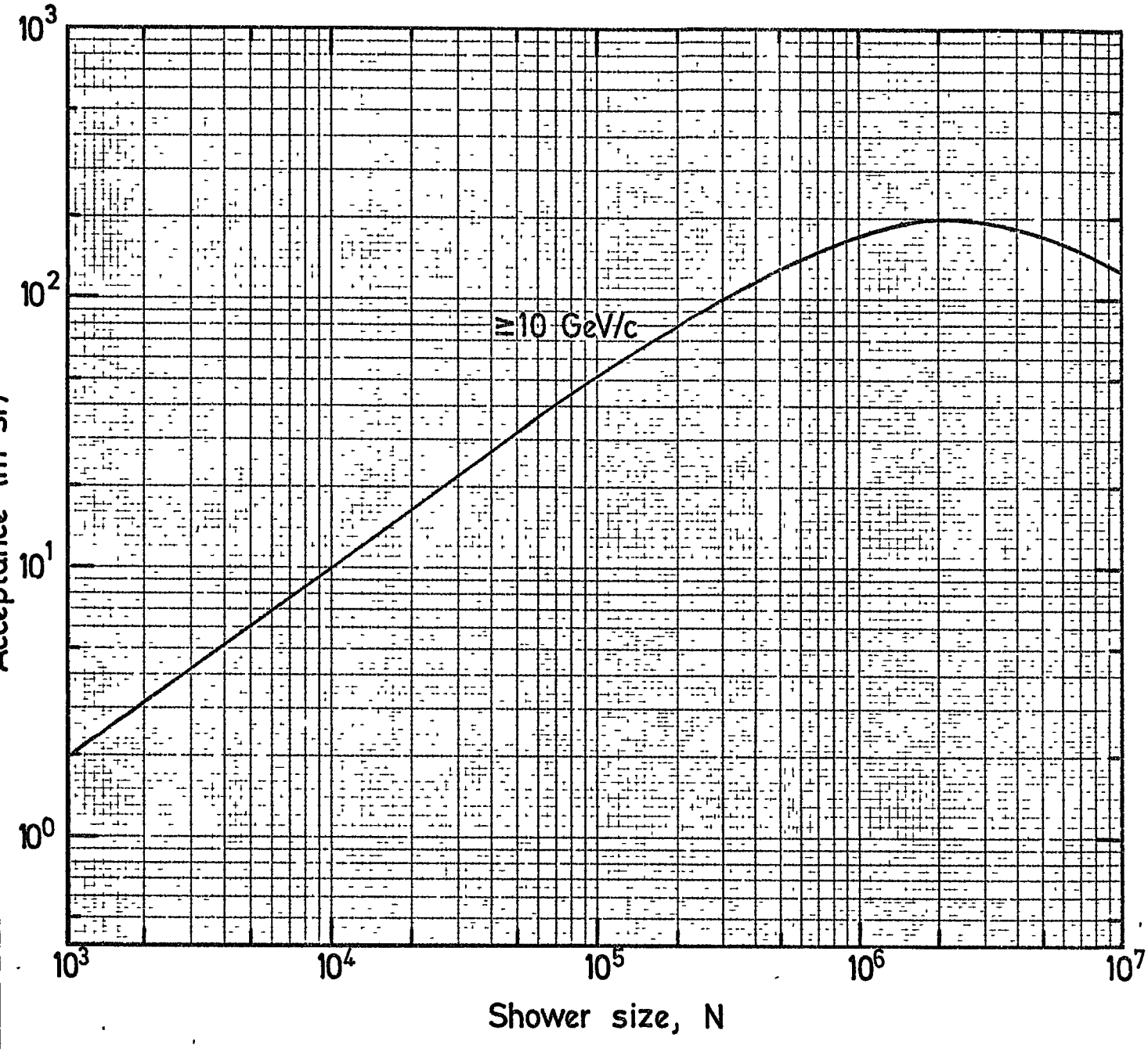

Figure 3.8. The acceptance of M.A.R.S. to single muons in air showers of size N falling on the array within the array acceptance criteria. The array triggering probability is unity.

Calculation of the muon's momenta and sign is a simple process in theory but is non-trivial in practice. In the M.A.R.S. case account must be taken of spuriously flashed tubes, the occurrence of bursts and knock-on electrons which could make the track fitting process less well defined. The M.A.R.S. data analysis takes these factors into account and provides for various fitting options depending upon the quality of the data present. In its basic form the trajectory of a muon traversing the spectrograph is defined by the five measuring trays of flash tubes. These flashed tubes enable a track of a certain curvature to be clearly defined and from this a momentum may be assigned according to

$$p_\mu = Be\, r_\mu$$

where B = 16.3 kG and r_μ is the radius of curvature of the muon's trajectory. The sign of the muon is given by the direction in which the trajectory curves.

All of the M.A.R.S. data is digitised and analysis is carried out on IBM 1130 and IBM 370/168 computers.

3.7 The Hadron Chamber

The second major cosmic ray research programme in the laboratory in Durham is the investigation of hadron phenomena by the use of a chamber of over 11000 flash-tubes. At present this is being used to investigate hadrons in regions of large particle density in cosmic ray air showers. It has been used in the past in the search for quarks in shower cores. Figure 3.9 shows the chamber.

Hitherto the triggering requirement has been to use a local particle density exceeding some preset level on the top of the chamber and this effectively selects showers of greater than a particular size for investigation. Increasing the density discrimination level will increase the mean shower size that is capable of inducing a trigger. Consequently, data have been obtained from this experiment with only limited knowledge of the individual air showers that have caused the events. It is hoped that when the air

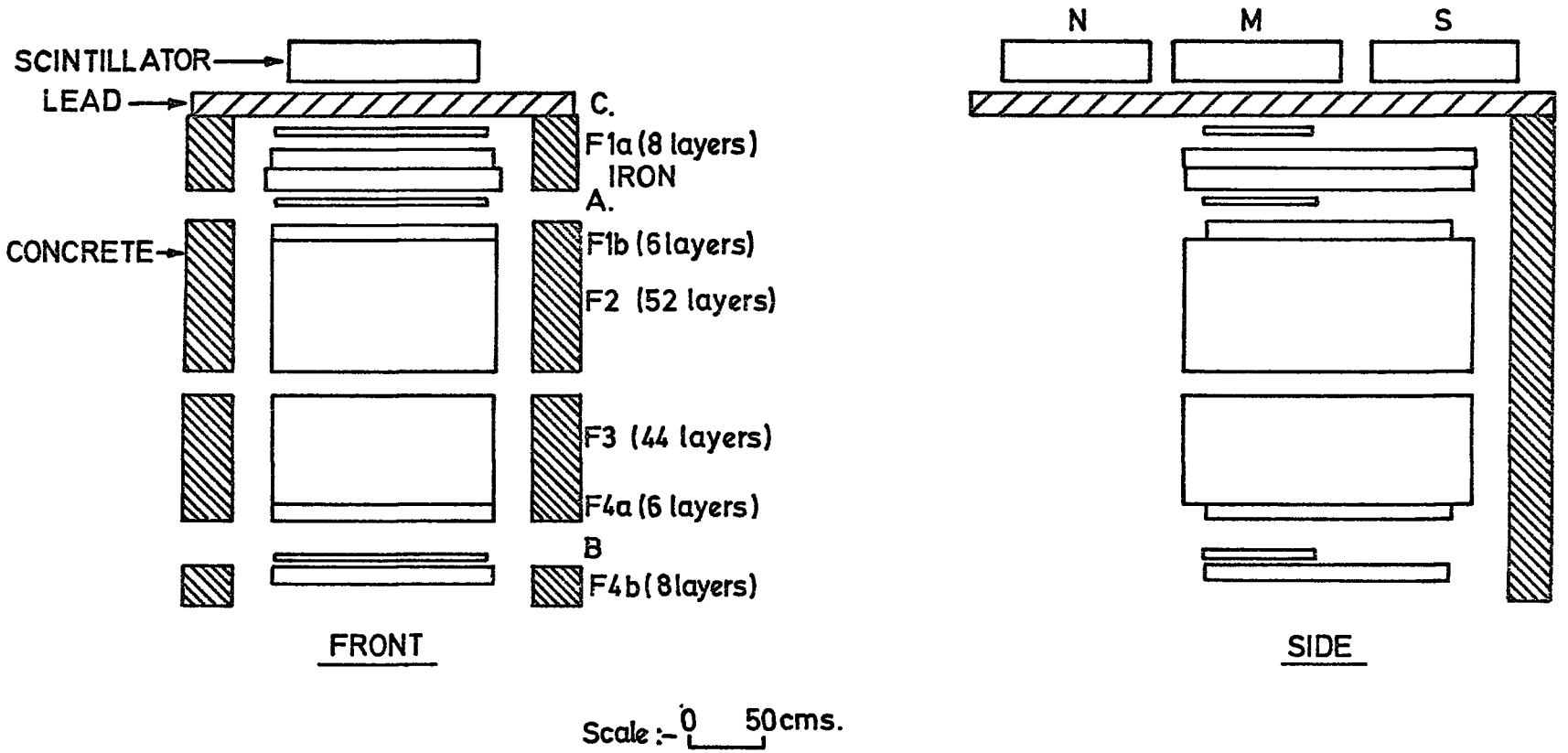

Figure 3·9. Scale diagram of the Flash Tube Chamber. (After Cooper, 1974).

shower array is used with the chamber much more detailed information will be able to be extracted from it.

The data from the hadron chamber are produced on photographic film. When the chamber fires, a camera photographs the flashed tubes and then the camera is wound on to the next frame. After a running time of the order of a day the film is retrieved and developed. This is then scanned by eye for events of interest and then analysed according to the quality of the data. With a system as complex as this chamber digitisation and computer analysis would be extremely difficult since it would be a very complex task trying to quantify the pattern of tubes flashed. A visual scan, although much more subjective, does allow for a greater degree of flexibility in the search for interesting events and because of the low triggering rate (about one per hour) digitisation is not justified. The response of this chamber has been calculated for a local electron density greater than 40 m^{-2} by Cooper (1974) and is shown in figure 3.10.

3.8 Measurable quantities

From what has been seen in the preceding sections it is evident that using the air shower array with these two major experiments a great deal of detailed information may be obtained for each individual air shower event. The muon spectrograph can provide accurate measurements on muon momenta from less than 7 GeV/c to momenta in excess of 5000 GeV/c for vertical muons. From an assembly of the muon data the charge ratio as a function of shower size and momentum can be derived. The hadron chamber is capable of providing more detailed data on the electron, muon and nuclear active particles structure functions for showers than is the case for the air shower array alone. By selecting appropriate trigger criteria for the experiments in combination any one or more of these features may be investigated.

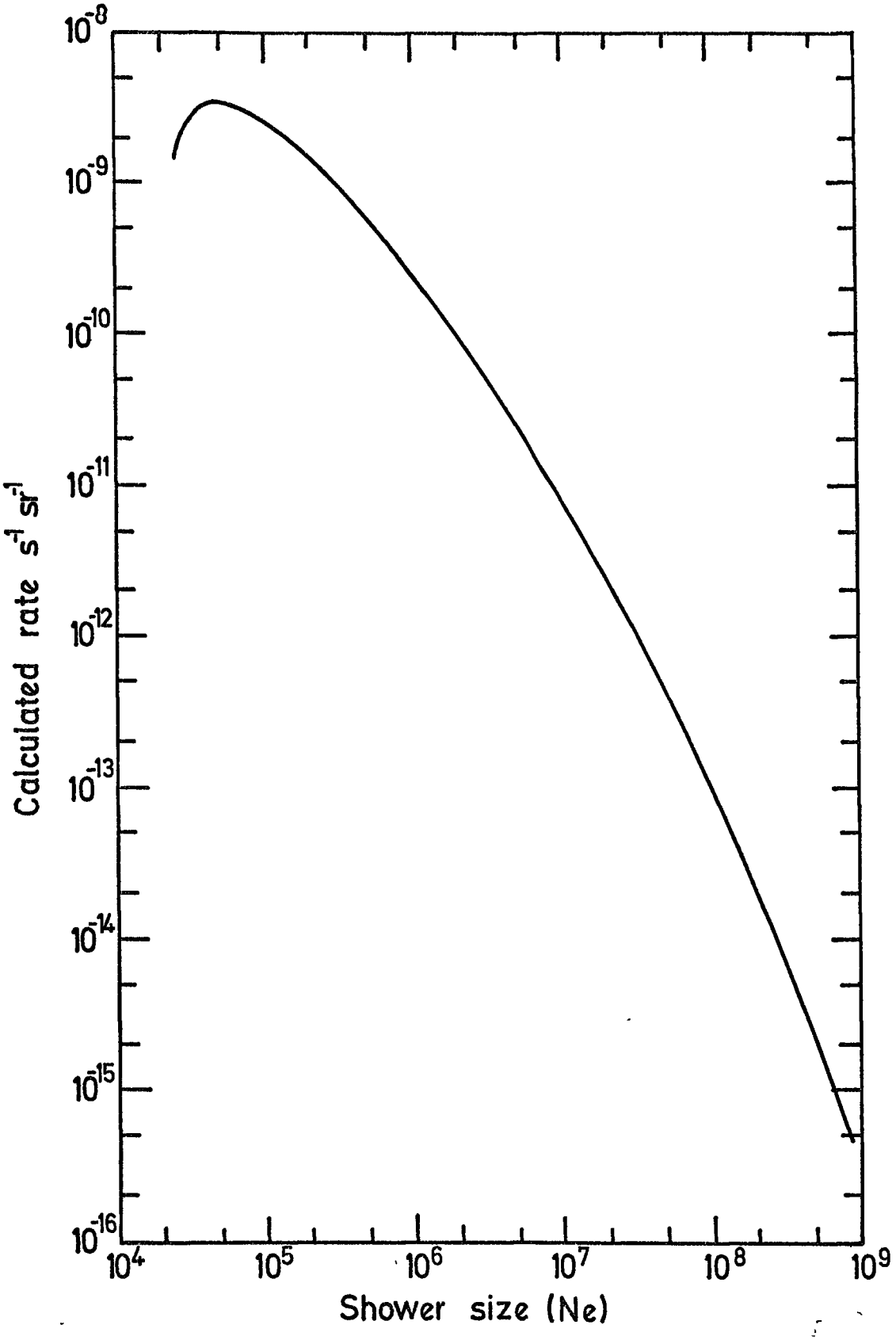

Figure 3.10. The rate of triggers produced at the Flash Tube Chamber by showers of size Ne in which the local electron density at the chamber exceeds 40 m^{-2}. (After Cooper, 1974.)

3.9 Accuracy of Measurement

Accuracy in the measurement of a physical quantity is of prime importance if any detailed understanding is to be gained from the study of it. The accuracy to which the parameters outlined above may be determined vary and are functions of the instruments. In the case of the muon momenta what has usually been done, with many previous spectrographs, is to add the maximum detectable momentum correction in quadrature with the multiple scattering correction to define an error on the momentum δp_μ given as

$$\delta P_\mu = P_\mu \left(c^2 + \left(\frac{P_\mu}{P_{m.d.m}} \right)^2 \right)^{\frac{1}{2}}$$

Here c is the scattering correction of 0.16 and P_{mdm} is the spectrograph's maximum detectable momentum.

An error on the sign of the charge of the muon only begins to be significant for momenta in the region of the m.d.m. of the apparatus. Above this momentum the charge ratio tends to unity. For the purposes of studying muons in extensive air showers this is not an important consideration as associated muons with momenta in excess of 5000 GeV/c would be very rare occurrences. For determining particle densities in air showers the Hadron Chamber is very useful. This is because the individual tracks of the cosmic rays are rendered visible and thus may be easily counted. The knowledge of the extent of the absorber on and in the chamber will give a measure of the energy threshold that the particles must exceed. The chamber projects a three dimensional event on to two dimensions, consequently reducing the amount of extractable information from it, but in some applications this loss is not important. As with many associated air showers it is of prime importance to know the main parameters of the air shower, viz: the core location, size and arrival direction. The errors present on these quantities will be dealt with in detail in Chapters 6 and 7.

3.10 Versatility required for data collection

As one of the built in features of the array was the requirement of

versatility. The electronics have been so designed that the array may trigger, or be triggered by, an external device such that associated events can easily be collected. Because of the existence of several other cosmic ray experiments in the laboratory it became a fundamental factor to enable these and future experiments to be triggered when an air shower event occurs. Conversely, it could be desirable to trigger the array when an event of interest has occurred in another experimental arrangement. This is possible with the present system.

CHAPTER FOUR

THE AIR SHOWER ARRAY AND ITS FEATURES

4.1 Introduction

The detector layout of the Durham Array, established partly by calculation and partly by the availability of detector sites, is shown in figures 3.2 and 4.1. Each of these detectors samples the particle density of an air shower event and relays it to the laboratory. Seven of the detectors give time markers when the shower front passes through them and these, too, are relayed to the laboratory where they are converted into relative time differences and stored. The process of calibrating these detectors and delivering the pulses into the laboratory is necessarily complex and formed a large part of the array preparation and construction. In what follows the methods by means of which the data arrive in the laboratory are discussed. The various kinds of detecting elements are described and how the calibrated pulse height information is presented to the data handling electronics where it is coded and stored.

4.2 The Air Shower detecting elements

Many techniques have been employed in the detection of particles in air showers. Early workers relied on cloud chambers and geiger counters to detect and investigate air showers' properties. In some applications these devices are still used, for example Hazen et al. (1975) use a $3m^2$ cloud chamber in a quark search in the cores of small air showers but geiger counters have, in general, been superseded by different detection devices which are more reliable, electronically easier to handle and capable of providing more detailed information. Neon hodoscopes, spark chambers and scintillation counters have tended to replace the earlier devices as detection techniques become more sophisticated and in the present experiment plastic scintillators are used throughout.

One major problem associated with the use of scintillator material lies in its light attenuation length. This is the characteristic length of

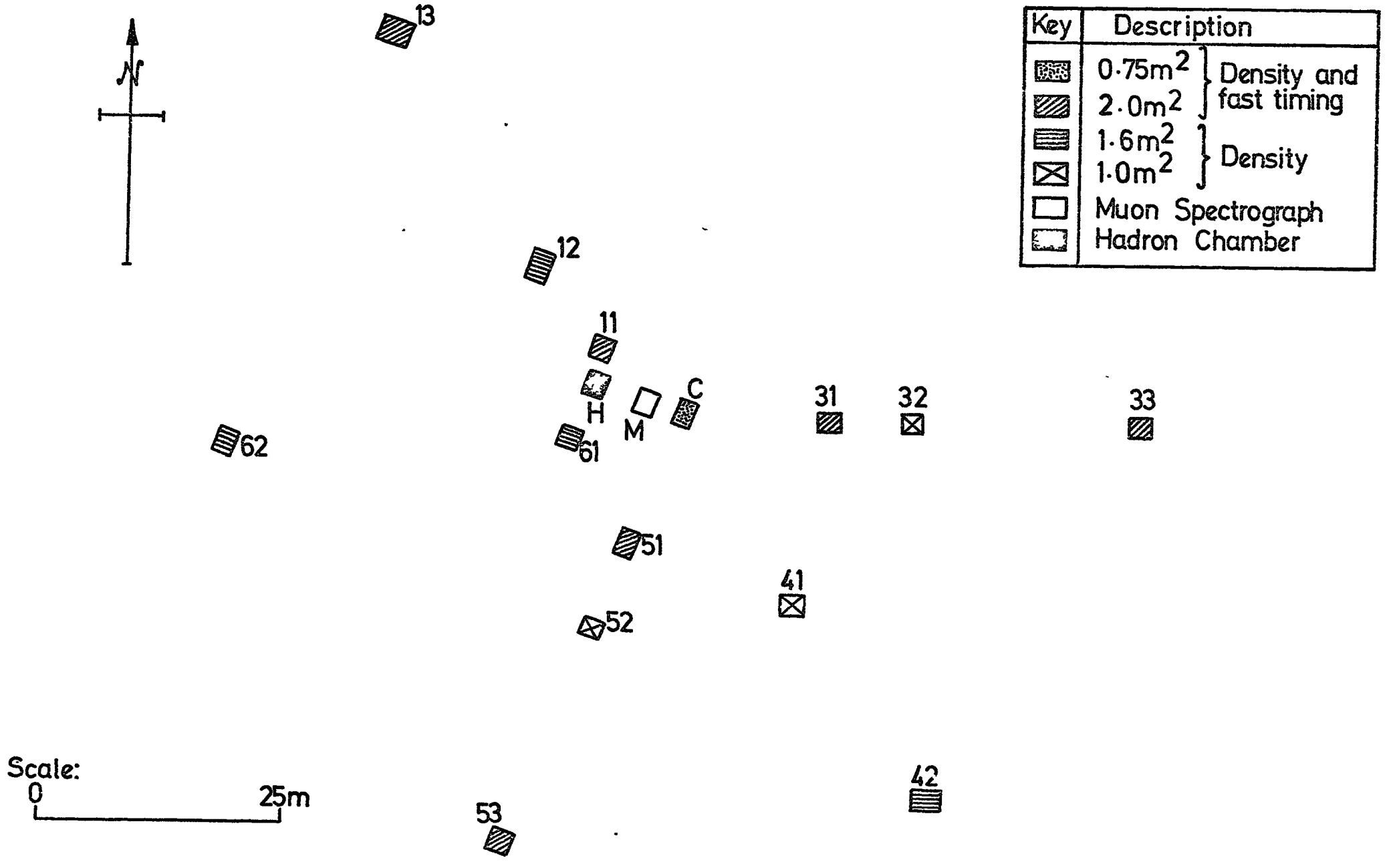

Figure: 4·1. The Durham Extensive Air Shower Automated Research Array.

scintillator down which the light intensity decreases by e^{-1}. Consequently, for large area detectors, account must be taken of the non-uniformity in response whereas in the case of geiger tubes, spark chambers and similar devices, these corrections are unnecessary. Scintillators do have a great advantage in that they can be made in large areas relatively cheaply and the associated electronics required to detect the emitted light is capable of long term stability. It was for these and other reasons that scintillators are used in the Durham Array.

There are four types of scintillation detector in present use in the array and they may be conveniently distinguished from each other by the fact that they have different areas. The variation in detector area ($2.0m^2$, $1.6m^2$, $1.0m^2$ and $0.75m^2$) is due to their availability. The $2.0m^2$ were specially fabricated for the array by Nuclear Enterprises of Edinburgh. Figure 4.1 shows that, whereever possible, detectors with the same areas have been placed at equivalent positions within the array to enhance the symmetry. This disposition also helps in the monitoring of the detectors' responses which is discussed in Chapter 5. Characteristic of all of the detectors is the similarity in how the scintillators are housed. Figure 4.2 shows this. The boxes that contain the scintillators, photomultiplier tubes and associated electronics are made from wood and are weather proofed with bitumen paint and aluminium foil. On one edge of the box the E.H.T. unit (§ 4.3.1), the head amplifier (§ 4.4) and the services box (§ 4.5) are mounted. Each detector box rests on an angle iron bed to raise it off the ground surface both to prevent damp and to assist the circulation of air around the box. Each of the several legs are adjustable in height to allow for uneven resting surfaces. Enclosing the detector box and bed is a weather proofed hut, also made from wood that is covered in either cedar wood of roofing felt. A louvre panel on the front and rear assist the air circulation around the detector. These panels can be removed to gain access to the detector electronics. Each of the various types of detector have been constructed in slightly different ways to take advantage of their size or shape and will be discussed separately.

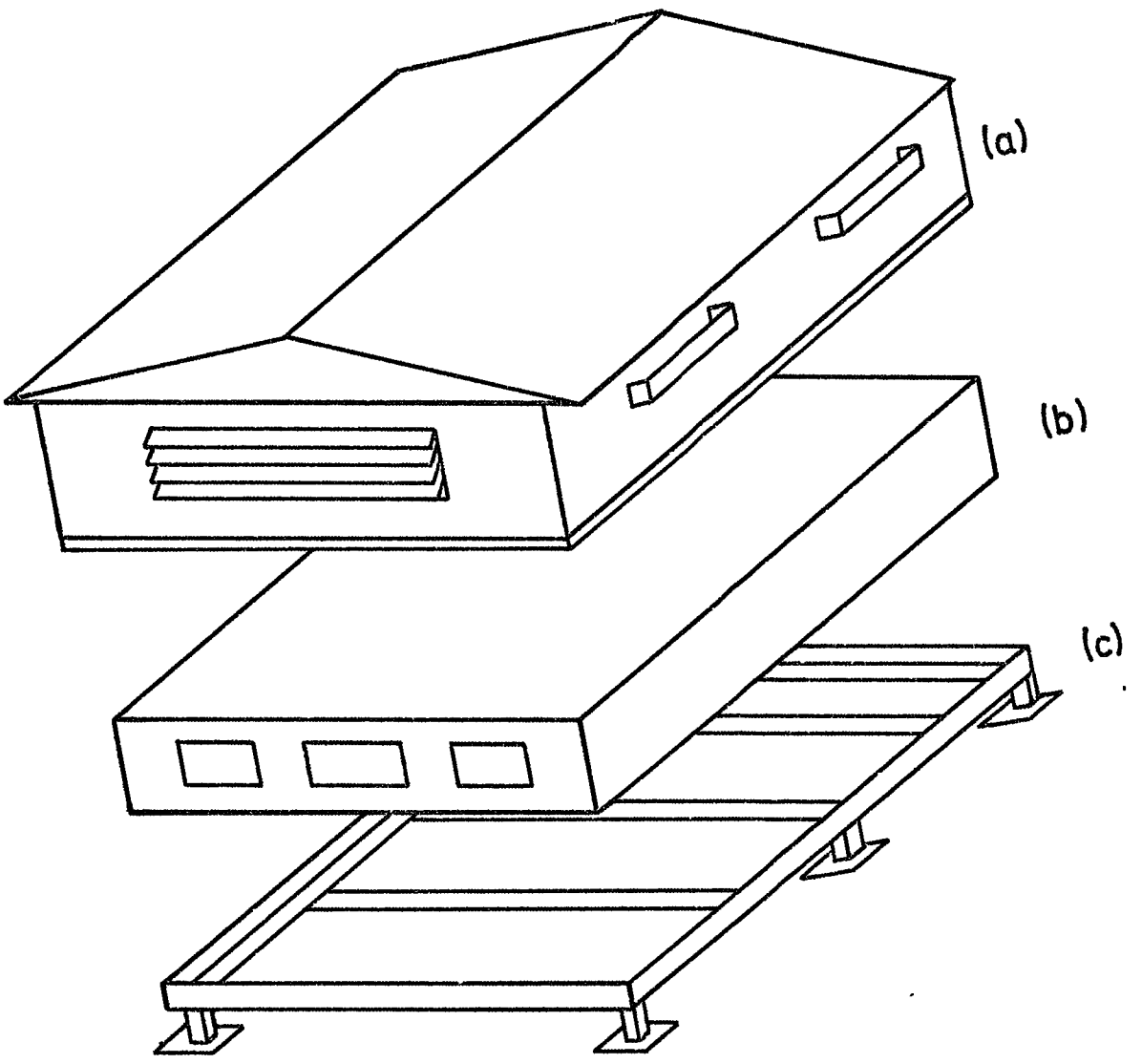

Figure 4·2. A typical detector arrangement.
(a) weatherproofed wooden hut.
(b) weatherproofed wooden box containing scintillator and associated electronics.
(c) angle iron bed.

4.2.1 The Central Detector

The central detector, 'C' in figure 4.1 is of a type that is not found elsewhere in the array. It has a geometrical area of 0.75 m^2 and because of its uniqueness it was decided to locate this at the central position. Figure 4.3(a) shows the salient features of this detector. It consists of two identical halves. Each half consists of a 5 cm thick slab of NE102A plastic scintillator that is viewed by two Philips 53AVP photomultipliers via perspex light guides, one on each end. Attached to one of the light guides on each half is a Philips 56AVP photomultiplier which supplies the timing pulse to which all of the other timing pulses are referred. The two halves are positioned side by side on an angle iron bed on the Physics Department roof and define the spatial and temporal origin of the array coordinate system.

4.2.2 The 2.0 m^2 detectors

There are six $2m^2$ detectors and these form the backbone of the air shower array and it is with these and the central detector that an event is established. They consist of a 2m x 1m x 2.5 cm slab of NE110 plastic scintillator that is noted for its long ($\sim$ 4m) attenuation length. The phosphor is viewed by four 5" diameter EMI 9579B photomultiplier tubes for particle density measurements and one 2" diameter Philips 56AVP photomultiplier tube for fast timing. Timing measurements are only taken on these and the central detector to give a total of seven time markers. Figure 4.3(b) shows this detector's features. The 'slow' phototubes view the long edges of the phosphor and have no interviewing light guide as they were found to be unnecessary. The "fast" phototube is attached to a long edge of each phosphor with NE580 optical cement.

4.2.3 The 1.6 m^2 detectors

These detectors, of which there are four in all, consist of four identical individually light proofed quarters. Each quarter is a 2.5 cm

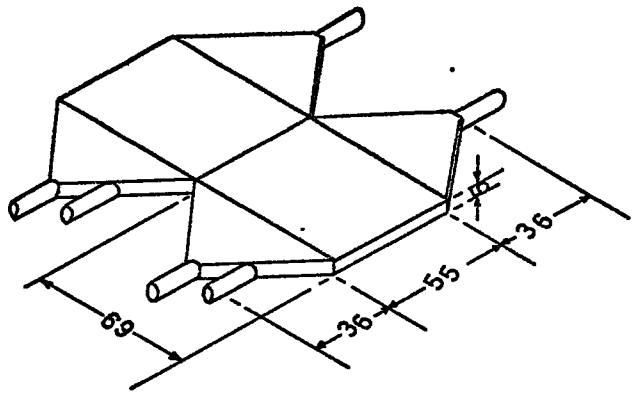

(a) The central detector (NE102A)

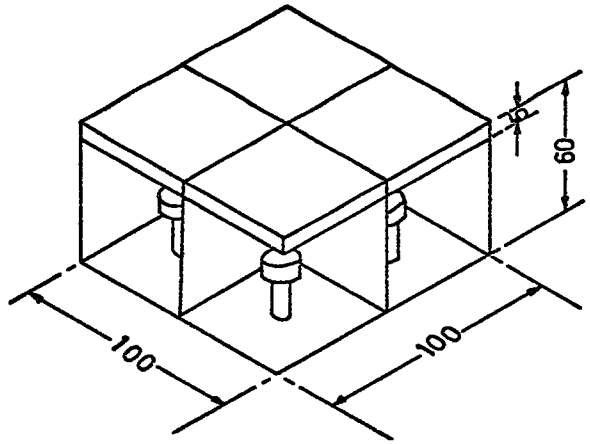

(d) A 1·0 m² detector (composition unknown).

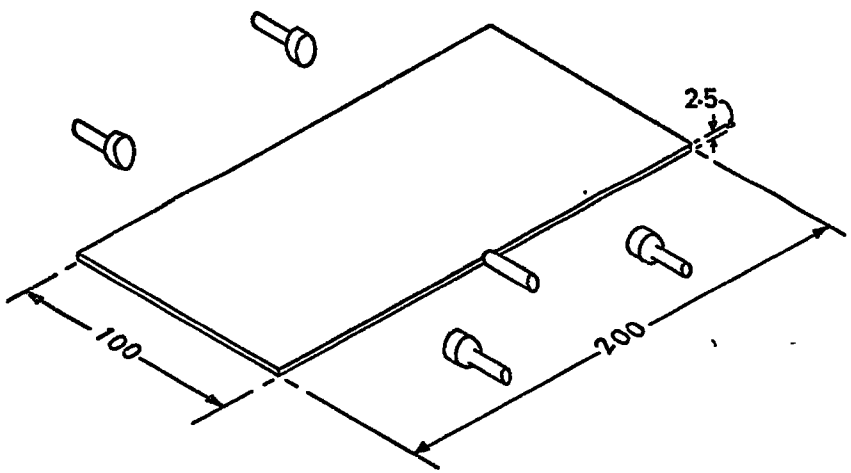

(b) A 2·0 m² detector (NE110)

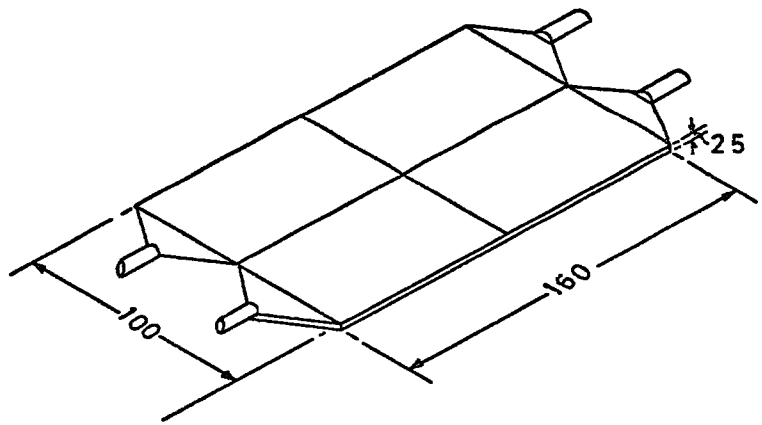

(c) A 1·6 m² detector (NE102A).

Figure 4.3. The Array Scintillators.

thick slab of NE102A plastic scintillator and is viewed by a Philips 53AVP photomultiplier tube through a perspex light guide, on one of the short ends, for the measurement of particle density. Figure 4.3(c) shows the detector and how the scintillators are situated in relation to each other.

4.2.4 The 1.0 m^2 detectors

Three of these detectors are to be found in the air shower array and each is located at about 25 m from the central detector. They are notably different from the other detectors in the respect that the photomultiplier tubes view the broad faces of each of the 25 cm x 25 cm x 5 cm slabs of scintillator. This naturally increases the detector's response to almost unity over all of its area. As with the 1.6 m^2 detectors, each detector consists of four identical quarters that are individually light proofed. The scintillator is of an unknown composition and not of the highest quality, thus necessitating the type of photo-tube arrangement shown in figure 4.3(d).

4.3 The Array Photomultiplier Tubes

Photomultiplier tubes are used with the plastic scintillators in the array to convert the light output of the scintillators into electrical signals that may be recorded and interpreted in terms of shower front parameters at the detectors coordinates. In all there are three types of tube in present use: EMI9579B with a 12 cm photocathode, Philips 53AVP with a 5 cm photocathode and Philips 56AVP also with a 5 cm photocathode. All possess standard S-11(CsSbO) photocathode and have their peak response in about the same region as the scintillator response. Figure 4.4 shows the much broader photocathode response that completely encloses the scintillator's spectral response such that any light quanta incident on the photocathode could result in an electrical signal.

The base circuits are illustrated in figure 4.5 and are of the high current design. This was chosen so that good linearity could be obtained for large pulses and so that saturation effects would be reduced. The tubes run on a negative E.H.T. supply and the output pulses from the 'slow' tubes are

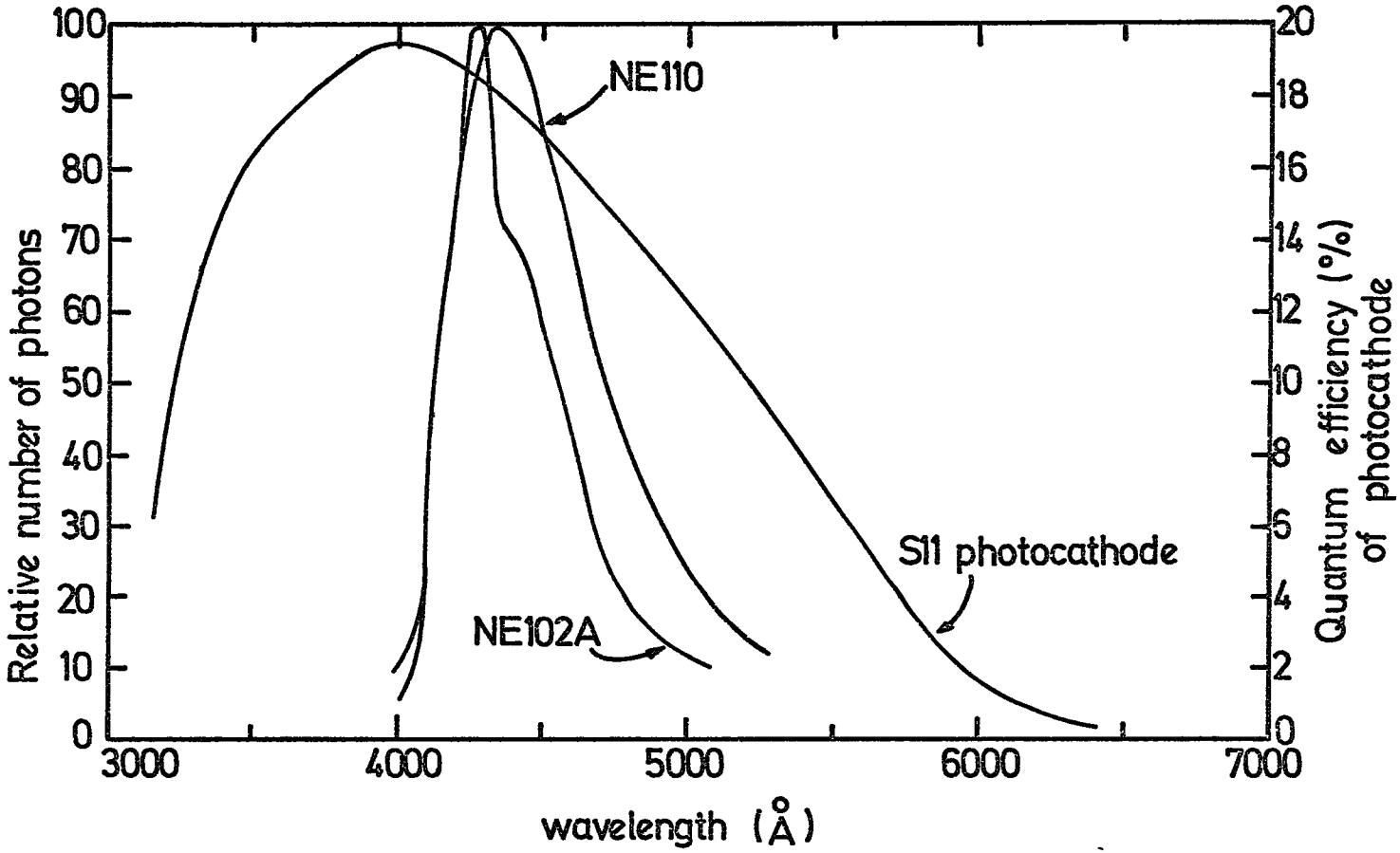

Figure: 4·4. Spectral response of the Array's scintillators and photomultiplier tubes.

Base circuit for EMI 9579B PMT

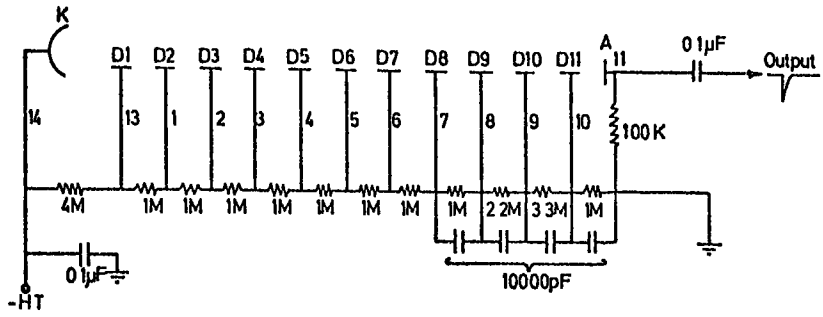

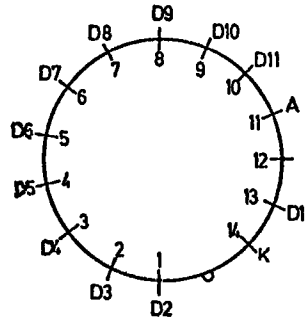

Base: 14pin Mullard FE1001
EMI B14A
Viewed from beneath

Base circuit for PHILIPS 53 AVP PMT

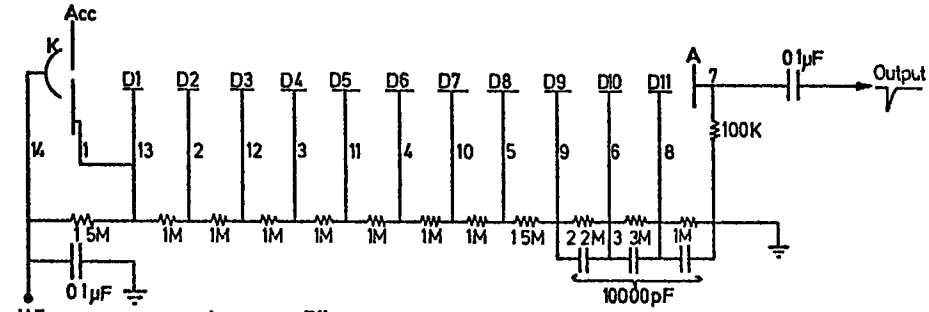

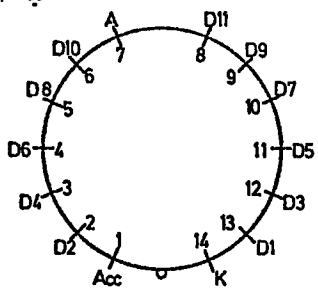

Base: 14pin Mullard FE1001
EMI B14A
Viewed from beneath.

Base circuit for PHILIPS 56 AVP PMT

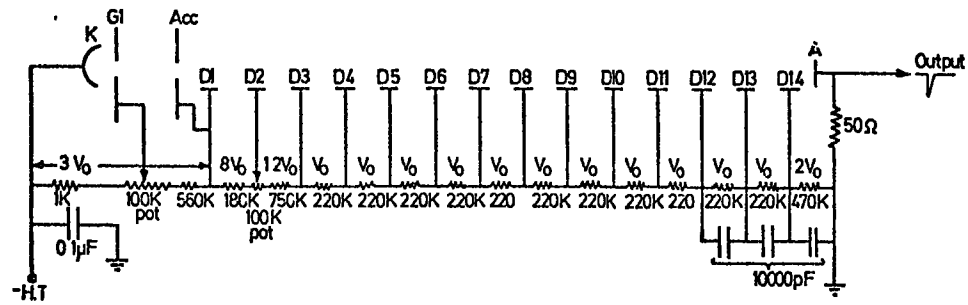

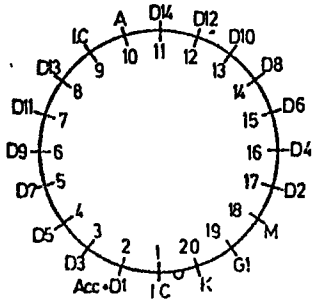

Base: 20pin Mullard FE1003
Viewed from beneath

Figure 4.5. The Array photomultiplier base circuits.

negative with an exponential decay time constant of 20 microseconds. The 'fast' tubes similarly run on a negative E.H.T. supply and have a negative pulse of ~5nS f.w.h.m. The photomultiplier tube base circuits are non-standard in the respect that the k-D1 voltage is unstabilised. This was constructed in this way following the usual practice in the laboratory but it was decided to investigate the tubes' gain for various light inputs and E.H.T's to check on any deviation from linearity. Three methods of ascertaining the photomultiplier tubes response were tried, each based on a device that could provide light pulses that could create large (of the order of a few volts) signals from the tubes. The light output from the device was then reduced by using high quality polarising filters in a crossed polariser technique.

Of the three light emitting devices used - an ^{241}Am alpha-source in NE110 plastic scintillator, a neon tube operating in its relaxation mode and a pulsed light emitting diode - the pulsed L.E.D. showed greatest promise. In detail it was found that the ^{241}Am source in the plastic scintillator produced fast rise time pulses, of a similar kind produced in the scintillation detectors, but whose intensity was too low and rendered the device unuseable. The neon tube had a very slow (~ mS) rise time and was thus unsuitable because it did not provide light pulses of the kind that were to be measured in the detector and because the photomultiplier tube pulse rise time was severely affected by the light output rise time of the neon tube. The pulsed L.E.D. was considered most satisfactory because more control could be exercised over the shape of the light pulse. A simple T.T.L. bistable circuit was constructed to provide voltage pulses of ~80nS width and with this driving a standard L.E.D. reliable and consistent phototube pulses were obtained of such an intensity that crossed polarising filters could be used. The phototube pulses were identical in shape to the pulses obtained from genuine cosmic rays in large area scintillators and consequently the L.E.D. technique was deemed satisfactory for the phototube gain investigation.

The method used was to pulse the L.E.D. at about 1kHz with the narrow voltage pulses. The light output from the L.E.D. was then reduced in intensity by polarising filters shown in figure 4.6. By varying the angle Θ between the planes of polarisation of the two filters the intensity of light falling onto the photocathode was altered according to the $\cos^2\Theta$ law. The output from the anode of the photomultiplier tube base circuit was then taken directly to the oscilloscope and the peak height noted. The linearity curves for the EMI9579B and Philips 53AVP photomultiplier tubes are shown in figure 4.7. Typical operating voltages are about 1.6 kV and 1.9 kV for the EMI9579B and Philips 53AVP respectively. It can be seen that for these voltages the phototube linearity, over the range of output pulses used, is good.

4.3.1 The E.H.T. Distribution

Two E.H.T. units supply the high voltage to the two distinct types of photomultiplier tube that are used in the array. The 'fast' tubes are run off an NE4646 E.H.T. unit which is capable of servicing the seven tubes. The 'slow' tubes run off an Ortec 456 and is set to 2.4 kV in the laboratory. This unit can supply the appropriate voltage to all of the 'slow' tubes within the array. Going to each detector is one co-axial cable that carries the 'slow' tube power and this is distributed amongst the four tubes in the detector using a resistor chain, illustrated in figure 4.8, which enables each tube's voltage to be adjusted independently of the others. This is necessary as no two tubes work at exactly the same voltage. In the case of a detector's 'fast' tube a single co-axial cable carries the power and at the detector there is a similar resistor chain to adjust the voltage across the tube as required.

4.4 The Detector Head Amplifiers

The output pulses from each of the four density measuring phototubes

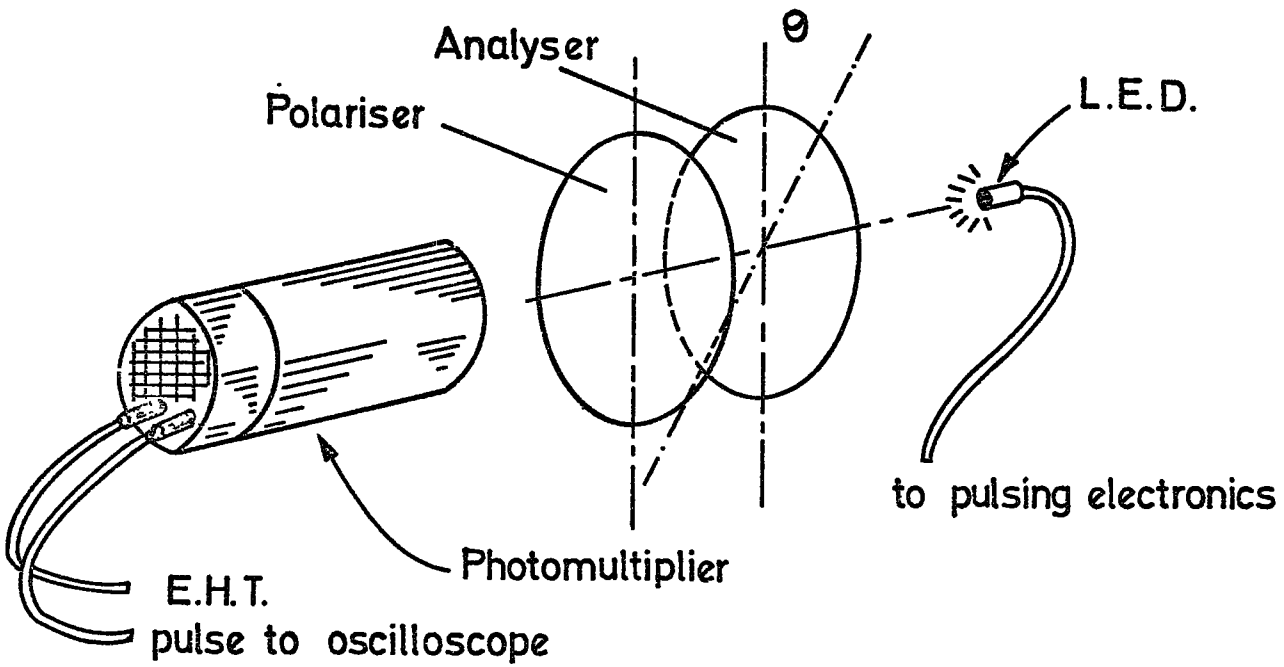

Figure 4.6. The arrangement for the photomultiplier gain investigation.

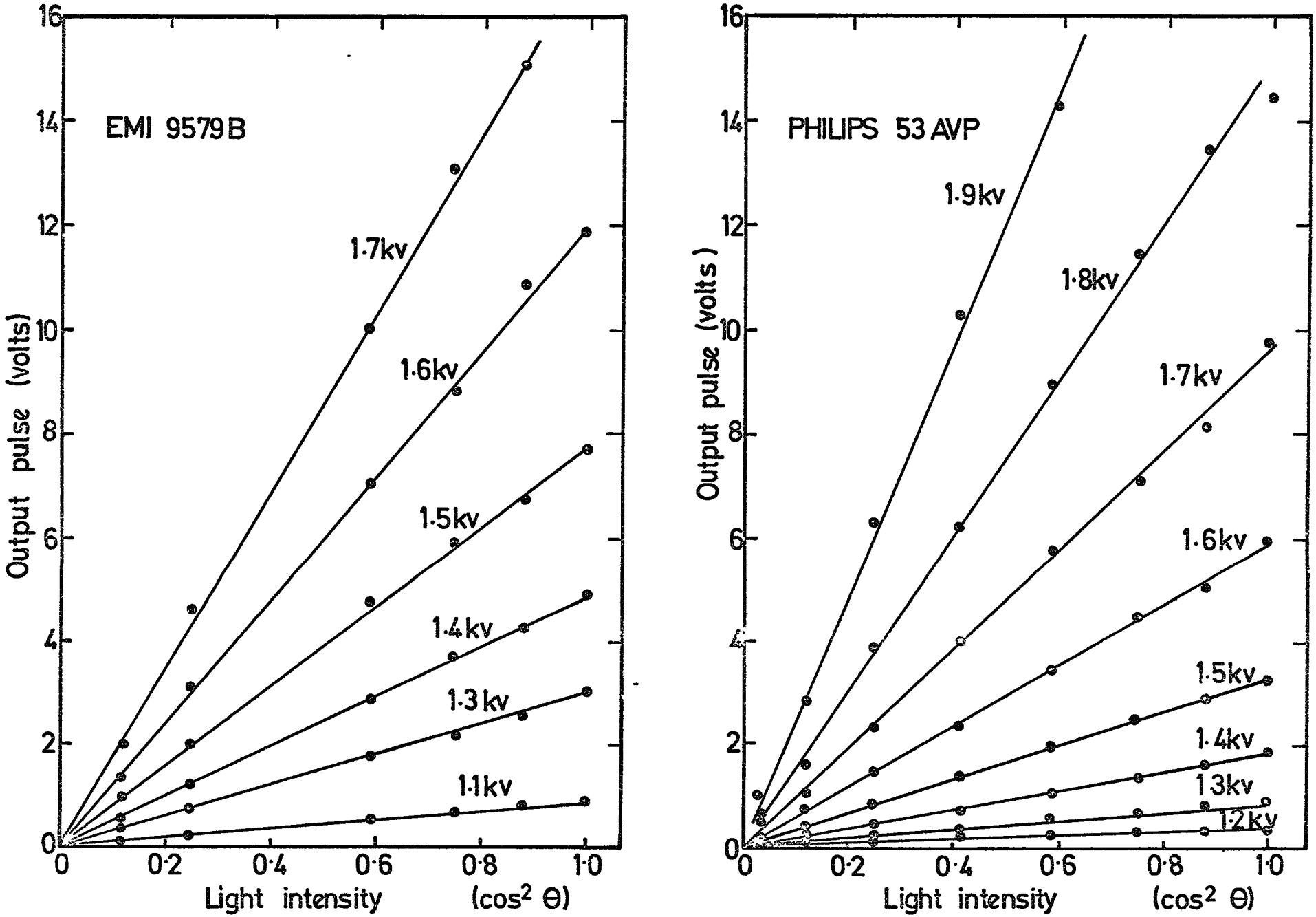

Figure 4·7. The linearity of the Array particle density measuring photomultiplier tubes.

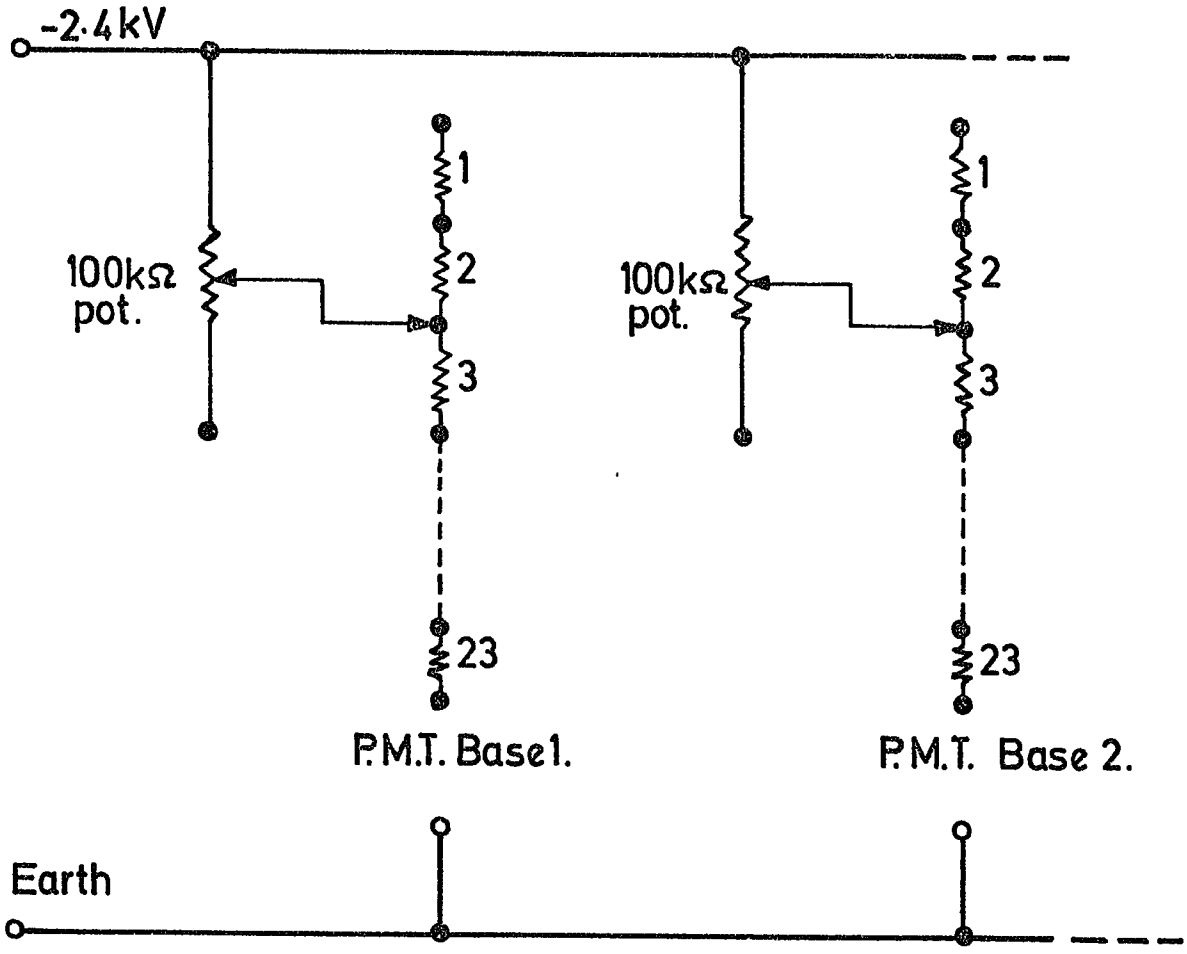

Figure 4.8. The sections of the four E.H.T. distributions at each detector. All resistors are 100kΩ, 2% tolerance.

are summed in a mixer-amplifier at the detector. The amplifier (figure 4.9) essentially consists of four emitter followers whose outputs are summed and amplified in a μA702C differential amplifier integrated circuit. The output of this device is then fed into another emitter follower circuit such that the now positive signal can be driven down the long lengths of cable into the laboratory.

Because many of the amplifiers are used out of doors they become susceptible to variation in temperature and thus it is important to know the temperature characteristics to see if any temperature correction need be applied to the output pulses. This was done by covering an amplifier in a watertight jacket and immersing it in water of a known and stabilised temperature. When it was considered that the temperature of the amplifier had also become stabilised a measure of the gain was taken. This was done for a variety of temperatures above and below $0^{o}C$ and for the range of temperatures to be encountered the gain did not vary sufficiently to warrant correction terms in the analysis procedures. The amplifiers have been made in such a way that they can be easily removed from the detector thus aiding pericdic checking and servicing. A stabilised 24 volt, 3A power supply unit in the laboratory supplies the power to all of the amplifiers in the array.

4.5 The Services Box

At each detector telephone and soldering iron facilities are provided to enable audio contact between the detectors and the laboratory and also to assist in electrical repairs. A spare twin flex, similar to the ones carrying the soldering iron power, is included should it be required at any time in the future.

4.6 The Array Cables

Figure 4.10 shows the layout of the array cable distribution amongst the detectors. In order to economise on cables and to reduce the number of

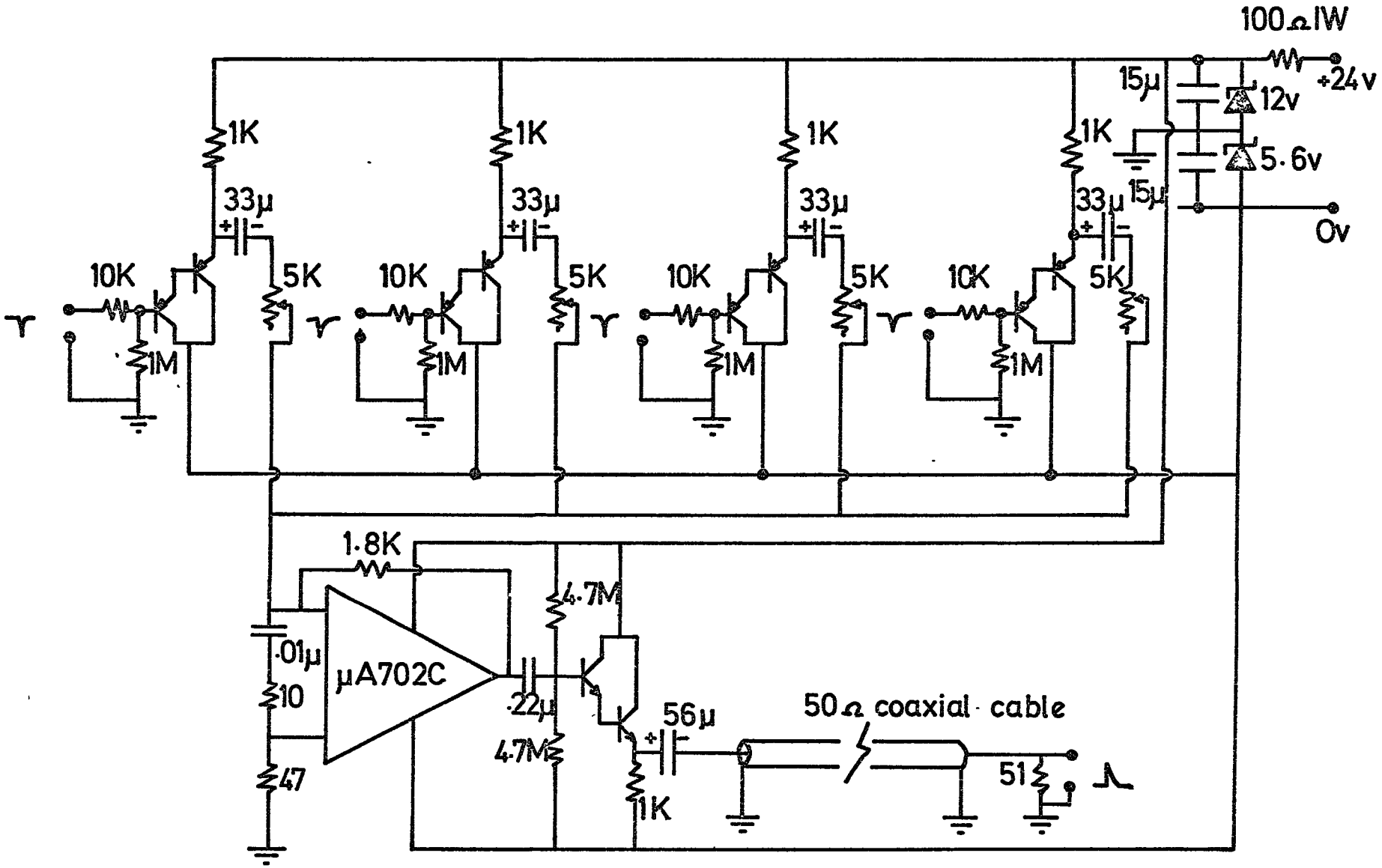

Figure 4·9. Four input gain five mixer-amplifier.
(Transistors: PNP ZTX501, NPN ZTX301)

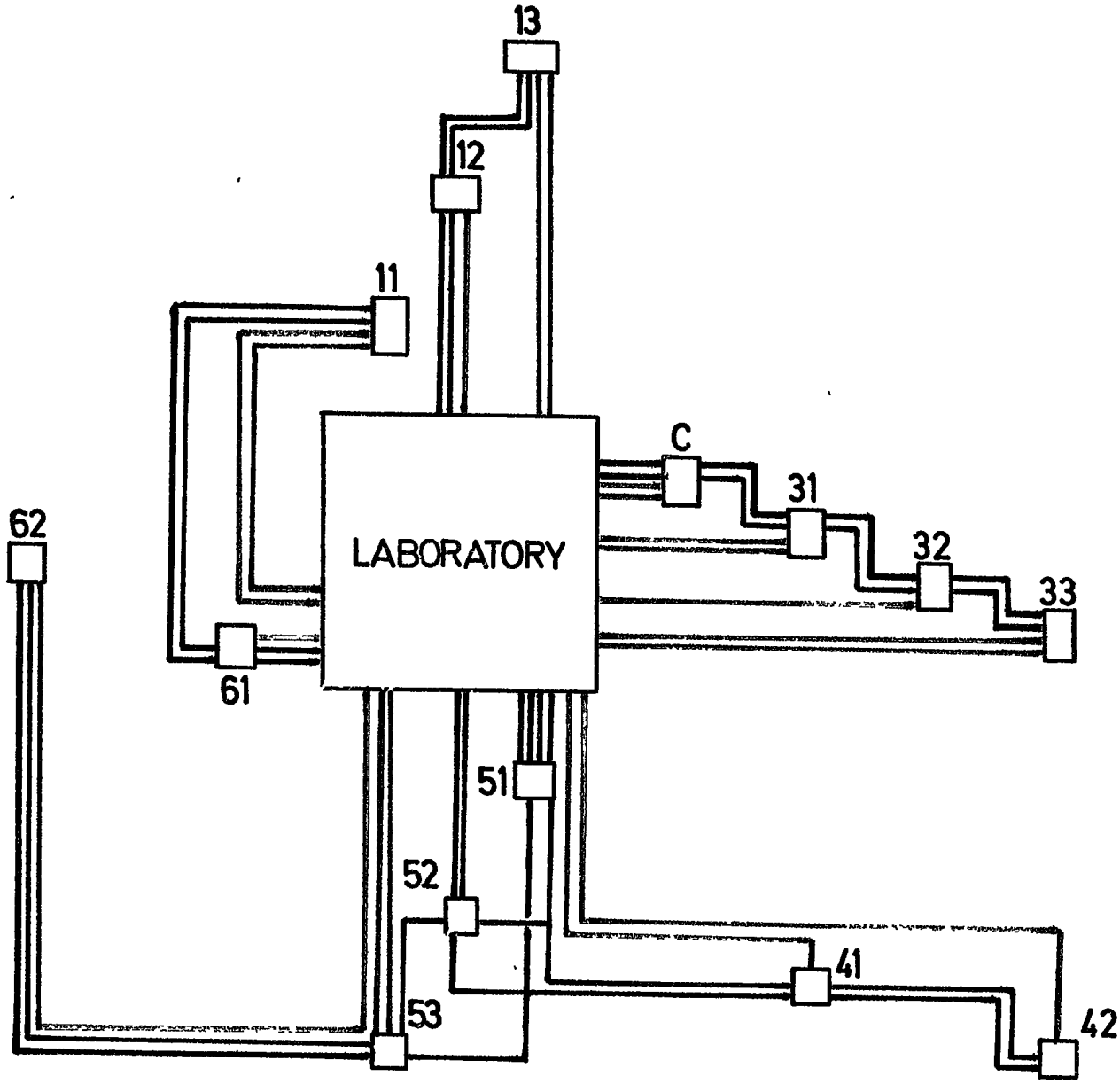

Figure: 4·10. Cable distribution of the Air Shower Array.

cables coming into the laboratory the cables carrying the 'slow' E.H.T., telescope E.H.T. (§4.7), low tension and services, go from detector to detector along the various arms of the array. The 'fast' E.H.T. and pulse carrying cables are individual cables which go directly from the laboratory to the various detectors. The 24V low tension is carried on screened four core cable (BICC 16.2.4C). Two of these carry the 24 volts, the other two are spare. The coaxial cable is RG58 C/U 50Ω cable throughout down which the pulse information propagates with a 0.9dB per 100 m loss. This loss in signal can be compensated for by increasing the photomultiplier E.H.T. to increase the size of the signal before being introduced to the cable. The frequency response of the cable is such that no significant change to the pulse shape can be seen for either the density pulses or the fast-timing pulses.

4.6.1. The Temperature Dependence of the Pulse carrying Cables

In the case of those cables carrying the timing pulses it is necessary to know their electrical length as distinct from their physical length so as to be able to determine the time delay that is introduced by the cables from each detector. It was thought that this could be a function of temperature and humidity and so these characteristics were investigated.

Two cables of similar length (100m) were coiled. One was maintained at room temperature in a dry environment and constituted the reference cable. The second was enclosed in a dry temperature controlled environment and a measure of the propagation delay of identical pulses down the cables for varying temperatures were recorded with the aid of a fast time base oscilloscope and an accurate variable time delay unit. After the dry environment characteristics had been obtained the cable was immersed in water and the temperature characteristics again measured. There was no observable difference between the wet or dry characteristics over the temperature range investigated (15^{o}C to 47^{o}C). The cable in the wet test was continuously monitored for a week and again no observable departure from the dry test was seen, thus

indicating that the cables are waterproof.

Over this temperature range a temperature coefficient of (-6.0 ± 0.2) 10^{-4} nS m^{-1} $^{o}C^{-1}$ was found and for the temperature ranges encountered on the ground surface and at subsoil levels of 30 cm no correction term need be applied. The expected variation is less than $\pm$ 0.6 nS per 100m length.

4.7 The Telescopes

Two additional coaxial cables go to each detector and they provide for the operation of a subsidiary scintillator telescope at each detector. The telescope is used in the calibration and checking of the detectors' responses. The technique utilised is to use one cable to supply the telescope photomultiplier E.H.T. and to carry the tube pulse back into the laboratory and this is achieved by using charge sensitive amplifier-discriminators in the laboratory. By using the telescopes in this way the number of cables to and from each detector is reduced and the requirement of an additional low tension power supply and head amplifiers is obviated. The telescopes themselves are used to select genuine cosmic ray pulses from the detector photomultiplier tubes such that the particle spectra may be acquired on a multi-channel analyser (M.C.A.) in the laboratory.

4.8 Calibration of the Density Measuring Photomultiplier Tubes

Each type of scintillator used in the array possesses its own charactertistic response qualities and thus each must be individually calibrated so that a complete understanding of the detectors' response is obtained. As mentioned earlier, the detectors are not uniform and a contour map of each detector's response to a single particle has been constructed, using the subsidiary telescope, to define that region of the detector that was under investigation. Figure 4.11 shows the linearity contour maps for the mean pulse heights of the various scintillators used in the array.

These contour maps contain vital information regarding a detector's response to cosmic ray particles. Because the contours are present one needs to define a mean pulse height per particle per detector. Having

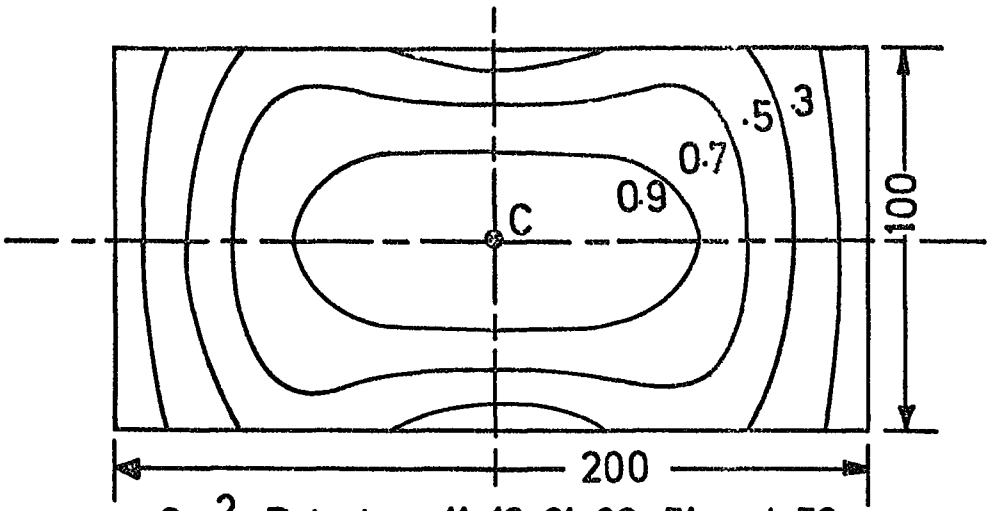

$2m^2$: Detectors 11, 13, 31, 33, 51 and 53.

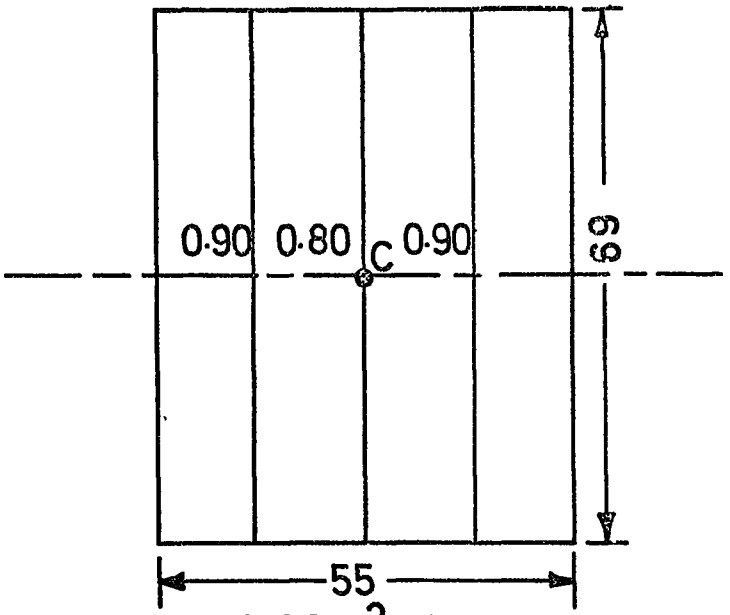

$2 \times 0.38 m^2$: Central Detector.

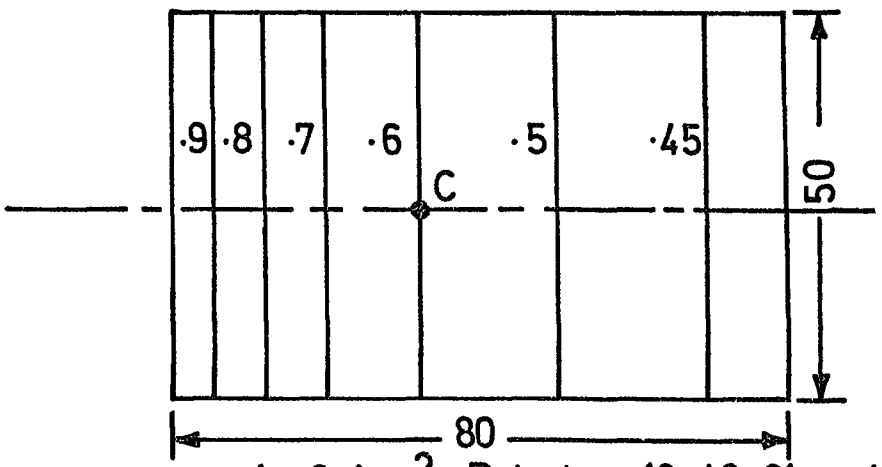

$4 \times 0.4\ m^2$: Detectors 12, 42, 61 and 62.

Figure: 4·11. Pulse height contour map of the Array's Scintillators.
Dimensions in centimetres.
C represents the calibration points.

obtained a contour map and a point on the scintillator where calibration is done (obtained from geometric considerations) the value of the pulse height at this point with respect to the defined mean pulse height is derived. It is this pulse height that is then used in the calibration.

4.8.1. Method of Calculating the Calibration Pulse Height

The aim of calibration is to set each detector's photomultiplier tubes to have an identical response such that for a summed pulse from all four tubes in the detector when divided by 100 mV will give the number of particles per square metre at the detector.

For a detector of total area Am^2 and with n photomultipliers viewing the same single piece of phosphor one calibrates on a mean pulse height of

$$\frac{100}{An} \quad \text{mV per p m t per particle per } m^2$$

When a particle distribution has been acquired on a M.C.A. the most easily measured quantity that can be related to the average pulse height is the maximum, or mode, of the distribution and it was felt that it would be quicker to calibrate on this value rather than the mean. To introduce this quantity into the calibration procedure and still retain the desired 100 mV/particle m^{-2} the relationship between the mean and the mode had to be found. For each type of scintillator used the ratio mean/mode was accurately determined at the calibration point. In fact it was found that this ratio did not vary more than $\pm$ 4% over the total scintillator area of any detector. Consequently, the use of this ratio, R, modified the calibration pulse height to

$$\frac{100}{AnR} \text{ mV p m t } {}^{-1}m^{-2} \text{ at the mode of the single particle distribution.}$$

For those detectors which were not calibrated at the coordinate where the mean pulse height occurred account had to be taken of this fact because of the phosphors' non-linear response. The ratio of the pulse height at the calibration point to the pulse height at the mean pulse height coordinate, g,

becomes another term which has to be applied to the calibration pulse height. The pulse height calibration equation thus becomes

$$H = \frac{g100}{AnR} \text{ mV per p m t per particle } m^{-2} \text{ at the mode of the single particle distribution at the calibration point.}$$

These values for the various detectors are shown in Table 4.1.

4.8.2 Experimental Method of Calibration

The scintillator telescope used in the calibration consisted of a 23 cm x 23 cm x 3 cm slab of NE102A plastic scintillator viewed by two Philips 53AVP photomultipliers in a light tight duraluminium box. The phototubes use positive E.H.T. and both the pulse and the E.H.T. are carried on the same cable. The two telescope cables from each detector go to NE4675 charge sensitive amplifiers in the laboratory. Each of these amplifiers supplies the E.H.T., removes the photomultiplier tube's pulse, amplifies and discriminates it above a preselected threshold level to give a standard logic signal at its output. These logic pulses then go to a simple T.T.L. coincidence unit, the positive output signal of which opens a gate on an Analogue to Digital Converter (A.D.C.) on a M.C.A. enabling the particle pulse from the air shower detector to be stored in the M.C.A. memory.

In this way a pulse height distribution is built up on the M.C.A., from that region of the air shower scintillator as defined by the telescope, and after some tens of minutes a sufficiently accurate distribution is obtained to gauge whether that particular detector's photomultiplier is being supplied with a voltage that is either too high or too low. The E.H.T. is consequently adjusted and another particle distribution is accumulated. When the peak of the distribution nears the calibration value, extended acquiring times become necessary to gauge the value of the peak of the distribution accurately. When the peak is within $\pm$ 2% of the calculated calibration value that photomultiplier is said to be calibrated. This process is employed for all of the array's density measuring photomultiplier tubes.

TABLE 4.1

DENSITY MEASUREMENT CALIBRATION PARAMETERS

Letector.	Total area (Am^2).	No. of p.m.t's. Total.	Viewing each piece of scintillator (n).	Calibration co-ordinates (centre of scintillator is (0,0)).	mean mode (R)	Pulse ht.at calibration pt. mean pulse ht. (g)	Calibration pulse height (HmV).
C	0.76	4	2	(0,0)	1.53±0.01	0.89	38.3
11,31,51,13, 33,53	2.0	4	4	(0,0)	1.83±0.01	1.41	9.6
12,42,61,62	1.6	4	1	(-7,0)	1.60±0.01	1.00	39.1
32,41,52	1.0	4	1	(0,0)	1.40±0.01	1.00	71.4

4.8.3 Calibration of the Fast-timing Photomultiplier Tubes

The fast-timing photomultiplier tubes can be calibrated in a variety of ways depending upon how much information one wishes to extract from them. Unlike the density measuring tubes whose pulses are 60μs long (t_b=20μs), the fast-timing pulses are only ~5 nS f.w.h.m. and unless these can be stretched to widths of the order of several microseconds pulse height distributions cannot be acquired. This is because the A.D.C. has a finite sampling time of this order. Using an Ortec LG105 fast pulse stretcher a pulse height distribution of the 56AVP pulses can be stored on the M.C.A. By gating the fast-timing pulses, with the pulses from the density measuring tubes viewing the same phosphor, noise may be eliminated giving a clear particle spectrum. The E.H.T. to the fast-timing tubes can then be adjusted until the correct pulse height distribution is obtained. Calibrating in this way enables one to select only those timing pulses that exceed a value as determined by the fast discriminators in the laboratory and thus may be related to a specific particle density such that time markers are produced only when a certain particle density has been exceeded.

A much simpler alternative method can be used since all that is required from the fast-timing tubes is a time mark when an air shower front passes through that detector. This method is to adjust the counting rates of the fast tubes to be equal using some low discrimination level. Although in this case particle density information is lost, it may be obtained from the density measuring tubes in the analysis procedures. At present this simpler method is used but the first method will be employed if it is found to be required.

4.9 Summary

Two sets of air shower data are acquired by the array electronics for each air shower event. One set consists of fourteen analogue signals representing the shower particle densities at each of the array's fourteen detectors which can be reduced to particle densities by dividing by 100mV.

The second set represents the timing information which consists of seven time markers. One of these markers defines the origin of the timing coordinate system and all of the other time markers are referred to this. These relative time differences may then be used to obtain the zenith and azimuthal angles of the shower front. The timing data does, however, contain delays introduced by the finite propagation time of the electrons down the fast photomultiplier tubes the delay in the pulse carrying cables and the delays in the electronics, all of which must be removed before the data can be analysed.

These voltage signals represent all of the experimentally available data that can be extracted from the electromagnetic cascade by this array. The reduction of these data to useful quantities will be fully discussed in Chapters 5 and 6. This chapter has attempted to show how the air shower array data are initially collected and transmitted to the laboratory in such a form that the data handling and storage electronics may handle it before it is eventually analysed.

CHAPTER FIVE

THE DATA HANDLING ELECTRONICS

5.1 Introduction

Chapter Four described how data are initially produced at the several detectors and then followed the progress of these data to the point where they entered the laboratory in a form ready for processing. It is with these data that the parameters of the air shower events are eventually evaluated in terms of shower size, core location and arrival direction. Before these values can be produced the incoming data to the laboratory needs to be coded and stored, in a form that can be interpreted in terms of particle densities and time measurements, that can be retrieved from storage to be analysed. Storage of the data is primarily on magnetic disc as binary information and it is one of the major features of the Durham Array that it is on-line to an IBM 1130 Computer. The on-line facility enables rapid data collection (an event is coded and stored within 2 mS) and the obviation of any photographic means of data recording. Such a system saves on analysis time and reduces the dead time of the apparatus.

The aim of this present chapter is to describe how an air shower event is established and how the raw data are manipulated, coded and stored such that the next stage in processing, which is the event analysis, can take place on the larger IBM 370/168 computer.

5.2 The first stage of Data Processing

For the eventual digitisation of the air shower data the first stage in the processing of it is to convert each signal into analogue form. Data from the detecting elements of the array arrives in the laboratory essentially as analogue information but the fast-timing data are not in a form that can be directly stored. The particle density data arrive as positive 20μ S decay time exponential pulses and the timing data as negative 5 nS wide semi-gaussian pulses. The particle density information is directly related to the particle density at the corresponding detector, as is described in §4.8 but the

fast-timing pulses, although their heights are related to particle density, are used only as time markers that refer to the passage of the shower front through the detector.

5.2.1 The Density Pulses

The density pulses from each set of photomultiplier tubes at the detectors have already been summed, amplified and calibrated before they reach the laboratory and so very little is done to them at this stage. The pulses are, however, fed into a discriminator and buffer unit which acts as an interface between the input pulses and the various devices in the air shower array data handling electronics. Figure 5.1 shows a schematic diagram of this discriminator/buffer unit of which there are 24 in all. On it there are two analogue outputs. One goes to the Analogue Multiplexer, which will be described later, and the other is a buffered linear output that is available for general use in the laboratory. The discriminator is a leading edge type (figure 5.2) that uses a μA710 high speed comparator as its basic element. The discrimination level is preset internally and may vary from 40 mV to 7 V. The discriminator outputs may be used in a variety of ways; the most important being in the monitoring of the count rate of each detector (§5.9) and in providing logical signals for a coincidence unit (§5.5.1). The input impedance of the combined unit is 10 kΩ, and this is in parallel with the Analogue Multiplexer's 50Ω. As with all of the data handling electronics in the laboratory, it is N.I.M. standard and each discriminator and buffer unit consists of eight discriminators and buffers, mounted on circuit boards, in a double width N.I.M.

5.2.2 The Timing Pulses

Up to seven timing pulses enter the laboratory from the fast-timing detectors (see figure 3.2). They appear as pulses in time but it is the relationship between the pulses that is of interest and which will give the arrival direction of the shower. To reduce, then, these time differences to useful quantities, and in particular analogue signals, Time to Amplitude

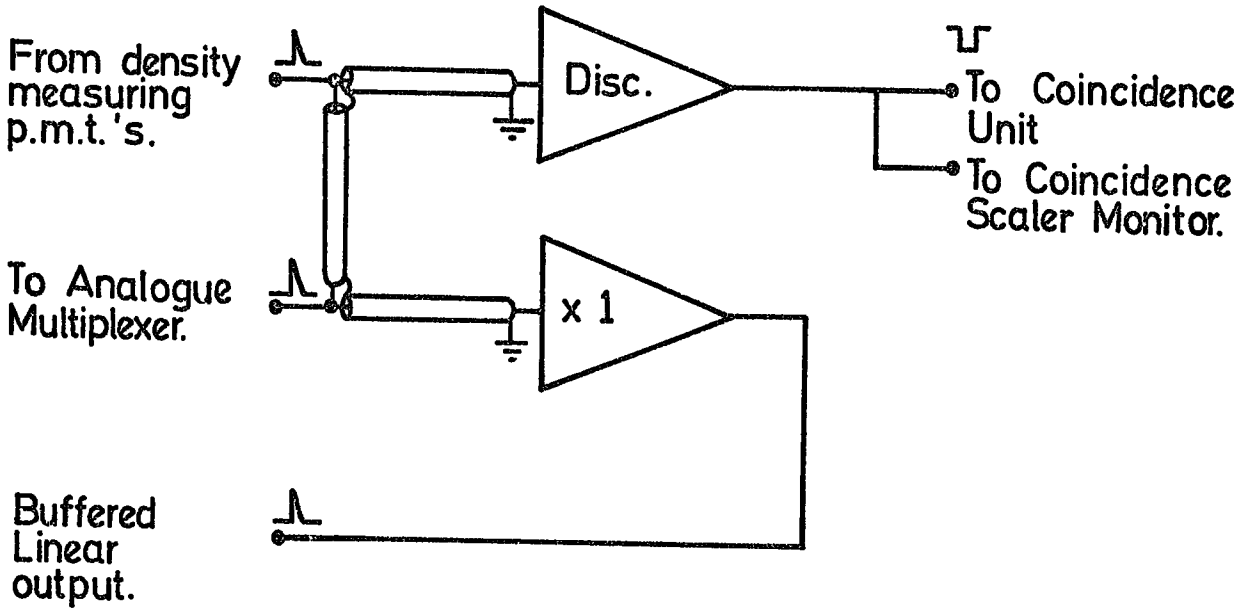

Figure:5·1. The Linear Fan Out and Discriminator.

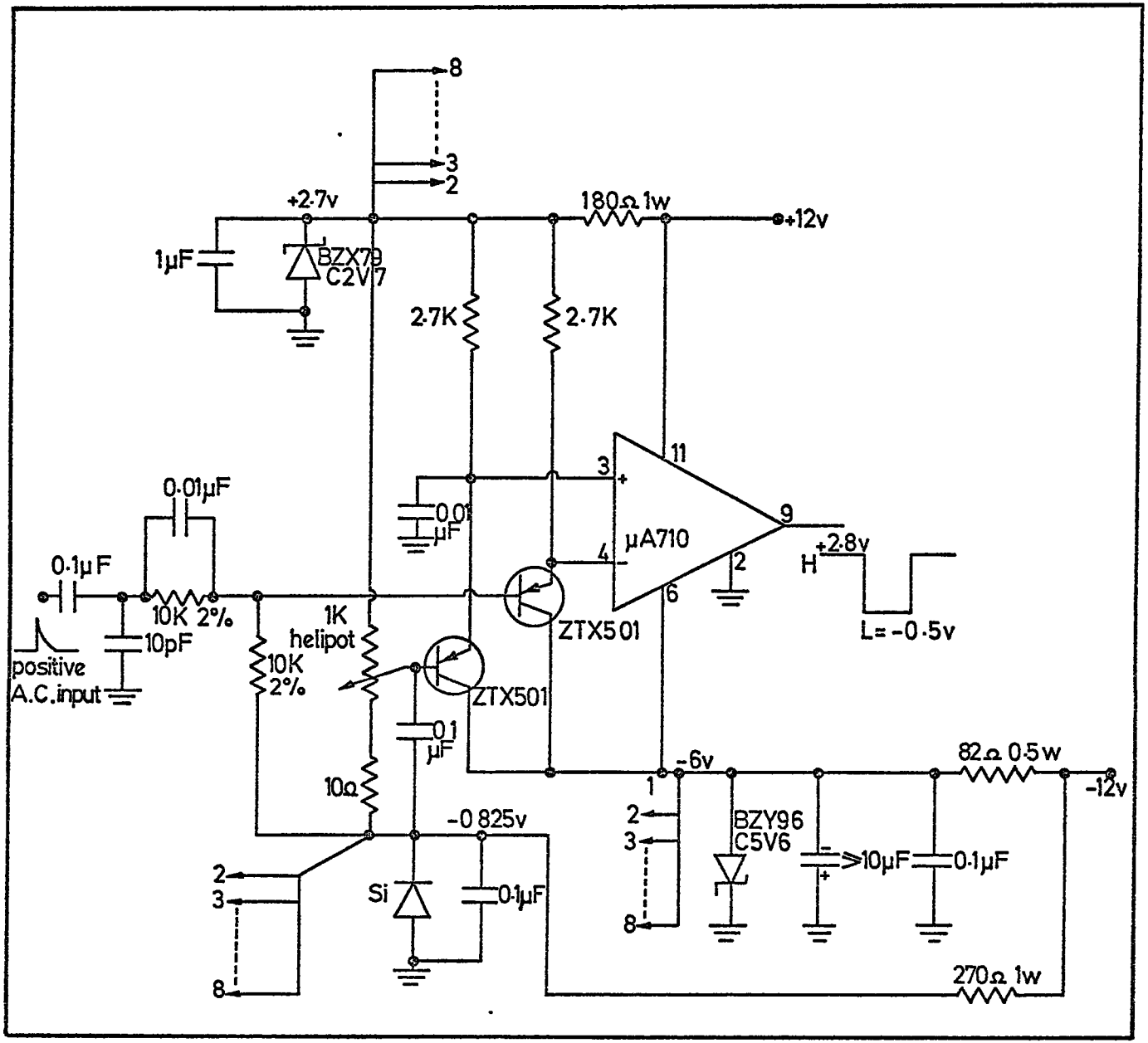

Figure : 5·2. Octal Discriminator

Converters (T.A.C's) are used. By using a common pulse to 'start' the T.A.C's and using the detectors to furnish the 'stop' command an output voltage pulse is generated whose height is directly proportional to the time difference between the 'start' and 'stop' commands. By using the central timing detector pulse to start the T.A.C's and ensuring that, for whatever angle an air shower should arrive, this pulse always arrives in the laboratory before any other signal, the T.A.C. outputs will bear a simple relationship to this moment in time. The central detector may then be used to define a position along the time axis such that for those detectors that the shower front passed through first have smaller T.A.C. outputs than for those detectors which the shower front passed through later. The analogue signals, which are positive, 5_{μ}S wide rectangular pulses, contain as part of the pulse height, not only the shower front relative times but time periods as a result of propagation delays down the various cables and through the various electronic devices of the system which must be removed before sense can be made of the T.A.C. output. This will be discussed in §5.9 and Chapter 6. What is important at this point is that the time marks between the ith and central detector have been reduced to analogue signals, even though there appears to be contamination from other sources.

Figure 5.3 illustrates the event handling electronics in which the T.A.C.'s are shown at the top right. Devices necessary for the successful operation of the T.A.C.'s include fast amplifiers and fast discriminators, also shown. When the timing pulses first enter the laboratory they are amplified and then discriminated. The fast N.I.M. logic signals then either 'start' or 'stop' the appropriate T.A.C. The discriminators possess two outputs, the second of which goes to a coincidence unit and can be used to establish the occurrence of an air shower event (§5.5.1). Accurate delay boxes are included in the timing circuitry to remove any small delays introduced by cables in the laboratory.

The T.A.C. outputs go to two devices for further processing. One is

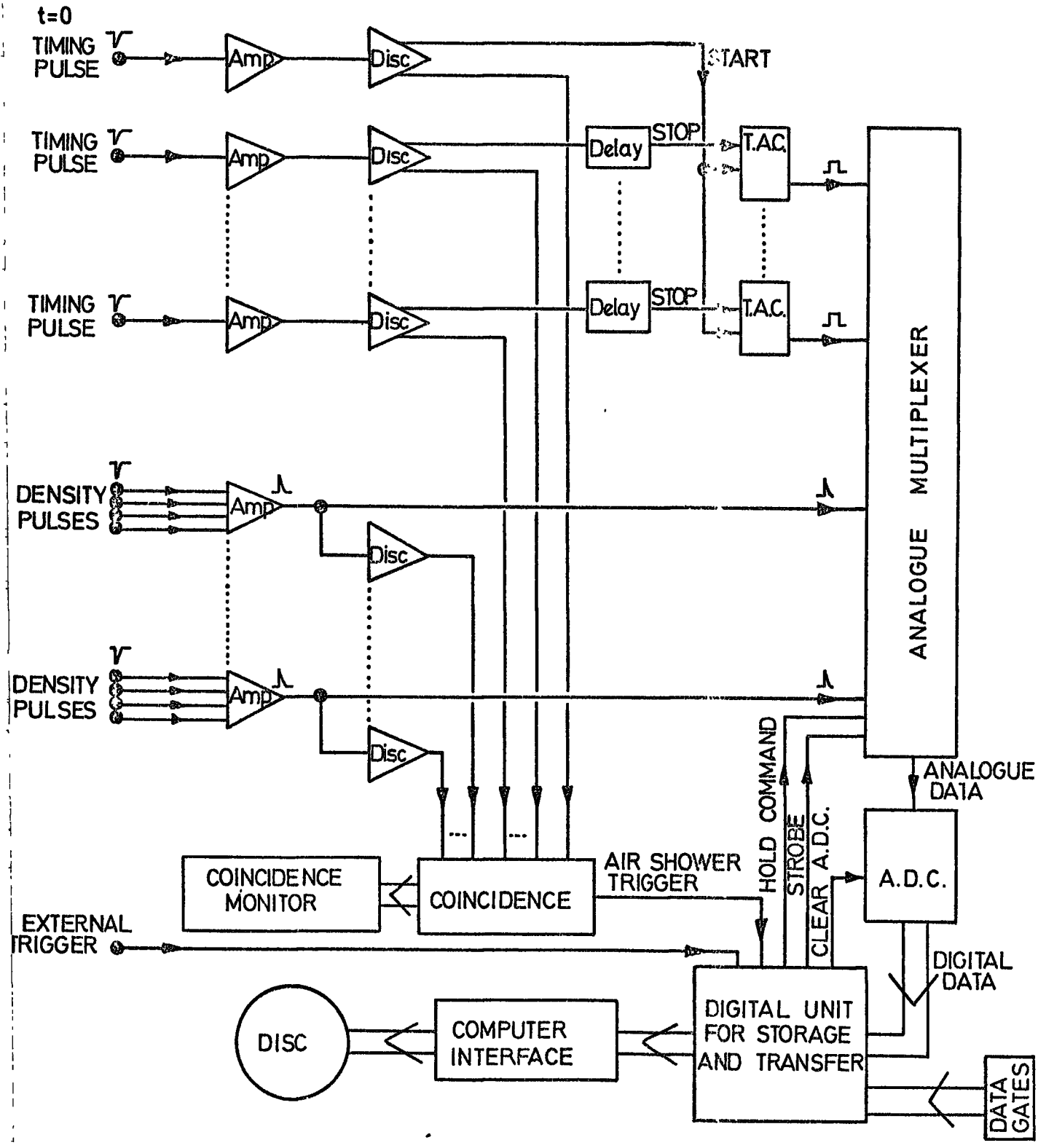

Figure: 5·3. The Event Handling Circuitry

a set of linear buffers and discriminators (§5.2.1) and the other is the Analogue Multiplexer. At this point, all of the data that have been obtained from the array detectors have been transformed into analogue signals. The heights of the pulses contain all of the dynamic data, that is, data obtained from the shower front. What must now be done is to find some means of permanent storage.

5.3 The Analogue Multiplexer

Tha Analogue Multiplexer (A.M.) is a device that was specially designed for use with the array. Its chief function is to store a shower's dynamic data for a short period of time (about 2 mS) after an event has been established such that the analogue signals may be converted into a form more suitable for permanent storage.

The A.M. consists of two basic modules, again N.I.M. standard. The first is the Master Unit which defines how many pulse heights are to be stored and which contains the external triggering command circuitry. The second is a Slave unit. (Plate 1). There may be as many as twelve Slave units in the total system, but this depends upon how many analogue signals there are. Both the Master and Slave modules have the capability of storing eight pulse heights and the maximum number that may be stored by the full system is 99. The present system employs one Master and two Slaves making a total of a maximum of 24 pulse heights that can be temporarily stored. A command to initiate the A.M. data 'hold' cycle may be produced in two ways, depending upon how one wishes to trigger the system. The first and simplest method is to use the 'external trigger' on the master unit. (see Plate 1). If a positive 5 v 2μS width pulse is applied to the external trigger socket then whatever data are present on the Master and Slave units will be stored in those units. The second method is more rigorous. On each Module exists two sets of thumb wheel switches to select conditions that must exist before an internal 'hold' command is generated. The switches select an "X out of Y" coincidence criterion in which at least X pulses from the first Y (maximum 7) inputs must be present. With the 'X of Y'

criterion, which can vary from 0 of 0 to 7 of 7, is an additional restriction of the presence of a positive signal on the master input of any of the multiplexer modules. For a data 'hold' command to be generated, then, there must be a positive pulse on any module's master inputs and the 'X of Y' condition must be satisfied on any module. The selection method used in the present experiment lies between both of the above techniques in which the A.M. is set such that a pulse on the master input of the Master module is sufficient to cause a data 'hold' within the three modules. Acquisition by this method has one great advantage - that the pulse used to initiate the data 'hold' cycle may be of a constant size enabling the output amplifier (common to all 24 channels) to be continuously monitored throughout the running of the experiment and of being able to use an external coincidence circuit to establish the occurrence of an event.

The A.M's inputs have 50 Ω impedence and accept pulses between 0v and 10v in amplitude. This corresponds, for the present system, to a dynamic range of approximately 0 to 100 particles m^{-2}. When used on the 'X of Y' data hold method the X pulses must exceed the internal preset discriminaters level (variable between 100mV and 500 mV) and must be coincident to within $\pm$ 150 nS of the master input signal. The outputs are rectangular 4μS wide voltage pulses with a gain of 0.40. These output signals appear spaced in time according to the frequency at which they are emptied by the Data Flag pulses. The droop on the outputs is 250 mV/V/sec and becomes significant ($\sim$1%) in this experiment only if the data storage cycle takes over 40 mS.

With the aid of the Analogue Multiplexer the dynamic array data can be temporarily stored. What can now be done, once that the analogue data are in this condition, is to take each pulse height, digitise it and store it in a way that is more permanent and accessible by electronic means.

5.4 Digitisation

Data storage of analogue signals is a difficult and expensive technique. Transfer of the data from one device to another requires devices

whose gains are well known, which makes systems very large and electronically cumbersome if large amounts of data need to be stored. This is why there is the need for digitisation. By reducing the analogue signals to binary numbers, each digit of which may be represented by memory elements being either 'on' of 'off', large quantities of data may be stored efficiently and easily. This is what is done in many applications of data storage, for data in this form can be easily manipulated and transferred from one location to another.

Conversion of the analogue information is most easily and conveniently done with an Analogue to Digital Converter (A.D.C.). This is a device which accepts analogue signals and converts them into binary numbers whose magnitude is proportional to the height of the input signal. Thus we have a technique to digitise the dynamic data.

For each air shower event that is collected a certain amount of information relating to its identification and under what circumstances it was acquired is as equally important as the analogue data when it comes to the interpretation and analysis of the air shower event. This information may be essentially described as bookkeeping and for each event that is stored by the data handling electronics a large amount of pertinent information is stored alongside the dynamic data. These data are the 'static' data and are generally constant or slowly varying throughout an experimental run.

5.4.1 The Data Gates

The static data are initially assembled in devices called Data Gates (D.G.), Plate 1, and perform several functions in the computer interpretation of the event and in the computer analysis. These gates either contain or transfer digital information to the central command modules, D.U.S.T. (§5.6) and consist of:

(i) An Event Header to identify the beginning of the data for a particular event,

(ii) A Run Number to identify a particular data collection series,

(iii) An Event Number to identify individual events,

(iv) A Trigger Mode Data Gate which serves to identify how the data storage cycle was initiated,

(v) An Operational Units Data Gate. This is used to inform the computer analysis programmes which detection devices were in operation at the time that an event was collected.

(vi) A Clock. This transfers real time information to the storage electronics and represents the time at which an event was collected and

(vii) Event End Data Gate to signal the end of the data for an event.

5.4.2 The Event Header

The event header is a 16-bit word which is constant throughout the experiment and defines the start of an event's data. The word, BFFF (hexadecimal), is set up by the use of NAND gates in a way similar to that shown in figure 5.4(a). As the number is constant, the switches in this figure should be omitted and the input to the gates held high or low depending on the bit in the word.

5.4.3 The Run Number

This is a 16-bit word that is set by toggle switches on the front panel of the Run Number Data Gate. It is used to define a particular series of data collection and is usually incremented every few days.

5.4.4 The Event Number

Each event can be identified by this 24-bit number. The event number scaler that supplies the binary number is a common scaler to several experiments in the laboratory and therefore each event from the separate experiments may be related to each other through this scaler. If any experiments should have coincidental events then their event numbers will be identical. This is useful in relating muon events in M.A.R.S. or hadron events in the Hadron Chamber to air shower events.

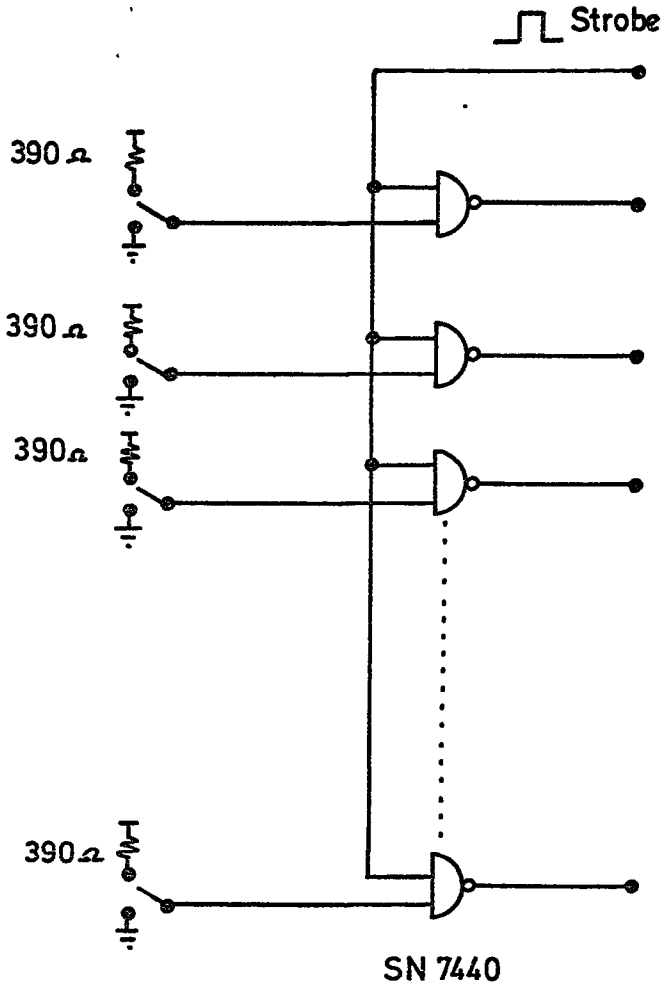

Figure 5·4 (a). The standard Data Gate. The switches are omitted for those gates which transfer data from elsewhere.

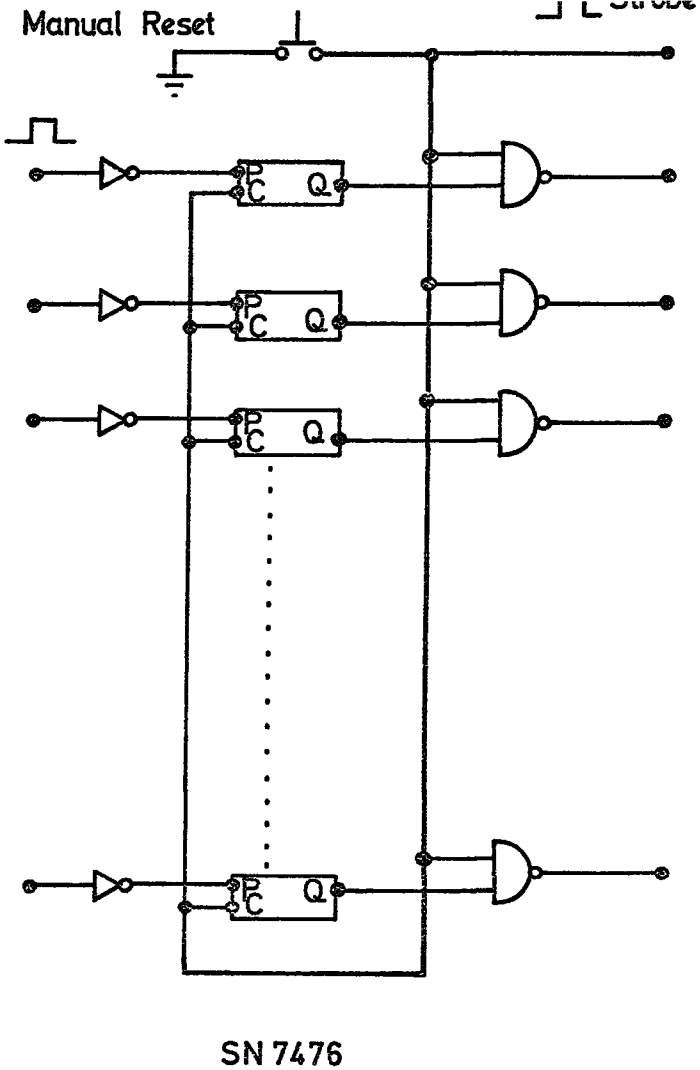

Figure 5·4 (b). The Trigger Mode Data Gate. The flip flops are reset by by the negative edge of the strobe pulse.

5.4.5 The Trigger Mode

This is an 8-bit word and instructs the computer analysis programmes how the data storage cycle was initiated. Its circuitry is shown in figure 5.4(b). The various input pulses to the flip-flops come from the triggering experiment which also provides a pulse to start the data acquisition cycle. Eight different experiments can be accommodated by the Trigger Mode data gate and for every event at least one bit should go high. It is possible for all bits to go high, indicating a multiple coincidence.

5.4.6 The Operational Units

Because there are so many detectors for density and fast-timing measurements there is the possibility that all of the detectors will not be operating at any one time due to faults with the detectors. So that the analysis programmes can be instructed to use only those devices that are operational this data gate is used. The 32 toggle switches, some of which are spare, indicate by either being 'on' or 'off' whether a device is operational or not. Figure 5.4(a) illustrates the circuitry used to perform this function.

5.4.7 The Clock

In some work it may be necessary to know when an event occurred. For example, to deduce galactic coordinates for the arrival direction of a shower or to relate this array's events with another experiment in another laboratory. The real-time data gate is connected directly to a special scaler that is counting at the rate of 1 kHz and is crystal controlled to better than 2 parts in 10^8.

5.4.8 The Event End

When all of the array static and dynamic data have been stored in the buffer memory the last word is written in. This is a constant number, EFFF, and indicates that the event's data have finished and that another

event may now follow in storage. This circuitry is similar to the Event Headers.

5.4.9 Digitisation: Summary

By using the Analogue Multiplexer with an A.D.C. and with the Data Gates already supplying binary information we have the situation where all of the relevant air shower data are in digital form. What is done with this digitised data will presently be discussed but before the data may be stored an event must occur.

5.5 Establishing an Event

An event may be established in two ways: by either an 'internal' air shower trigger, in which several preselected detecting elements in the array register coincident signals, or by an 'external ' trigger in which the presence of an air shower need not be required (see figure 5.3). The external trigger method can be used, for example, when another experiment, which records an event in its apparatus, wishes to interrogate the air shower detectors to see if an air shower is present. In this case a shower trigger may or may not be present and this method is useful in investigating phenomena in which small air showers ($\sim 10^4$ particles) initiate this other experiment as the shower triggering mode may be insensitive to this size of shower.

5.5.1 The Coincidence Unit

The coincidence unit is a simple device which, by preselection of detectors by toggle switches on its front panel, provides a coincidence pulse $1\mu S$ after the central detector pulse arrives in the laboratory. In relation to the occurrence of an air shower event this is about $1.2\mu S$ after the shower front passes through the central detector. When this pulse is produced it is directed into three devices. One is to increment the event scaler so that a new event number is ready to be read into the buffer memory, the second sets the appropriate trigger mode data gate flip-flop and the third goes

to the master control module, D.U.S.T. and initiates a data storage cycle. The master control module now controls the order in which the data are coded and stored in a temporary buffer memory where the digitised data may remain for about half-an-hour.

5.6 The Digital Unit for Storage and Transfer (D.U.S.T.)

D.U.S.T. is a complex device that controls the entire data acquisition and data dumping functions. It supplies all of the appropriate commands such that the data are written into the correct addresses in the buffer memory and in the correct order. When the memory (1024 x 8-bit words capacity) becomes full it instructs the on-line IBM 1130 to read out all of the stored data and to dump it on to magnetic disc where it will remain for a few days before being transferred to the larger IBM 370/168 computer for analysis. No attempt is made to give a detailed account of the circuit description but from what follows a general understanding of its functions may be appreciated.

5.6.1 General Principles

There are three modes of operation of D.U.S.T. which may be selected by the MT/AN/T switch on D.U.S.T. II (Plate 1). These three modes (Memory Test, Analysis and Test) may be used to perform operations which may, from time to time, occur in the running of the experiment and to check that D.U.S.T. is acquiring data in the correct manner. With the MT/AN/T switch on T, D.U.S.T. may be manually reset prior to data storage at the beginning of each run. When D.U.S.T. is reset four 8-bit words are read into the first four addresses of the memory. These words 00, 00, FF, FF are written in each time D.U.S.T. is reset, manually or automatically, and serve to label the core load of data as air shower data, and are used in the analysis programmes as an identifier. With the MT/AN/T switch still in this position individual 8-bit words may be read in manually by depressing the CYCLING

button. This facility is used in the daily checking of the instrument to ensure correct performance of the system.

With the MT/AN/T switch on Analysis the device is ready to accept air shower data. A 'start cycle command' enters the device at (FF,18) on figure 5.5 which originates from either an external or air shower coincidence signal. This command immediately presents a 'hold' command to the Analogue Multiplexers which now temporarily stores all of the available particle density and fast-timing data that was present on its inputs. The 'start cycle' command also increments the Shower Event Scaler (Plate 1) and paralyses D.U.S.T. for the duration of a data read in cycle. During this time, which is about 2 mS, no further air shower events may be acquired. With D.U.S.T. now in this condition it begins to read in the Data Gate information.

The first Data Gate to be read in is the Event header. This is followed by the Run Number, Event Number, Trigger Mode, Operational Units and the Clock Data Gates. The digital data are read in as 8-bit words but in general most of the data to be read into the memory are in the form of 16-bit words. Consequently as each D.G. is strobed the most significant part is read in first and then the least significant part second. All of the D.G. information is read into the Mullard MM1501 Core Store in about 540 μS. When the last 8-bit word of the D.G's have been read in a Data Flag pulse is sent to the Analogue Multiplexer to release the first pulse height to be digitised by the A.D.C. When the A.D.C. has completed conversion which takes

$$(6.0 + 0.02N)\,\mu S$$

where N is the A.D.C. channel number, the A.D.C. presents a READY ((X,1), figure 5.5) signal to the D.U.S.T. circuitry to indicate this and then the digitised data appear on the D.U.S.T. data input lines (E,26). As in the case of the D.G.'s the most significant part of the word is read in first and then the least significant part. The A.D.C. word consists of 10 bits. The two most significant bits being read into a memory 8-bit word leaving 6-bits permanently low. Upon completion of the two half-16-bit word read-in

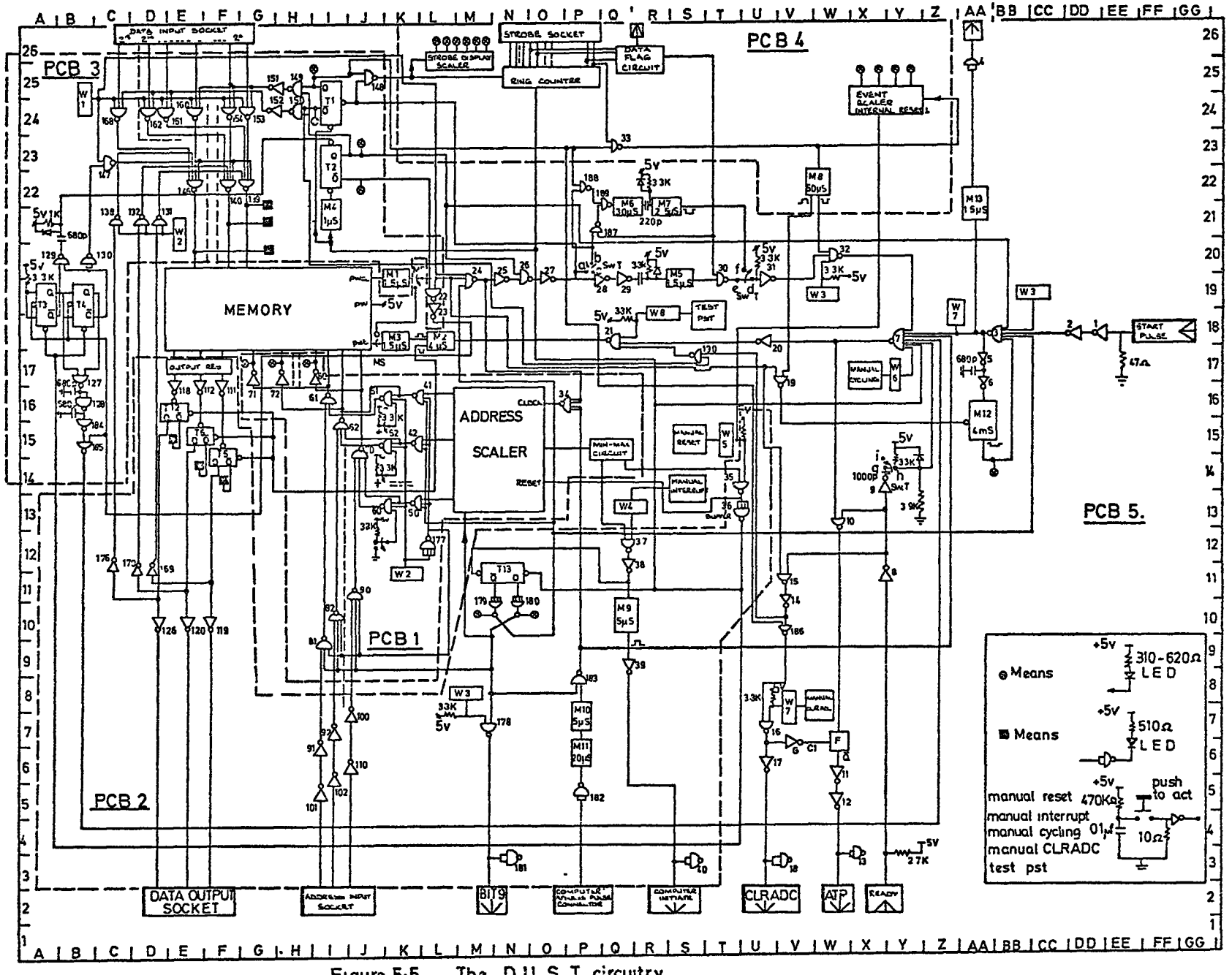

Figure 5·5. The D.U. S.T. circuitry.

cycle D.U.S.T. sends a clear A.D.C. signal to clear the A.D.C. output scaler and to wait in readiness for the next A.M. pulse. After this has occurred a second Data Flag is sent to the A.M. whereupon a second analogue signal is digitised by the A.D.C. and stored in the memory. This process continues until all of the 24 A.M. channels have been interrogated. The A.D.C. is again cleared, in readiness for the next air shower event data read in cycle and the final Event End D.G. is read in. Meanwhile the A.M. has automatically cleared itself and waits for the next 'hold' command. When the last D.G. has finally been read in the paralysis of the D.U.S.T. circuitry is removed and the device waits for the next Start Cycle command. A maximum of 11 events may be stored in the buffer memory in this way and when the 11th event has been stored the memory must be emptied before more air shower data may be acquired.

5.6.2 The Fan In Unit

The digitised data are presented to D.U.S.T. by a method of strobing the appropriate D.G. to enable it to release its data and by feeding those data through the Fan In Unit. Figure 5.6 clearly shows that the device, which consists of 16, 11 input NOR gates, acts like a funnel: channelling the several D.G.'s (including the A.D.C.) to one set of common outputs. The data, as initially assembled in the D.G.'s are real numbers, the outputs of the D.G.'s are the compliments of these numbers and because of the way they have been designed have all of their bits high when not being strobed. Only when a D.G. is strobed does it release its complimented information to the Fan In Unit which then decompliments it so that it can be correctly read into the D.U.S.T. memory in terms of two 8-bit words.

5.6.3 The Laboratory Computer Interface

Because there are three separate core stores in use in the laboratory, and only one cable connected to the IBM 1130 from the laboratory, a device to enable just one core store at a time to be emptied was constructed prior to

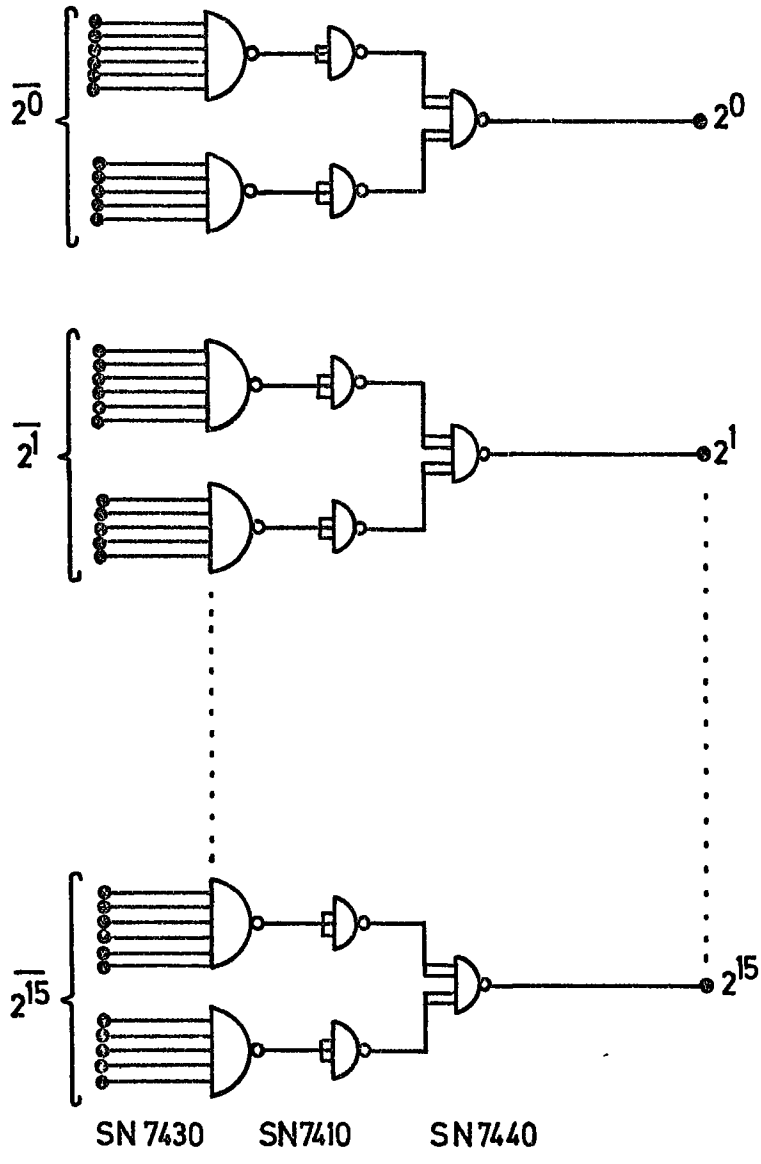

Figure 5·6 The Data Fan-In circuitry
This comprises 16, 11 input NOR gates. The inputs are connected to the outputs of the Data Gates. The inputs from the ADC have 1KΩ resistors to +5v

the author joining the group. This is required such that if two core stores need to be emptied simultaneously data will not be lost due to a confusion of data being presented to the 1130. In essence it allows one core store to be emptied at a time whilst the others are temporarily restrained until the previous one has completed its dumping cycle.

In the case when D.U.S.T. has stored the eleventh event in the MM1501 core store commands are sent to the 1130, via the laboratory interface, to indicate to the computer than D.U.S.T. is waiting to be emptied. The 1130 then acknowledges these pulses by returning with a sequence of binary numbers, which are interpreted as core store addresses ((I,2), figure 5.5) and simultaneous computer address pulses (P,2). With the computer supplying the appropriate core store addresses, starting at Ø, and a 'word-read-out pulse', i.e. the computer address pulse with each address, the memory is gradually emptied. When the last word has been read out the computer address procedures are inhibited and all of D.U.S.T.'s internal scalers are reset. D.U.S.T. then reads into its first four core store locations the core identifier 0000FFFF.

During the data read out cycle, which takes about one second, data acquisition by D.U.S.T. is inhibited and only after the core identifier has been successfully read in is D.U.S.T. again ready to accept more data.

5.6.4 Other D.U.S.T. Facilities

The third mode of operation, with the MT/AN/T switch on Memory Test, the contents of the memory may be interrogated to ensure that data have been successfully read into the appropriate core store address. By selecting the toggle switches on D.U.S.T. 1, at the address of interest and then by depressing the TEST PST push button on DUST II the contents of that address will be displayed on 8 red light emitting diodes on D.U.S.T. I, labelled Memory Output. Because the memory works on a read-write cycle the data at that address must be re-written into it within 0.4μS otherwise the data are lost. This re-read in is enabled by the D.U.S.T. circuitry gates 131-138

(D,21) in figure 5.5.

D.U.S.T. has been designed to be as versatile as possible within the limitations of size and complexity that such a device could be built. Its main feature, in the line of versatility, is that it can be easily adjusted to store up to 52 Analogue Multiplexer pulse heights per event and as many events that could successfully accommodate the memory. The D.U.S.T. complex was designed by Mr. J. A. Zabierowski and the author and was made into its operational form by the author.

At this stage the data now resides on magnetic disc in the department's IBM 1130 computer. The way that it is stored and how it appears on the disc will now be discussed.

5.7 The 1130 Data

The digitised data are stored on magnetic disc as a sequential file which contains all of the data from the three core stores of the M.A.R.S./Array apparatus in the order in which they were written onto the disc. The various core loads are identified by their core-identifier and may be manipulated accordingly. A typical example of an air shower's digitised data is shown in figure 5.7(a). The figures are hexadecimal digits; two digits making one 8-bit word that has been individually stored at an address within the buffer memory of D.U.S.T. From this figure can be seen where the D.G. data are stored in relation to the 'analogue'data. Figure 5.7(b) shows an event's data more clearly. In this case both the Event Header and Event End have been removed and the data are presented in a more readable form.

5.8 Summary: The on-line technique

The data as it now stands, on magnetic disc, remains in this condition for one or two days depending upon the availability of space on it. It is now in a form that is permanent and easily accessible by programming techniques and may be manipulated at will. The on-line technique enables rapid data collection resulting in quicker acquisition efficiency, reduced dead time

```
4520 4620 9191 9292  9393 9494 9595 9696  FF03 3058 340A 4061  9191 9292 9393 9494
9595 9696 FF04 438A / 4421 9191 9292 9393  9494 9595 9696 FF05  45C6 5004 9191 9292
9393 9494 9595 9696 / 0000 FFFF / BFFF 0048  6240 9C04 AA00 AAFE  FFFF FFFF FFFF 0000
0000 0000 0000 0000  0060 0000 0000 0000  007C 004F 0000 0017  0000 0000 0000 0017
0000 0000 / 004F 0061  0000 001E 0024 0000  0000 0000 0000 0000  0000 0000 0000 0000
0000 FFFF / BFFF 0048  6240 AD04 AA00 AAFE  FFFF FFFF FFFF 0000  0000 0000 0000 0000
C089 0000 / 017B 0000  007C 0062 0000 0019  0000 00AB 0000 0093  0000 0010 0065 0172
0035 005C 0039 0000  0000 0000 0000 0000  0000 0000 0000 0000  0000 FFFF / BFFF 0048
6240 C104 AAC0 AAFE  FFFF FFFF FFFF 0000  0000 0000 015D 0000  0000 0000 / 0000 0000
007B 0000 0000 0071  0000 002F 0000 000F  0000 00B2 0000 0000  0000 0030 001E 003B
C000 0000 0000 0000  0000 0000 0000 0000  0000 FFFF / BFFF 0048  624D CD15 AA00 AAFE
FFFF FFFF FFFF 0000  0000 0000 0077 CCC0  0000 0000 / 0176 0000  007A 0250 0000 0096
CC00 016A 0CC0 0149  0000 0131 01A1 02FF  02CB 03A9 0227 0016  0000 0000 0000 0000
0000 0000 0CC0 C000  0000 FFFF / BFFF 0048  6240 F904 AA00 AAFE  FFFF FFFF FFFF 0000
C0C0 C000 0144 0000  0000 0000 / 01BB 0CC0  007D 0047 0000 0028  0000 0000 0000 001F
0000 0025 / 0C0A 00JA  0010 0025 007D 0262  0000 0000 0000 0000  0000 0000 0000 0000
0000 FFFF / BFFF 0048  6240 FA04 AAC0 AAFE  FFFF FFFF FFFF 0000  0000 0000 0116 0000
004A 0000 019A 0000  007A 001D 0000 0039  0000 0045 0000 0026  0000 0000 001B 0000
C000 0000 0017 0009  0000 0000 0000 0000  0000 0000 0000 0000  0000 FFFF / BFFF 0048
624E 0004 AA00 AAFE  FFFF FFFF FFFF 0000  0000 0000 0153 0000  012C 0000 / 0186 0000
```

(a) A typical sector of data written on to the 1130 disc. Air shower data begins with the core identifier 0000 FFFF. The data before these two words is part of a M.A.R.S. event sent to the 1130 before D.U.S.T. dumped this particular core load. Slashes separate individual events.

Data Gates.
7 timing channels,
1 standard pulse,
8 density channels

16 density channels
(last 8 are spare)

```
0048 624E 2504 AA00 AAFE FFFF FFFF FFFF 0000 0000
0000 0000 C000 0074 0000 0167 0000 007D 007B 0000 0011 0000 0020 0000 0012 0000
0000 0015 CC00 0011 0012 00C9 CC00 0000 0000 0000 0000 00C0 C000 0000 0000 0000

0048 624E 7004 AA00 AAFE FFFF FFFF FFFF 0000 0000
C000 01C5 00C0 0108 0000 01CE 0000 007C 0009 0000 0026 0000 0012 0000 000F 0000
0000 0000 C00F C000 0000 001A 0034 0000 0000 0000 0000 0000 0000 0000 0000 0000

0048 624E 7A04 AA00 AAFE FFFF FFFF FFFF 0000 0000
0000 0152 0000 00BC 0000 0130 0000 007A 0098 0000 0017 0000 001C 0000 008A 0000
0044 0040 0107 0031 0145 00BE 004C 0000 0000 0000 0000 00C0 C000 0000 0000 0000
```

(b) Three air shower events from the above sector of data with the core identifier, event header and event and words omitted for easier reading. There are 11 events per D.U.S.T. core load.

Figure 5.7. Typical Air Shower Data as it is initially assembled on magnetic disc

and obviates the need for any manual intervention with the data apart from the monitoring of the data acquisition electronics performance.

5.9 The Daily Running of the Experiment

Checks on the performance of all of the array electronics are carried out at least once per day. Some of the checks are manual, some are semi-automatic and others are fully automatic. The automatic checks will be described in this section and Chapter Six.

Before each new run and at least once per day, the Data Storage Cycle is checked to ensure that all of the Data Gates are operating and are being read in correctly and that the analogue data are being stored, digitised and read into the buffer memory in the correct manner. The fast-timing electronics, including the presence of pulses and its transformation to analogue data by the T.A.C.'s, are then checked. Tests done on the density measuring detectors, with the Coincidence Monitor (fig. 5.3), include the monitoring of the integral count rate above a preselected discriminator threshold for each detector. These are then plotted each day such that any general trends in their operation can be seen. Coincident rates between selected pairs and groups of detectors also keep a check on the detectors' performance and also provide some physics on the shower size spectrum and decoherence of particles in air showers.

Semi-automatic daily checks are done on all of the Analogue Multiplexer channels that have acquired data during a day. For all of the events collected each day, histograms of the pulse heights that have been stored in each separate multiplexer channel are created in the IBM 1130. Each detector and T.A.C. will have a similar pulse height histogram for each day of operation of the experiment if the triggering criterion remains constant and if the detector remains calibrated. Any deviation from that expected in terms of the measurement of the mean of the spectrum, would result in an investigation of the detecting element to see why the mean pulse height had changed. Typical daily 1130 histograms are shown in figure 5.8(a) and 5.8(b).

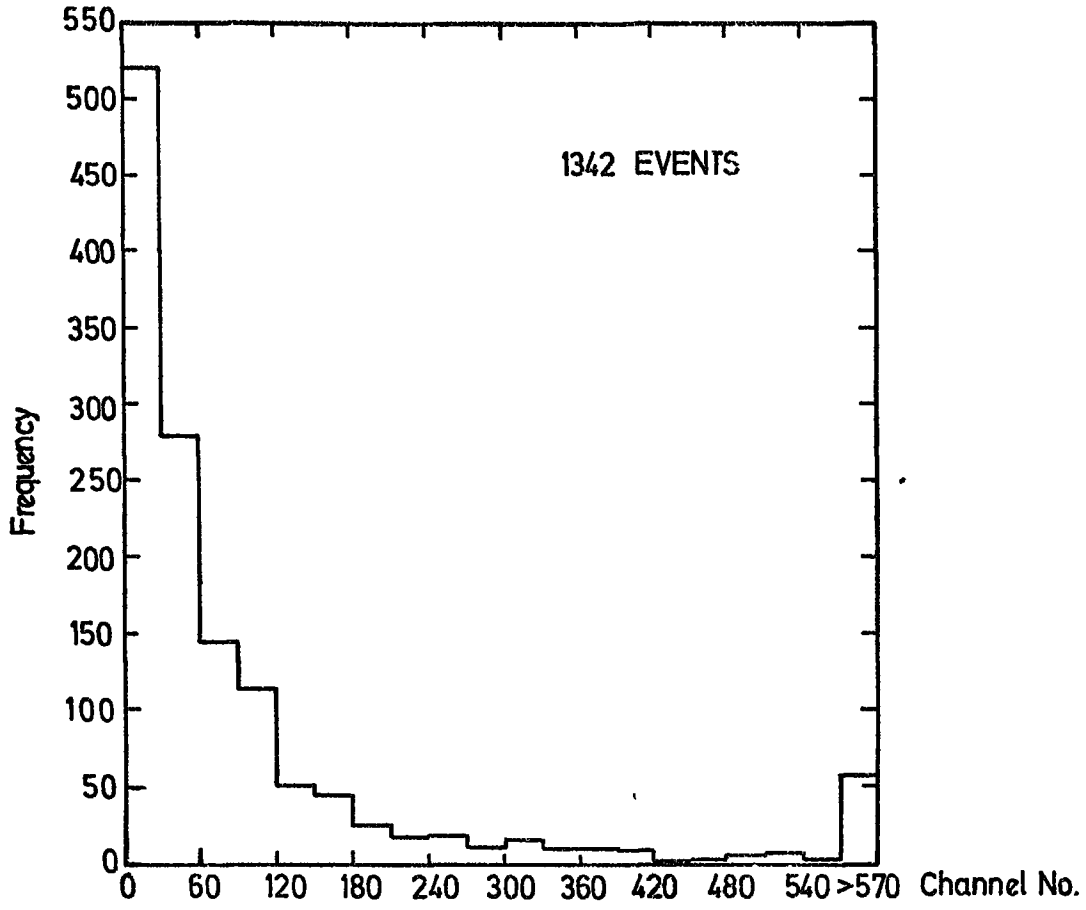

(a) Density pulse height histogram for the central detector

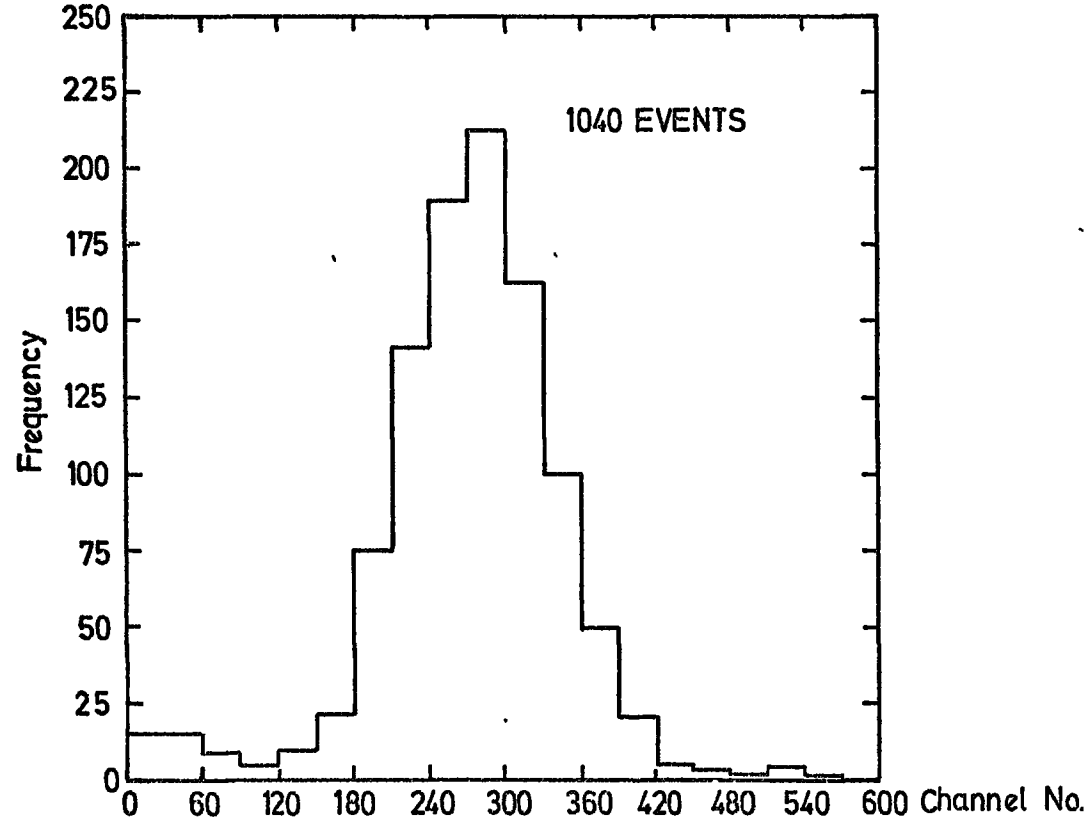

(b) T.A.C. distribution for detector 33.

Figure 5.8. Typical data produced by the 1130 for daily monitoring of the experiment.

For figure 5.8(a), which represents a pulse height spectrum of the central density detector, the mean pulse height is only of academic importance. In the case of figure 5.8(b), which represents the T.A.C. distribution for detector number 33, the mean (or, more particularly, the mode) takes on a more significant meaning. If showers arrive mainly from the zenith then the maximum of the distribution would correspond to a zero time delay with reference to the central detector (if both detectors were on the same spatial Z-plane). Consequently, the distance along the time axis would represent the constant time delay due to pulse propagation down the various cables and electronic devices. This property of the distribution allows for automatic calibration of the timing data. By defining t = 0 as the mode of the distribution for each detector, and for each separate run, variations in the drift and gain of the timing electronics are no longer quantities that need be monitored, with the view of including them in the analysis programmes to correct for drift from the originally calibrated value, since they could be recalibrated each time the events are analysed. These T.A.C. distributions are investigated in more detail in Chapter Seven as potentially useful distributions.

By including a standard pulse as one of the analogue signals presented to the Analogue Multiplexer, the gain of the output amplifier of the device may be continuously monitored with each event that is stored. Plotting this pulse's histogram in the same way as the particle density or T.A.C. pulses shows that the Analogue Multiplexer and A.D.C. gains are remarkably stable and vary by no more than about 0.1% over a period of several days.

5.10 The Time Sequence of Events in the Data Processing Cycle

From the instant an event occurs to it being finally, and as completely analysed as it can be, could take from three days to one or two weeks and consequently this is the order of the turn-around time and because of this there is the necessity to monitor as many variables as possible in the laboratory whilst the data are being acquired. In this way faults can

be rectified in a short time whereas if the computer output was awaited before repair several days of useless data would have been acquired in the meantime.

Figure 5.9 gives the time sequence of events on a logarithmic plot in the processing of the array data from its acquisition to final analysis.

5.11 Summary

In this chapter the processes by means of which the data, as they appear in the laboratory as dynamic or static quantities, are temporarily stored in the Analogue Multiplexer or Data Gates are coded and stored in the D.U.S.T. buffer memory have been discussed. The stage where the digitised data are then written on to a magnetic disc for more permanent storage has been described and how all of the array electronics is daily monitored, to ensure total efficiency of the system, has also been presented.

The sequence of operations to which the analogue signals are subjected are necessarily very important and must be fully understood to ensure that erroneous data will not be analysed in the final stages of an event's progress through the experiment. It is hoped that every aspect of the pulses' progress have been sufficiently investigated so that the digitised data contain no contamination that is not well known and cannot be eliminated.

Event occurs. Dynamic data begins to accumulate.

Dynamic data reaches laboratory & persists on A.M. inputs.

Event established. Dynamic data stored in A.M.

Static and Dynamic data coded and stored in the buffer memory. D.U.S.T. paralysed.

A.M. cleared. D.U.S.T. unparalysed. Ready for next event.

After 11th event D.U.S.T. is paralysed and the memory emptied. D.U.S.T. is then unparalysed & ready for next event.

Digitised data resides on magnetic disc.

Data transferred to magnetic tape or private disc.

Data analysed.

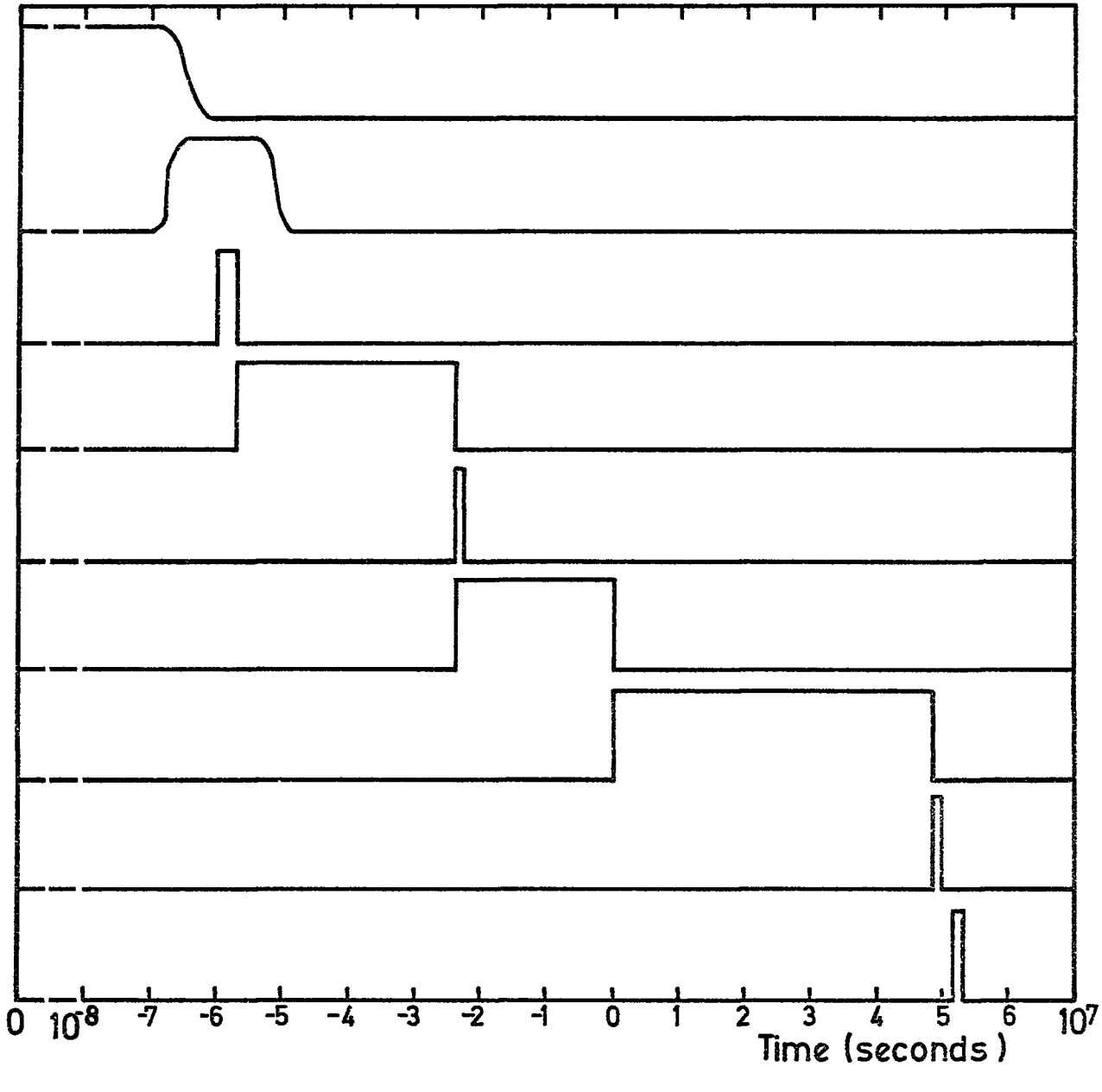

Figure: 5·9. Time sequence of the processing of an air shower event.

CHAPTER SIX

THE DATA ANALYSIS

6.1 Introduction

Using the techniques described in the preceding chapters it has been shown how the data relevant to an air shower event are coded and stored on a magnetic disc on an IBM 1130 Computer. This chapter is devoted to the data's interpretation by computer methods and takes the form of describing how these data are prepared for, and interpreted by, the analysis programmes. The data from the magnetic disc, in their first stage of analysis, are transferred to either magnetic tape or a private disc and stored in the Northumbrian Universities Multiple Access Computer's (N.U.M.A.C.) archives where they remain until required for analysis.

6.2 The Aims of the Analysis

In general there are several quantities that can be deduced from the digitised data for each event:

(i) the times of arrival of the shower front at the timing detectors,

(ii) the nominal particle densities at each detector in terms of electrons per square metre, and

(iii) the Data Gate information.

It is the object of the analysis procedures to reduce these data into quantities that yield as much information about the individual air shower as possible. Such parameters include:

(i) the arrival direction of the shower front,

(ii) the radius of curvature of the shower front,

(iii) the shower core position, and

(iv) the electron shower size.

The analysis of the data are carried out on the N.U.M.A.C. IBM 370/168 computer and is done in several stages. Briefly, these are to convert the

raw data, as initially assembled on the IBM 1130, into a form that can be handled by the IBM 370/168. This involves the conversion of the data into pseudo card images such that, as far as N.U.M.A.C. is concerned, the data are on cards. These data are then sorted into groups ('runs') and statistical quantities are calculated on these to monitor the data handling electronics and for use in internal calibration. The analysis is then performed according to the amount of data available for each event. The sequence of the analysis is important: data are first calibrated and converted into useable quantities, the shower arrival direction is then calculated followed by the core location and shower size.

6.3 Methods of Analysis

There are several methods by which air shower data can be analysed, but in general their aims are the same and these are to find the best estimates of the parameters from the data available. In every case accuracy is the main concern and thus primary assumptions about the raw data(that is, calibration) need to be correct since if not they may cause erroneous interpretations of what actually occurs at the detectors. Accuracy of the various shower parameters can be considerably improved by employing more detectors since then large fluctuations in particle density or timing measurements at individual detectors will not severely bias the eventual calculated quantities.

Numerical minimisation methods are techniques most widely used in the analysis of air shower data (see, for example, Dennis, 1964, Komori, 1975a, Kaneko, 1975) and in particular a Chi-squared minimisation is most often employed. Analysis of the Lodz array data (J. Wdowczyk, private communication) is a two stage process that initially finds an approximate core location using a simplified structure function and then uses this value as a starting point for a more detailed analysis using the Greisen (1960) lateral structure function. The Tien Shan analysis algorithm locates the

shower core using the assumption of shower radial symmetry and the monotonic decrease in the radial density of shower particles (Aseikin, 1975b).

6.4 The Analysis Procedures

The main features of the analysis programmes lie within the very versatile and comprehensive minimisation package (§6.4.2) in which a theoretical description of an air shower's structure is fitted to the observed quantities as measured by the various detecting elements in the array. This is enabled by initially converting the raw data into accurately calibrated quantities which necessitate a thorough understanding of the acquisition electronics at the detector and of the data handling in the laboratory. A second major feature of the analysis routines are that they can automatically compensate for any drifts in the acquisition electronics that may not have been corrected for in the laboratory or that are not capable of manual adjustment.

6.4.1 The Analysis Programme

The entry to the analysis programmes begins by calling the controlling subroutine CONTRL which directs the way in which the analysis routines are called depending on the analysis codes. These codes are read from a single line file which is also used to store the last analysed events run number and event number. These codes allow for various degrees of analysis and for the testing of the programmes with simulated data. The run number and event number of the last analysed event are stored such that event analyses are not duplicated. Upon entry to CONTRL an internal clock is started, to monitor the Central Processing Unit (C.P.U.) time consumed, the analysis codes are read in after which a title page is printed.

The various degrees of analysis allow either for a quick summary of the data in the data file, a summary and data print out (that is, no minimisation) or a full analysis including minimisation. Figure 6.1 shows a simplified flow chart of the analysis routines that are at present

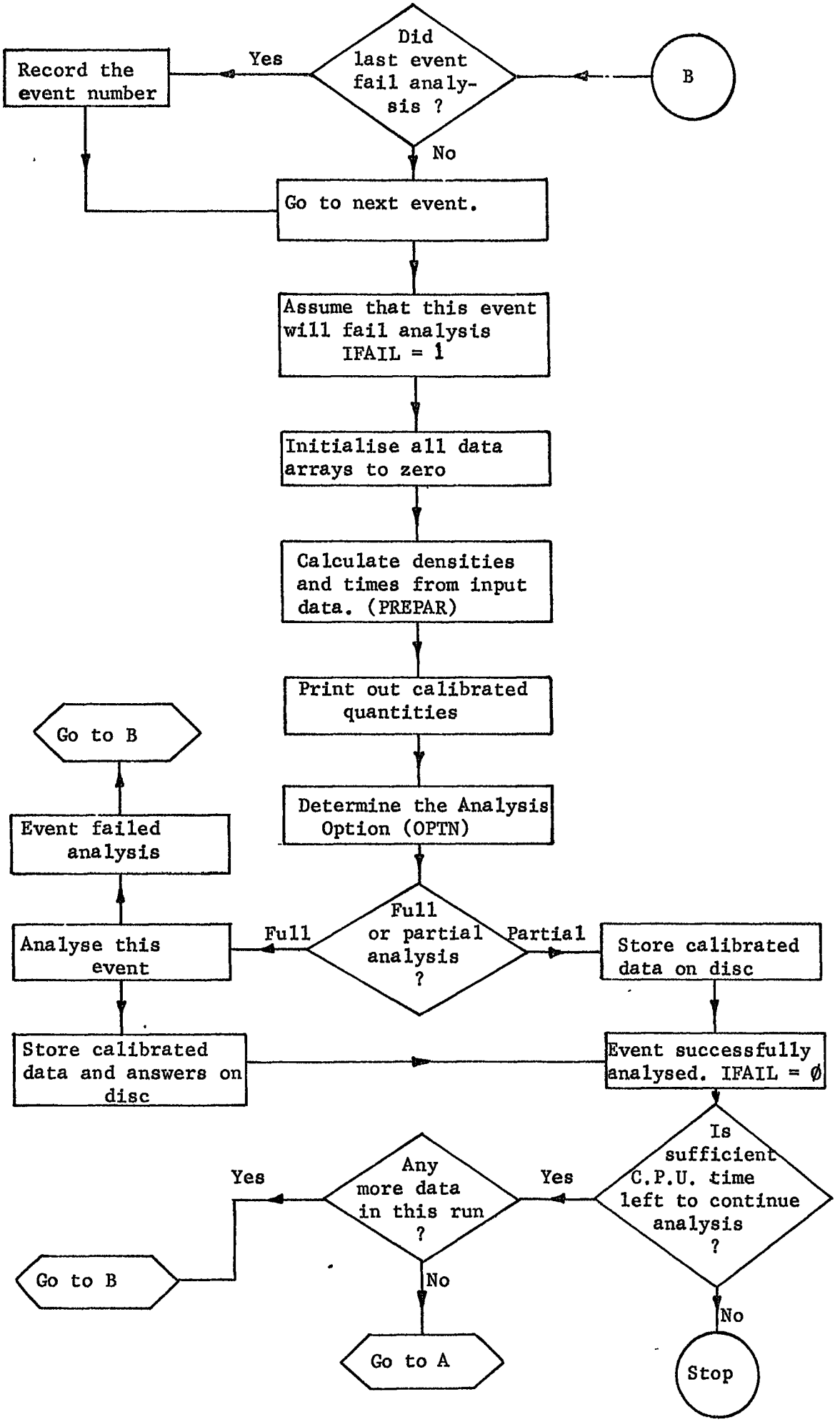
Did last event fail analysis ?
Yes
Record the event number
B
No
Go to next event.
Assume that this event will fail analysis IFAIL = 1
Initialise all data arrays to zero
Calculate densities and times from input data. (PREPAR)
Print out calibrated quantities
Determine the Analysis Option (OPTN)
Full or partial analysis ?
Full
Partial
Analyse this event
Store calibrated data on disc
Event failed analysis
Go to B
Store calibrated data and answers on disc
Event successfully analysed. IFAIL = ∅
Is sufficient C.P.U. time left to continue analysis ?
Yes
No
Stop
Any more data in this run ?
Yes
No
Go to B
Go to A

available and which are discussed in this chapter.

A full analysis begins by summarising all of the data present on the input file. The summarising subroutine produces a table that indicates which runs are present, how many events are in each run and where in the data file are the first and last events in each run. If no data are found in the specified data file then a message is printed and the programme terminates. This routine also checks for spurious runs that contain less than one D.U.S.T. core load of events (< 11) which would indicate a Run Number Data Gate fault. If any such runs are found they are added to the previous run and a revised summary table is printed. The summary table is used in several of the other routines to help in the data manipulation. Upon a successful exit from this routine the run in which the last analysed event occurred is found. This run's data are then read into an internal array by subroutine READ which also decodes the Trigger Mode and Operational Units Data Gate information. This routine also checks on the purity of the data and prints messages if any of the data looks impure. Such messages are printed if run numbers occur out of sequence (indicating a Run Number Data Gate fault), if event numbers occur out of sequence (indicating an Event Number Data Gate fault), if the Analogue to Digital Converter has not been cleared at the end of the last acquisition cycle of the previous event or has picked up between events (which would result in all of the data gate information in an event being in error) and if the data have been read in incorrectly from the source file. A message is also printed which indicates the number of events to be analysed in the current run being analysed. If the source file contains no data, as a result of it being erased or being full of zeroes, the analysis is terminated. These error messages are printed primarily to instruct the person viewing the computer output that he should be aware of the several faults in it and do not, in any way, attempt to correct the data before it is analysed.

A similar procedure to the daily 1130 histogramming is carried out following the data summary by subroutine COEFF. The routines that make up COEFF are very versatile histogramming programmes which can be instructed to display histogrammes of the input data and to calculate various statistical quantities for each Analogue Multiplexer input. For each Analogue Multiplexer input, the mode, mean and the standard deviation on the mean are calculated and returned to the main programme. These values serve a dual purpose. One is to monitor the state of the Analogue Multiplexer data and the other is to provide coefficients which may be used for internal calibration. These values are printed out and stored for future use.

When the monitor coefficients have successfully been evaluated the main analysis routine ANALYZ is entered. This routine is the main calling routine for the various analysis option fits and the analysis remains in this routine until the preselected C.P.U. time limit has been reached, as read from the internal clock. A previous routine has found the location in the data file which corresponded to the last event that was analysed. ANALYZ then begins analysing from the next record in the data file. The first stage in the analysis is to convert the data, as stored in the internal data array, from the integer data that it now is, which are essentially the numbers that were presented to D.U.S.T. by the A.D.C., into relative times of arrival of the shower front at the various detectors and particle densities as measured at each density sampling detector. To do this subroutine PREPAR (i.e. 'prepare') is called from ANALYZ. PREPAR first takes one event's timing data and subtracts from it the correspondong mode value of the T.A.C. distribution as evaluated in COEFF. This mode value represents time delays due to pulse propagation down cables and through electronic devices in the laboratory and is thus a constant quantity for this run and should be for the duration of the experiment. It is, however, recalculated for each run because of the possibility of drifting in the electronics, temperature induced propagation delays in the pulse carrying cables and because electronic

devices may have been damaged or altered in some runs as a consequence of maintenance. Figure 6.2 illustrates the time calibration procedure for the case when the timing detectors are not coplanar. It is found that these modal values do not change by more than two or three A.D.C. channels from one run to the next. The timing data thus obtained are now in terms of positive and negative A.D.C. channels. The appropriate combined calibration coefficient for the A.D.C., T.A.C. and Analogue Multiplexer (nS/channel) is then applied followed by a further term which adjusts the time values to their correct values should the Analogue Multiplexer output amplifier or A.D.C. have drifted away from their calibration values. This final term is obtained from storing a pulse of standard height with each event collected in the laboratory and comparing its average value over all the run with the calibrated value.

In a similar manner the density data for one event are taken and calibrated using the standard pulse and the combined 100 mV $p^{-1}m^{-2}$, A.D.C. and Analogue Multiplexer calibration factor. Application of a calibration coefficient obtained from COEFF is more difficult in this case owing to the greater statistical variation in the mean of each Analogue Multiplexer distribution. For this reason no adjustment of the density data are made but instead a daily check is made on the 1130 histograms (§5.9) to ensure that the various means are within the range that they should be. This routine then prints out the calibrated data as it now stands, along with the decoded Data Gate information, ready for the appropriate analysis. Subroutine PREPAR also checks for the presence of data and the saturation of detectors and adjusts the operational units arrays such that the appropriate detecting element will or will not be included in the minimising procedures. The total number of useful timing and density detectors are calculated to be used in the next routine that determines the analysis options to be used.

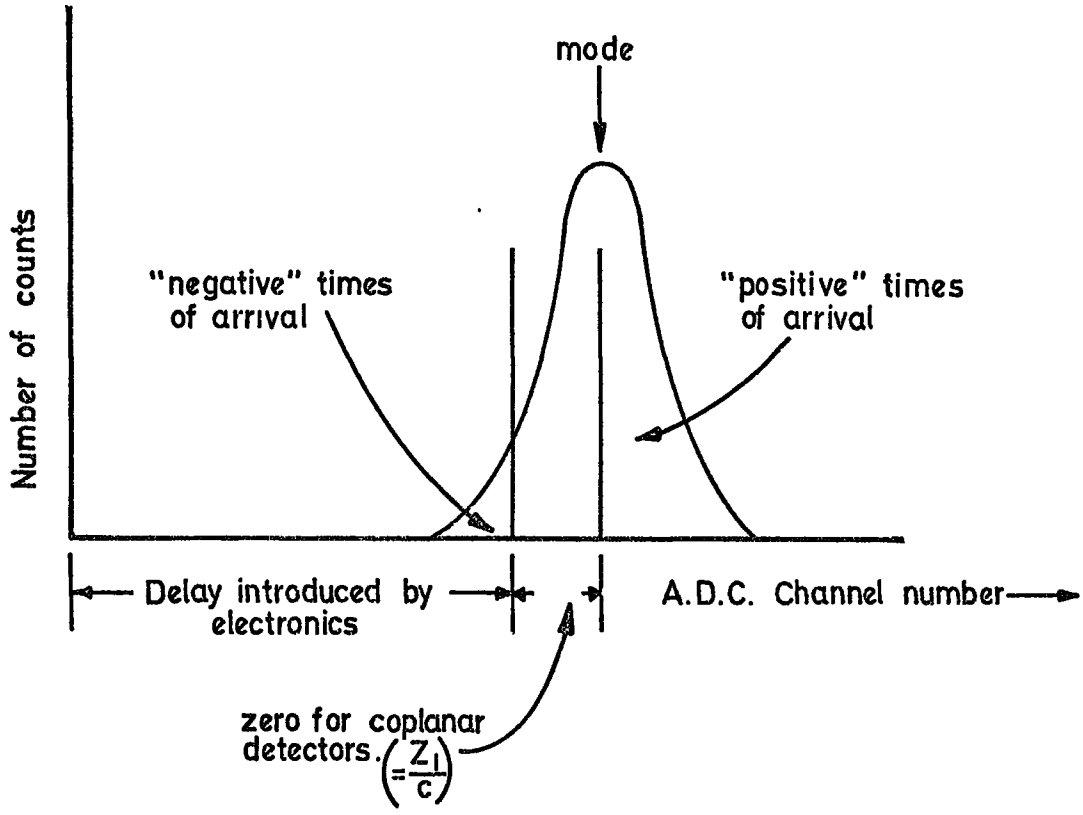

Figure 6.2. A schematic of a T.A.C. distribution.

There are four possible ways in which an event's data can be analysed. The various options depend essentially on the amount of data present and are given in Table 6.1 along with the quantity of data that are required for each option. The option chosen is then used in ANALYZ so that it may route the analysis according to the most appropriate analysis. After the analysis of each event by the minimising routines (§6.4.2) the answers are written out and a time check made to see if sufficient C.P.U. time remains for further events to be processed and analysed.

The several analysis options have been designed to make the greatest use of the available data. Analysis option 2, which is a three parameter fit to the density data with assumed zenith and azimuthal angles is not expected to yield accurate results. It is used such that some parameters may be derived from an event that would otherwise be considered unuseable.

6.4.2 The Minimisation of the Array Data

The basis of the analysis programmes lie within the minimisation routines. These comprise the C.E.R.N. programme MINUIT (James and Roos, 1971) which is a very versatile and powerful collection of programmes. Satisfactory performance of this programme is achieved through the use of various internal checks which ensure that minimisation of the appropriate function is being carried out correctly. If MINUIT fails to converge after a preselected number of tries (16,000) the attempt will terminate and the last parameter values will be returned.

In the case of the arrival direction minimisation of the timing data, t_i, from those detectors that are operational are fitted to a plane in three dimensions using a least squares technique. Because the air shower array is only 120 m in diameter the measurement of the radius of a shower front is very difficult. The typical deviation in times observed at the detectors from those of a plane would be about (6/R) nS where R is the radius of the shower front in kilometers. This deviation is thus too

Table 6.1

The Analysis Options

Analysis option	Meaning	# Times	# Densities
1	Insufficient data for analysis. No analysis done.	< 2	< 5
2	Insufficient timing data for full analysis. Three parameter (X_c, Y_c, N) fit to the density data, Θ assumed to be 0°.	< 2	≥ 5
3	Timing data used to calculate (Θ, ϕ).	≥ 3	<3
4	Full analysis. Timing data used to calculate (Θ, ϕ). Density data used to calculate (X_c, Y_c, N).	≥ 3	≥ 3

small to be measured with the present array and clearly justifies the shower plane approach. For a shower front of radius R (km), zenith and azimuthal angles (θ,ϕ) passing through detectors with coordinates $\underline{x}_i$ and $\underline{x}_j$, the time difference of the arrival of the shower front (t_i-t_j) can be given in

$$(x_i - x_j)l + (y_i - y_j)m + (z_i - z_j)n + c\left[(t_i - t_j) + \frac{(\underline{r}_i \cdot \underline{r}_i - \underline{r}_j \cdot \underline{r}_j) - c^2(t_i^2 - t_j^2)}{2R\,c}\right] = 0 \qquad (6.1)$$

where $l = \sin\theta\cos\phi$

$m = \sin\theta\sin\phi$

and $n = \cos\theta$

If the jth detector is used to define the spatial and temporal origin (see figures 6.3(a) and 6.3(b)) equation 6.1 reduces to

$$x_i l + y_i m + z_i n + c\left(t_i + \frac{(\underline{r}_i \cdot \underline{r}_i - c^2 t_i^2)}{2R\,c}\right) = 0 \qquad (6.2)$$

Clearly for $R = \infty$ the second term in the brackets disappears leaving

$$x_i l + y_i m + z_i n + ct_i = 0 \qquad (6.3)$$

which is uniquely soluble for two relative times and whose solution is given in Appendix A.

This analytical approach is perhaps the most efficient method to use in the case of 3 operational timing detectors since then there is a unique solution for (θ,ϕ). When the number of timing points exceed three a unique solution may not be possible owing to errors in the timing values. In this case a numerical minimisation approach can be useful and this is the technique employed. To simplify the analysis programmes a little, the numerical method is also used for three point fits as it is very efficient and does not require further programming.

The minimisation method involves the minimisation of the function

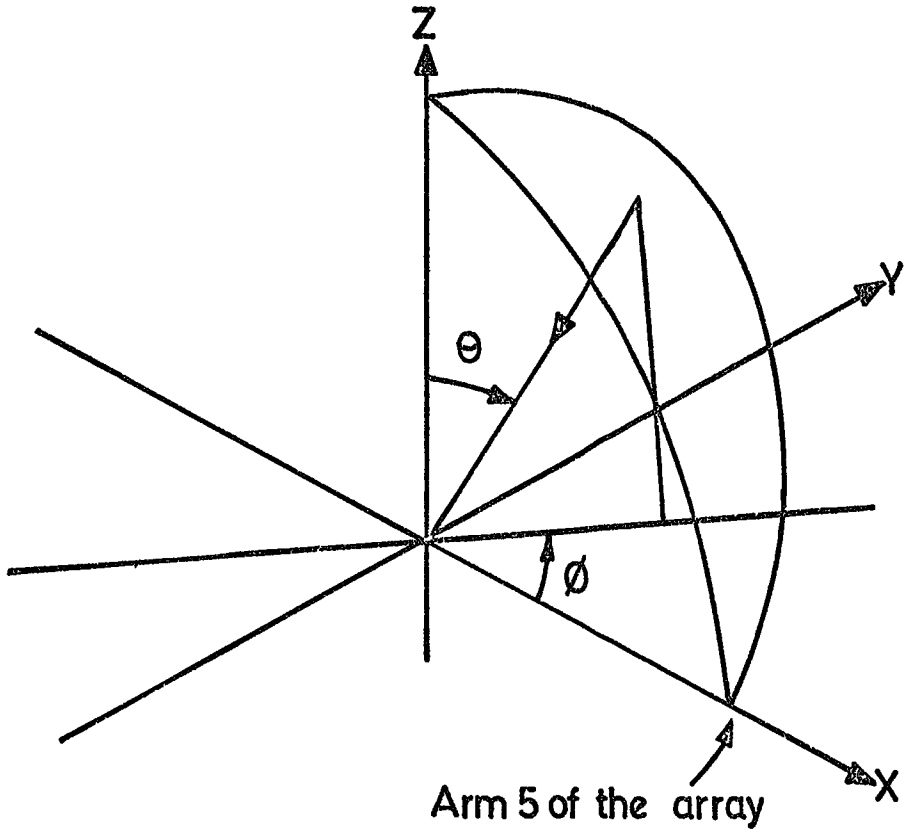

Figure: 6·3(a). The spatial co-ordinate system.

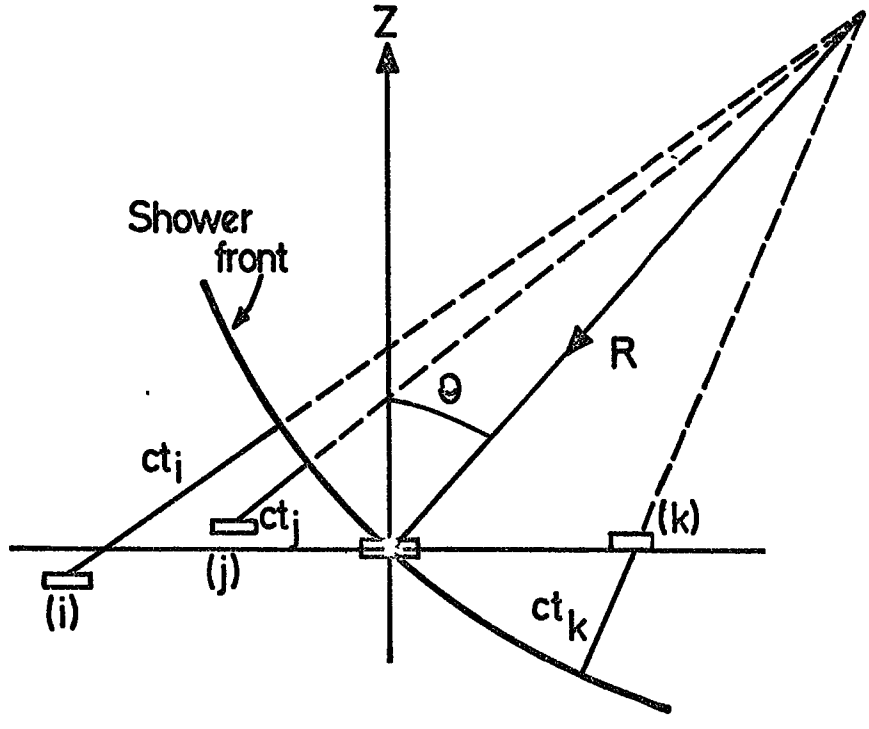

Figure: 6·3(b). The timing measurement convention.
(t_k is negative).

$$F_1 = \sum (t_{obs} - t_{calc})^2$$

with the summation extending over all operational timing detectors. Once a fit to the timing data has been completed (whether "successful" or not) and if there are sufficient density detectors operational the analysis proceeds by fitting a shower structure function to the density data by minimising the Chi squared function:

$$F_2 = \sum \frac{(\#_i calc - \#_i obs)^2}{\varepsilon_i^2 calc},$$

where ε_i calc is the estimated error on the calculated number, (see Appendix B). and $\#_i$ means particle number at the ith detector.

The structure function used in the core location procedures is that due to Hasegawa (1962) and was considered most appropriate for the initial analysis of the shower data since this distribution represents the air shower structure as obtained from plastic scintillator detectors.

In this stage of the analysis, the core location and shower size are minimised together as three independent variables. A typical option 4 analysed event is shown in figure 6.4 in which the various quantities are explained. The figure shows the calibrated input and the calculated answers.

6.5 Other Programme Features

6.5.1 The Handling of Multicore Events

The present array is insensitive to multiple cores in air showers but in those cases where the Chi-squared surface have local minima, which could be interpreted as sub-cores, precautions are taken to ensure that they are not returned as final answers. Only global minima are required and these are taken to represent the best fits to the observed data. The method used to make the programme jump out of a local minimum is that due to Goldstein and Price (1971) which consists essentially of transforming the function by dividing it by its quadratic part and thus removing the local minimum. The programme then proceeds to seek a new minimum. In

The numbers in brackets to the right of a time or density measurement refer to the Operational Units Data Gate.

1 = acceptable measurement, 2 = electronic fault in the D.U.S.T. read in of the number, (unacceptable measurement), 3 = density detector saturation.

The input density data (m^{-2}) of 21 values. 7 are at present unused.

Event no. — Run no. — Time of the event (clock not included in this event)

The input timing data (nS) (8 values)

```
E#: 5757073    R#:   59    TIME:***D**H**M**.***SECS.  TRIGGER MODES: 0,0,0,0,0,1,0,0
  0.0      (1)   0.0      (0)   0.0      (0)   0.0      (0)   8.74E 00 (1)   0.0      (0)   1.13E 01 (1)   0.0      (0)
  1.69E 01 (1)   0.0      (0)   2.42E 00 (1)   0.0      (0)   3.30E 01 (1)   0.0      (0)   4.99E 00 (1)
  6.22E 00 (1)   0.0      (3)   1.73E 01 (1)   3.03E 00 (1)   3.75E 00 (1)   6.43E 00 (1)   0.0      (1)
  0.0      (0)   0.0      (0)   0.0      (0)   0.0      (0)   0.0      (0)   0.0      (0)   0.0      (0)
** ANALYSIS OPTION 4 **
 -0.0             3.05E 01       4.77E 01       2.47E 00       8.74E 00      -5.15E 00       1.13E 01       1.55E 01
  5.34E 00        2.49E 02       2.70E-08
  2.85E-01        4.59E 00
NO. OF POINTS USED IN CALCS. = 3.
  1.62E 01        8.99E 00       2.61E 00       5.24E 01       3.28E 01       9.79E 00       2.68E 00
  5.48E 00        8.24E 02       1.60E 01       6.10E 00       6.64E 00       7.94E 00       2.06E 00
  1.62E 01        1.62E 01       1.62E 01       1.62E 01       1.62E 01       1.62E 01       1.62E 01
  2.66E 01        1.02E 01       3.80E 05       1.18E 01
  1.94E 00        4.42E 00       4.50E 04      -4.03E 04
NO. OF POINTS USED IN CALCS. =10.
```

x_c = 26.6m

y_c = 10.2 m

N = $3.8.10^5$

X^2 = 11.8

θ = 5.3°

ϕ = 249°

Least squares = 2.710^{-8}

The densities that should have been observed based on the (θ,ϕ) and (x_c, y_c, N) that have been calculated. The line or 1.62 E01 refers to detectors that have not yet been included in the array and have been temporarily assigned coordinates of (0,0,0).

The times (nS) that should have been observed based on the (θ,ϕ) calculated.

FIGURE 6.4 A typical Option 4 analysed event

effect the method causes the programme to jump out of a good minimum to find a better (deeper) one. If this search is unsuccessful it is assumed that the lowest Chi-squared has been found and this point is then related to the best estimate of the core position and shower size.

6.5.2 Contour Printout

If a printout of the contours used in the minimisation is required then a suitable command to the minimisation routines will do this. Figures 6.5(a) and 6.5(b) show sets of contours corresponding to the fitting of a plane to the timing data and of a shower to the density data.

6.6 Checking the Analysis Programmes with Simulated Data

Prior to the full implementation of the final analysis programmes tests were done to find out how well they responded to simulated shower data. Showers were simulated on the computer according to the Greisen (1960) lateral structure function (equation 2.1) and fired at the array at random zenith (modulated by a $\cos^{7}\Theta$ distribution) and azimuthal angles with random core locations to $\pm$ 100 m of the central detector. Errors on the times of arrival of the shower front and on the particle numbers were included in these simulations to a maximum of plus or minus five standard deviations and were modulated with a gaussian distribution, in the case of the times, and a poissonian distribution in the case of the particle number measurements. By examining the programmes' performances in this way, systematic effects introduced by the analysis could be identified and eliminated at some later stage.

6.6.1 The Arrival Direction Evaluation

The relative times of arrival of shower fronts as they pass through the array were simulated according to equation 6.3 and for each time measurement gaussian errors with a standard deviation of $\pm$ 5nS were introduced into them to a limit of $\pm$ 50. The computer analyses of these data into the shower arrival directions are shown in figures 6.6(a) and 6.6(b) for zenith angle θ and azimuthal angle ϕ. It is seen that for zenith angles

(a)

(b)

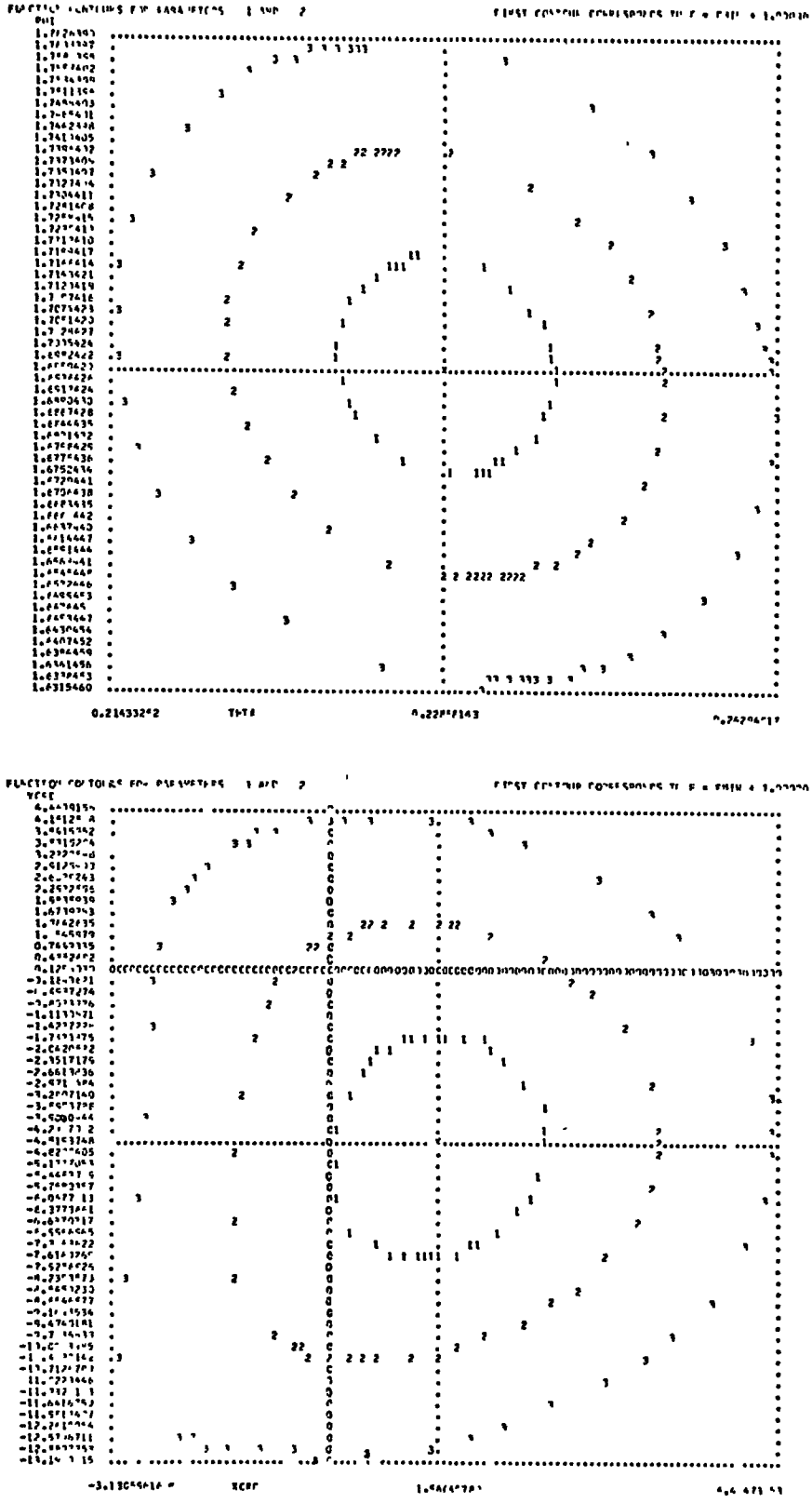

Figure 6.5. Typical computer contours for an analysed event.
(a) Least squares contours (Θ,Φ)
(b) Chi squared contours (X,Y,N)
The axes are scaled to enclose the third contour.

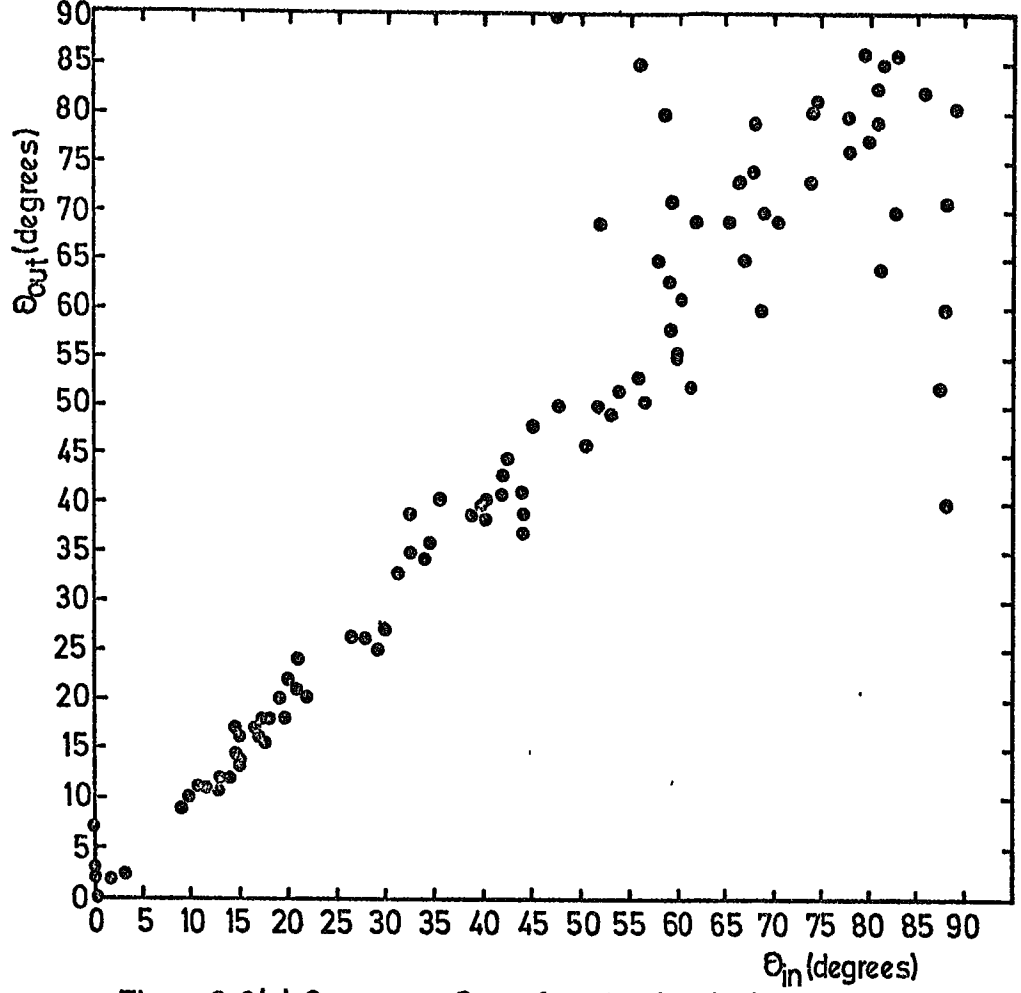

Figure 6.6(a). Θ_{in} versus Θ_{out} for simulated showers.

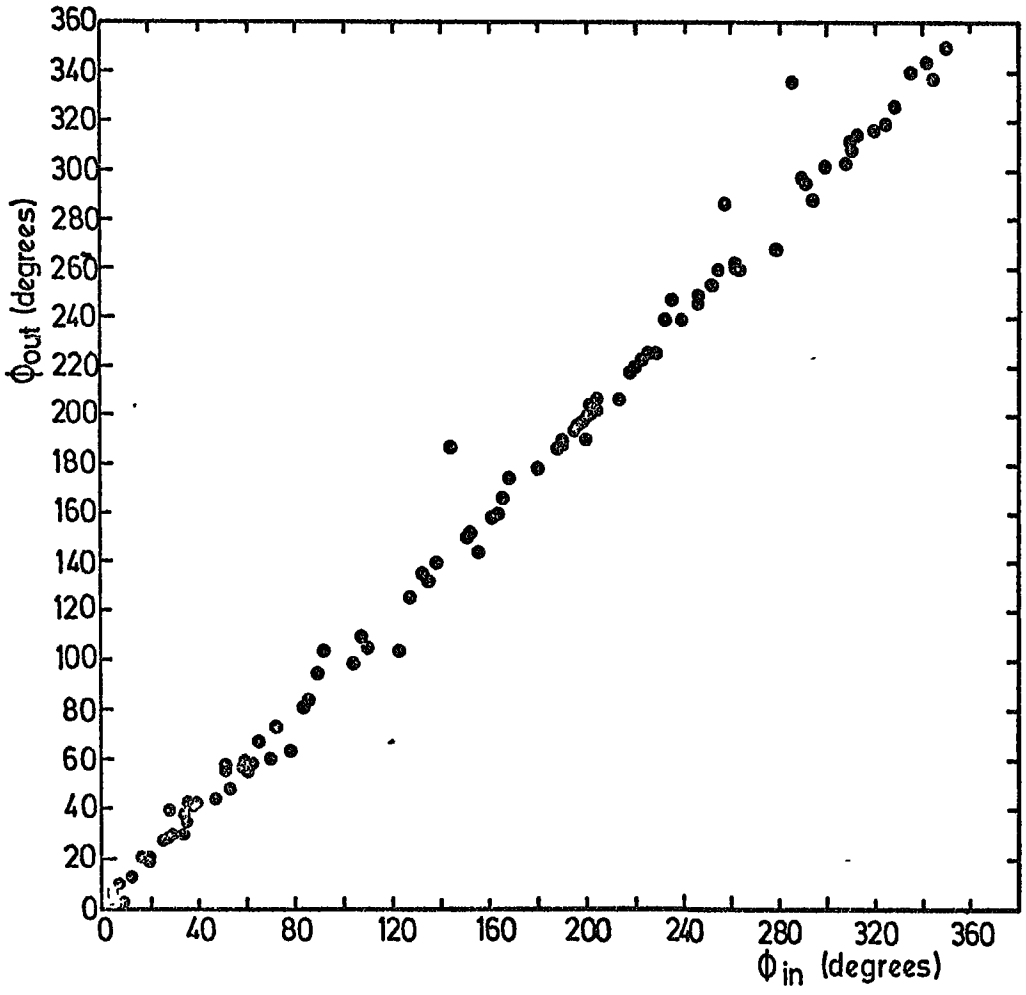

Figure 6.6 (b). ϕ_{in} versus ϕ_{out} for simulated showers. The three points off the main line had $\Theta<5°$.

greater than about 40^{o} the error on them becomes excessive. Consequently showers whose zenith angles exceed 30^{o} are not considered as suitable events with which to produce final spectra. These data refer to fits using only three timing values (three point fits). Four point fits are found to give better angular accuracy. The maximum error on the zenith angles is seen to be $\pm 3^{o}$ ($\theta \leqslant 30^{o}$) whilst that for the azimuthal angles is $\pm 7^{o}$.

6.6.2 Core Location Evaluation

Using the method described in §6.6 of simulating air showers in the locality of the array the shower axis coordinates before and after analysis were compared. Figure 6.7 shows the results obtained from showers whose axes were analysed to be within $\pm$ 100 m of the central detector and whose zenith angles were analysed to be less than, or equal to, 30^{o} for a shower of size 10^{6} particles. Errors on the number of particles incident upon each of the 11 detectors used in the simulation were modulated according to poissonian statistics, again to a $\pm 5\sigma$ limit. The figure shows than an accuracy of about $\pm$ 10 m can be obtained from the analysis programmes for this number of detectors employed and for showers that fall near to the centre of the array.

6.6.3 Shower Size Evaluation

From simulation of air shower events it is found that air showers are not, in general, analysed to give the correct (input) shower size but rather a distribution of shower sizes centred on the input value. This is because showers that fall at large radial distances can be analysed as being smaller showers within the array acceptance. The mean shower size of those showers that have been analysed as within the array acceptance is plotted in figure 6.8 against the shower size input. Figure 6.9 shows the ratio of the number of showers fired in the region of the array that have satisfied the array acceptance, to the number of showers as being analysed

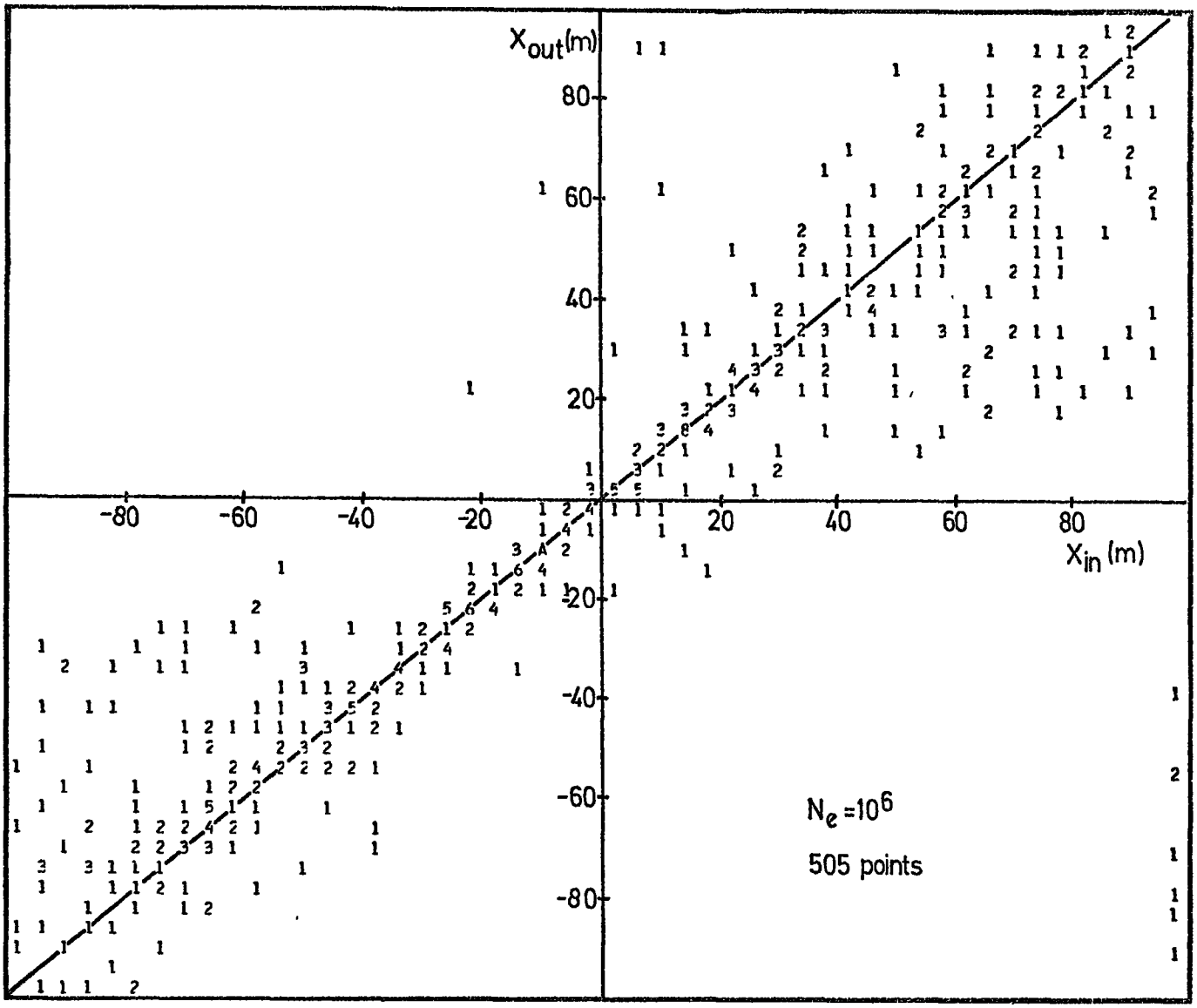

Figure 6.7 A computer plot of many simulated air shower events input and output core location coordinates clearly showing the poor core location accuracy for showers falling outside the array. ($\theta \leq 30°$).

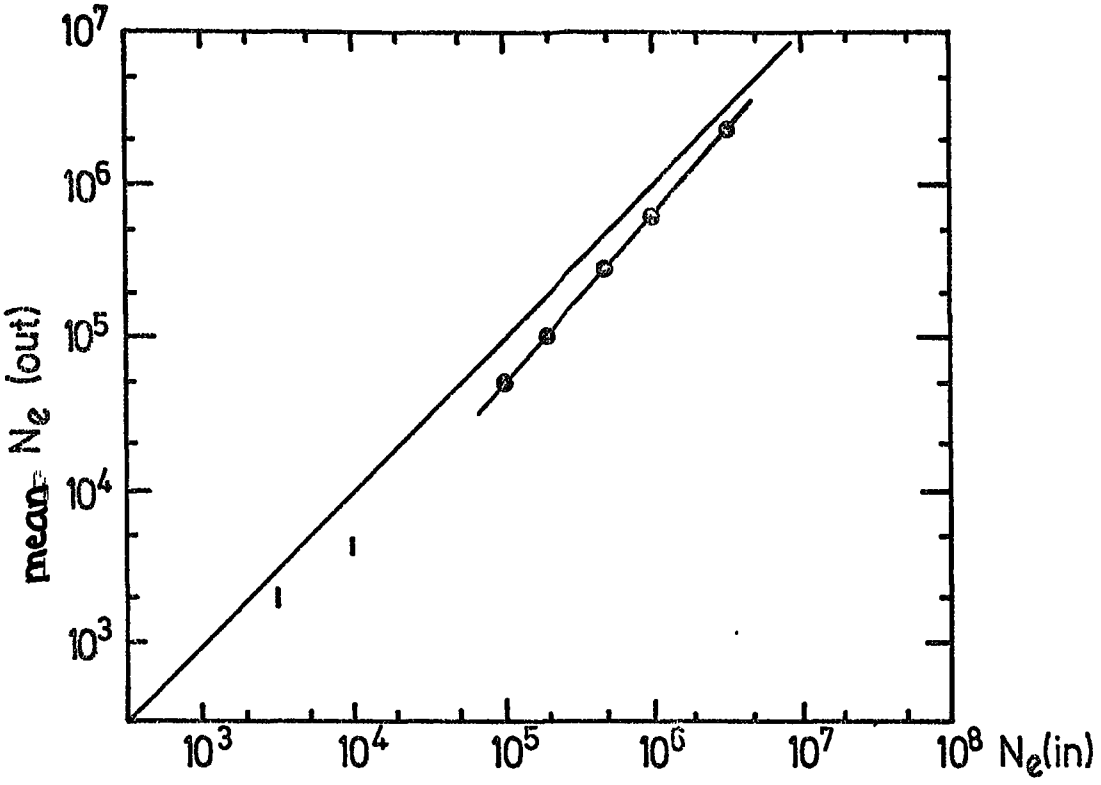

Figure 6.8. The response of the analysis programmes to simulated shower data. N_e(in) is the shower size fired at the array. N_e(out) is the analysed shower size.

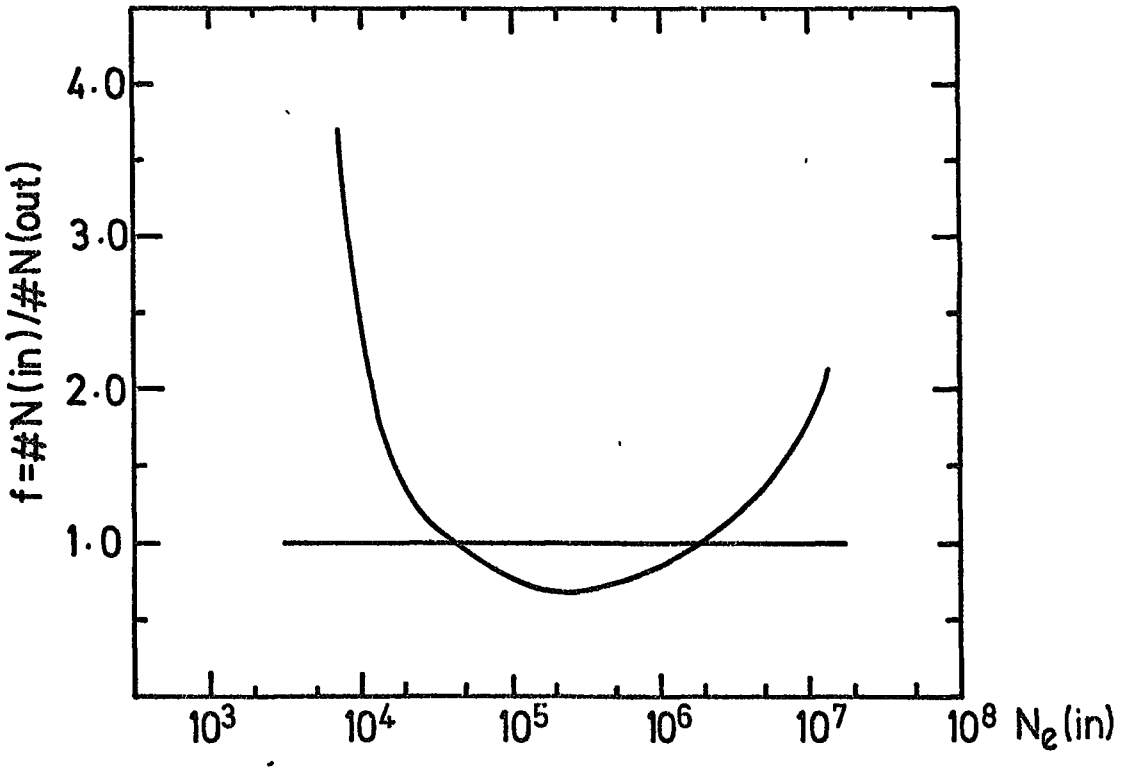

Figure 6.9. The response of the analysis programmes to simulated shower data. For a number of showers fired at the array of size N_e (in) a fraction f_i^{-1} are returned as being within the array acceptance. (Array triggering probability = 1.0).

within the array acceptance. The increase in f, for small showers, is due to the inefficiency of the analysis, essentially caused by the small number of detectors that contain particle density information, that makes minimisation more difficult. This makes the analysis programme attempt to fit larger showers at greater radial distances than correspond to the input values. The increase in f for large showers is due to more and more particle density detectors becoming saturated and consequently eliminated from the analysis procedures. Air showers with sizes greater than about 3.10^7 particles would, at present, saturate all of the detectors and thus be impossible to analyse.

These figures are used to remove systematic effects from the shower size spectrum which have been introduced as a consequence of the method of analysis and will be discussed again in Chapter Seven.

6.7 Analysis of Peripheral Experiments' Data

The data from the other major cosmic ray research programmes in the laboratory, M.A.R.S. (§3.6) and the Hadron Chamber (§3.7) are analysed independently of the array data. The Hadron Chamber data are collected photographically and thus each event is manually scanned during which the event is interpreted. The M.A.R.S. data acquisition and analysis follows closely the array method in which data are digitised and transmitted to the on-line IBM 1130 computer for storage and later analysis. The M.A.R.S. analysis has been described in detail in Wells (1973) and so only the basic features will be described here. For analysable events, which are uncontaminated by more than one muon and an excessive number of discharged flash tubes in the flash tube trays, the muon's momenta and sign are computed. A parabolic fit to the discharged tubes is attempted; the radius of curvature of the parabola being related to the muon momenta and the direction of curvature gives the sign of the muon's electronic charge. The maximum detectable momentum of M.A.R.S. is in excess of 5000 GeV/c and so this experiment can provide good accuracy for muon momenta less than this.

Included in the array analysis routines, and in the array electronics in the laboratory, lies the provision to time the arrival of high energy muons in M.A.R.S. with respect to the shower front. The time measurements are taken in a similar manner to the fast timing techniques described in §5.2.2 except that the muon time of arrival, detected by the bottom scintillator in M.A.R.S. (figure 3.6), is not used in establishing the shower zenith and azimuthal angles. What is done with the time measurement is to calculate the time difference between the arrival of the muon and the shower front at the same point. Hopefully this will be used to extract data on the height of production of muons and on their transverse momenta but the experimental arrangements in existence at present suggest that no data of any great detail can be obtained.

6.8 Summary

This chapter has shown how useful quantities are obtained from the laboratory acquired values and how these data are manipulated by the analysis programmes into parameters which characterise air shower events. The programmes have been shown to satisfactorily analyse these data by simulating air shower events on the computer and the versatility of the powerful analysis programmes has been illustrated. The following chapter describes how the analysed data are used to produce useful cosmic ray spectra and quantities of physical interest.

CHAPTER SEVEN

THE INTERPRETATION OF RESULTS

7.1 Introduction

Analysed data from the array are stored in data files separate from the original shower data and both are eventually dumped on to magnetic tape for permanent storage. Access to both the pre-analysis and post-analysis shower data is simply a matter of loading the appropriate data file on to a magnetic disc. These data files tend to be identified by their run numbers which indicate a particular set of events collected, over a period of a few days, under the same acquisition conditions. Each of the runs are analysed separately before being grouped together to increase the statistics of any particular distribution since some runs' data may not be considered suitable for some applications, for example in producing the shower size spectrum. The analysed data that is stored on magnetic tape, contains all of the information that is shown in figure 6.4, in a format that allows for efficient storage and economy of filespace.

As yet the air shower data represent only a preliminary evaluation of the array's capabilities and consequently the statistical accuracy of any measured parameter will have to be poor until many more events have been acquired and analysed.

7.2 Data Classification

The various analysis options, shown in Table 6.1, give a broad division of the air shower data into four main groups. Each group is defined by the amount of dynamic data (§5.2) that was recorded and stored with each event. Consequently, showers which were recorded in many detectors will be capable of being analysed more accurately than if not. Further classifications of the shower data are necessary and these may be defined by the restrictions imposed in manipulating the data to investigate particular shower properties and are defined in Table 7.1.

TABLE 7.1

Classification of the analysed air shower data

Class	Meaning
A	Well defined events: showers whose axes fall within the region of ~ 100% detection probability.
B	Well defined events but unsuitable for inclusion in the shower size spectrum.
C	Option 2 data: events useful only in conjunction with M.A.R.S. data.
D	Options 1 and 3 data, failed events.

7.3 All Shower Data

The daily monitoring of the array yields data relevent to showers but which may not be reduced to give information pertaining to any individual event. The quantities that are continuously monitored (§5.9) are such that the overall performance of the array and the data acquisition can be maintained in a satisfactory state. The daily 1130 histogramming systems check does provide useful data that, in the case of the Time to Amplitude Converter (T.A.C.) spectra (§5.9), may be indirectly related to the zenith angle distribution of showers. The density histograms cannot easily be related to the gross features of the average shower detected by the array and are consequently used only to monitor the state of individual detectors.

7.3.1 The Zenith Angle Distribution of Showers

The zenith angle dependence of showers is due to the absorption effect by the atmosphere on the air shower. With the increase in the amount of matter traversed, as the zenith angle increases, showers soon reach their maximum and die away. The dependence is most usually represented by

$$I(\theta) = I(0) \cos^{n}\theta \quad m^{-2} s^{-1} sr^{-1}. \qquad (7.1)$$

where $I(\theta)$ is the intensity of showers at a zenith angle θ and n is a function of shower size. Data from the daily accumulated T.A.C. spectra may be related to equation 7.1 through the histogram widths. Figures 5.8b and 6.2 illustrate what T.A.C. distributions look like. If showers are collimated to be progressively more vertical then the width of the distribution would decrease, hence $n = n(\sigma)$.

T.A.C. spectra were simulated on the computer by a process of firing showers (with an infinite radius of curvature) at the array according to the appropriate zenith angle distribution. Each of the T.A.C. distributions have different widths since each timing detector has different coordinates in space and thus each must be individually investigated. To obtain the simulated T.A.C. spectra 10,000 showers with gaussian errors to plus or minus five standard deviations (one standard deviation is 5nS) were fired at the array. For each distribution the standard deviation was calculated and plotted as a function of n. The observed standard deviations, as derived from the T.A.C. daily monitoring, were calculated from many shower events and then compared with the predicted curves. Figure 7.1 shows by how much the T.A.C. standard deviation for detectors 13, 33 and 53 vary with n. Three experimental measurements are also displayed. The value of $n = 10.0 \pm 1.5$ from these data can only be taken as an approximation since noise in the T.A.C. distributions will tend to make the values of n thus derived smaller than is the actual case. The mean shower size that corresponds to this zenith angle index is not known owing to the fact that large showers, falling outside the array acceptance, can trigger the array.

The zenith angle distribution constructed from individually analysed air shower events cannot be directly written in a form like equation 7.1. This is because a solid angle term, $\Omega_{1,2}$, needs to be applied to the observed data:

$$\Omega_{1,2} = 2\pi(\cos\theta_1 - \cos\theta_2) \text{ sr.} \qquad (7.2)$$

Here $(\theta_1 - \theta_2)$ is the zenith angle bin width. By dividing the observed frequency of events by the appropriate solid angle term the true zenith angle distribution can be deduced. Data from 977 Class A and Class B showers have been used for which the best fit zenith angle dependence to these data gives a zenith angle index of

$$n = 10.2 \pm 1.2,$$

for a median shower size of $4.5 \cdot 10^5$, and may be compared with the values of Ashton et al. (1975) of

$$n = 9.3^{+1.0}_{-0.8} \quad \text{and} \quad n = 10.0^{+1.9}_{-0.9}$$

for median shower sizes $2.7.10^5$ and $5.5.10^5$ respectively.

Table 7.1a shows the observed zenith angle data.

7.3.2 The Shower Attenuation Length

The zenith angle dependence of showers may also be interpreted in terms of the shower attenuation length, Λ, which may be evaluated from the expression

$$I(\theta) = I(0) \exp -\left(\frac{\gamma x_o}{\Lambda} (\sec\theta - 1)\right) \quad (7.3)$$

where x_o is the atmospheric depth of observation and γ is the integral shower size spectrum exponent. From the data of 977 Class A and Class B showers an attenuation length of

$$\Lambda = 165 \pm 40 \text{ g.cm}^{-2}$$ using $\gamma_1(<10^6) = 1.4$ and $\gamma_1(>10^6) = 2.0$.

has been derived using the method of Ashton et al. (1975). This value has been plotted in figure 7.2, from a survey by those authors, for a median shower size of $4.5.10^5$ and is seen to be consistent with these data. Possible interpretations of the shower attenuation length in terms of nuclear physical models of high energy interactions have recently been investigated by Popova and Wdowczyk, (1975) from which they observe that their predictions give larger values of Λ than observed. Interpretation of this discrepancy suggest that air showers develop more rapidly in the atmosphere than is

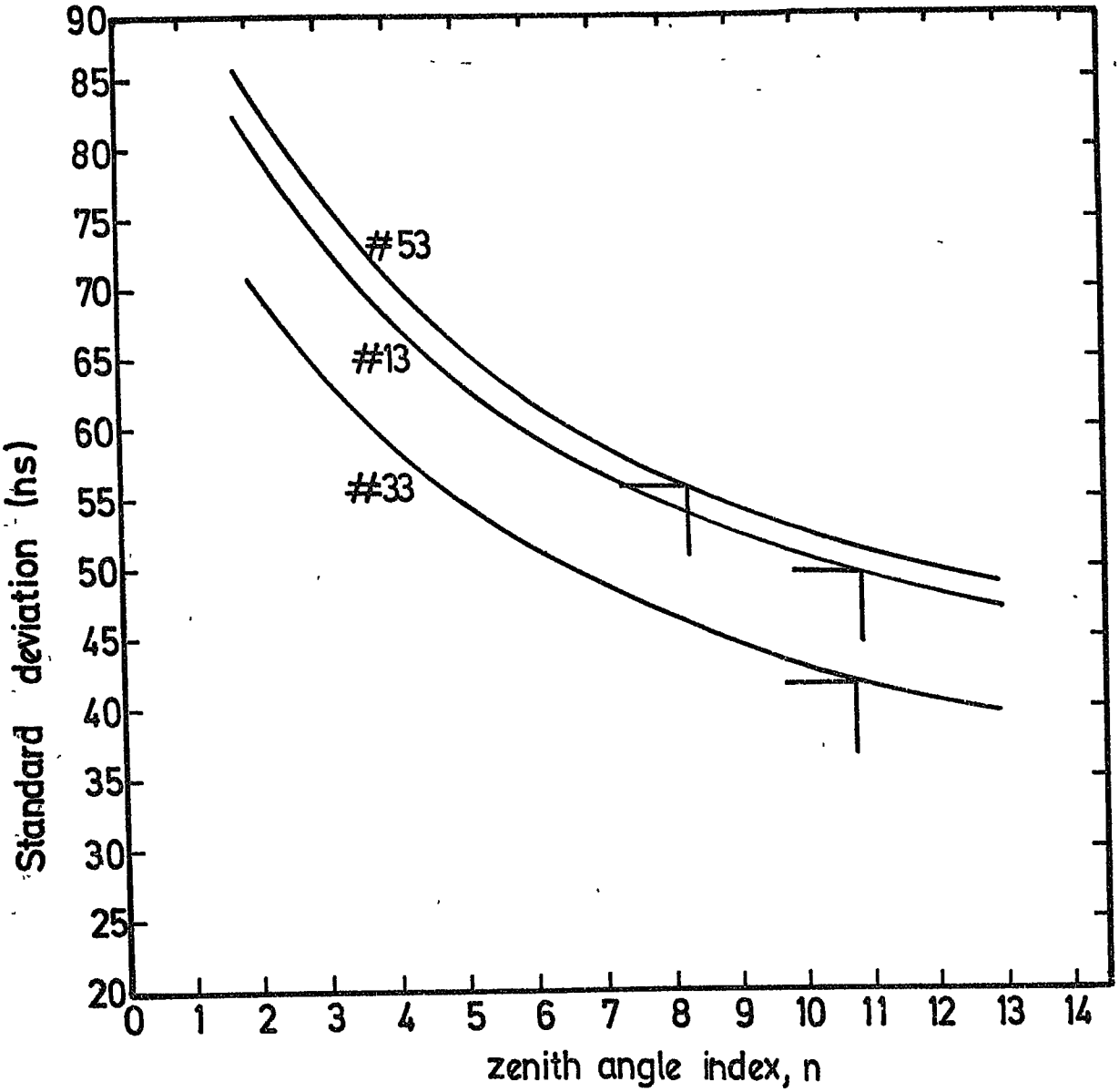

Figure: 7.1. The calculated T.A.C. standard deviation against zenith angle index for detectors 13, 33 and 53. $n = 10.0 \pm 1.5$.

Table 7.1a

The Observed zentih angle distribution of Air Showers detected by the array and analysed as being within 50m of the central detector and with $\theta \leq 30^{\circ}$.

Range of θ	No. Obs.	No. per steradian (normalised to 1st. bin)
$0 - 5^{\circ}$	55	1.00
$5^{\circ}-10^{\circ}$	137	0.83
$10^{\circ}-15^{\circ}$	214	0.78
$15^{\circ}-20^{\circ}$	222	0.58
$20^{\circ}-25^{\circ}$	169	0.35
$25^{\circ}-30^{\circ}$	180	0.31

A least squres minimisation of $\cos^{n}\theta$ to these data give $n = 11.2 \pm 1.2$. Removal of the areal $\cos\theta$ term gives $n = 10.2 \pm 1.2$

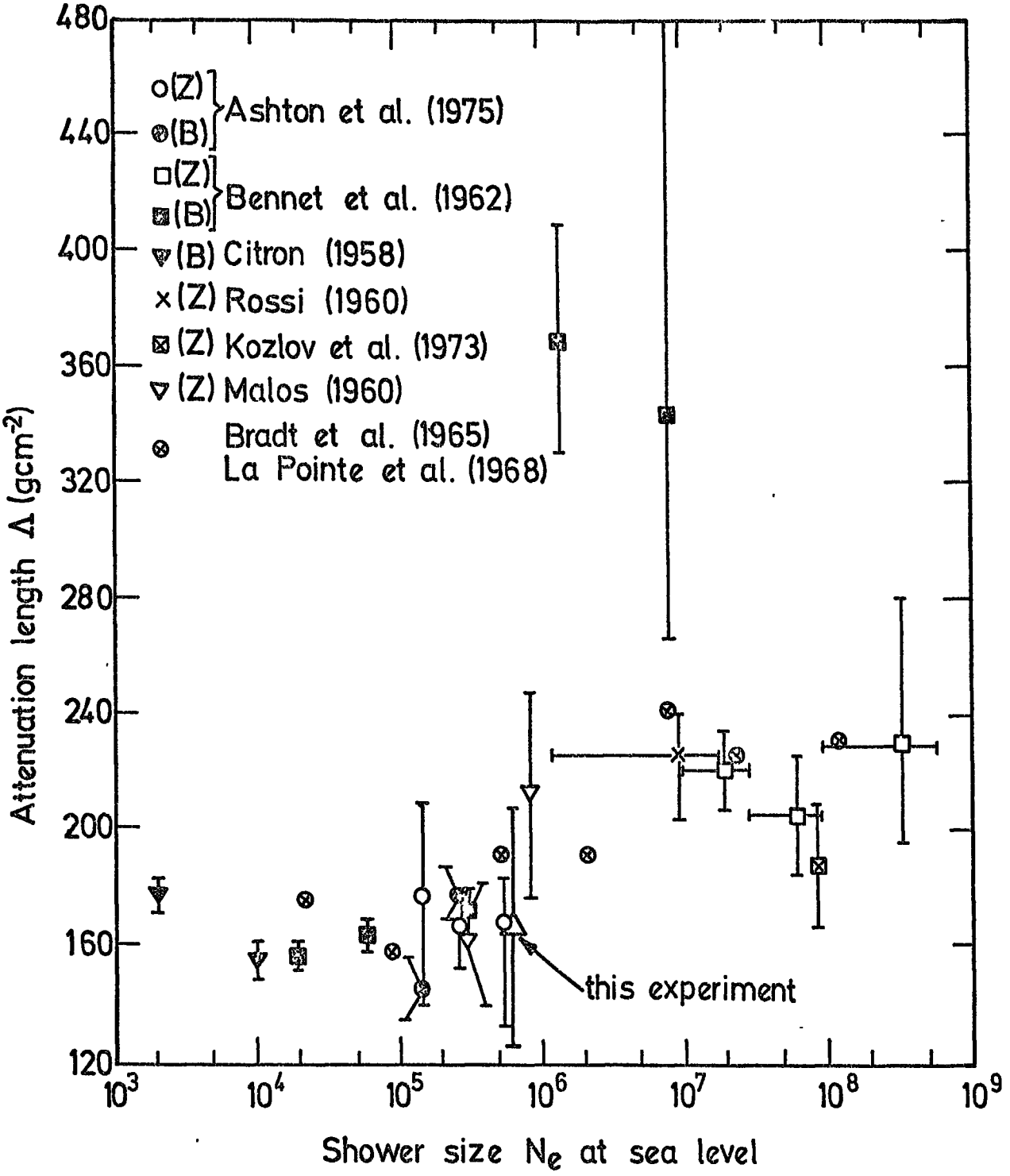

Figure 7.2. The shower attenuation length as a function of shower size at sea level (from Λ derived from barometric (B) and zenith angle (Z) measurements. (from Ashton et al., 1975)

predicted by the de Beer et al. standard air shower model. With more air shower data a more thorough and extensive investigation of Λ versus N may be undertaken with this array.

7.4 The Electronic Structure of Air Showers

The array data have been analysed according to the Hasegawa (1962) structure function with which the shower axes have been located and the shower sizes determined. This was used because it was considered most appropriate for scintillation detectors (Komori, 1975b) and because the average shower age parameter is almost constant over the size range investigated (figure 2.6). A more detailed investigation of shower structure would be possible by fitting a structure function with several parameters to the observed data, giving a greater insight into the characteristics of individual showers. Allowance has been made in the analysis programmes to include more parameters in the minimising process, if required.

7.4.1 The Chi-squared Distribution of Accepted Events

The structure function fitting procedure has been described in Chapter Six and the function that is minimised is described in detail in Appendix B. That minimised is the χ^2 function and, after the application of the event acceptance requirements on the shower data, a cut at some χ^2 must be made that will separate well defined events from ill-defined events such that only the 'good' events are used in deducing air shower properties. The magnitude of the cut, for the purposes of establishing the size spectrum and the attenuation length, has been set at the mean χ^2 plus two standard deviations. For the χ^2 distributions obtained this corresponds to a cut that encloses about 95% of the data; that is, those 5% of the data with the largest χ^2 are omitted. This cut is somewhat arbitrary and there is no cut that, statistically, presents itself as being more favourable than another. The χ^2 distribution of figure 7.3 is of 200 accepted events from Run 62 for

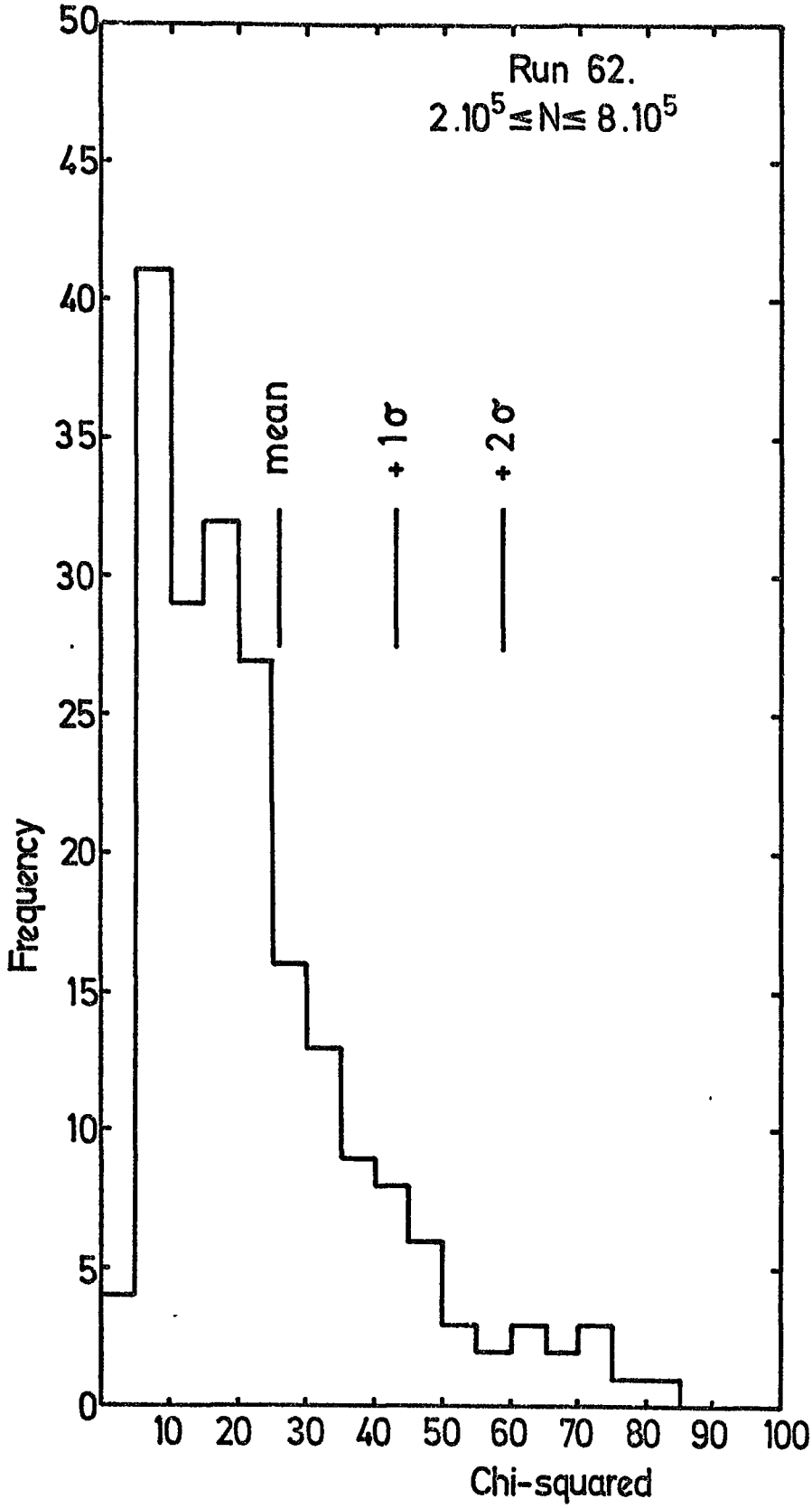

Figure 7.3. The Chi-squared distribution of 200 air shower events that satisfy the array acceptance criteria.

showers between 2.10^5 and 8.10^5 particles. This distribution is wider (by about a factor of 3) than that predicted based upon the assumption that all showers have the same age and this discrepancy is attributed to the age distribution of real showers. Further work on this aspect is required.

7.5 The Shower Size and Primary Energy Spectra

The size spectrum of air showers is studied mainly for the information that it bears on the primary energy spectrum. However, conversion from shower size to primary energy is not a straightforward process and is very much dependent upon the model of air shower development used to derive the relationship between them. This important aspect of air shower work has been, and continues to be, investigated by many workers (e.g. Dixon et al., 1973, Shibita, 1975 and Popova, 1975) and is still the subject of some uncertainty, due to the lack of knowledge of the appropriate nuclear physics. More uncertainty in producing an energy spectrum from air shower data comes from the complexity of unfolding the observed shower data and from the fluctuations in air shower development through the atmosphere to the observation level. Recent work into the E_p:N conversion ('transition coefficient') is summarised in figure 7.4. These data come from various theoretical treatments, mainly involving Monte Carlo simulations of air showers, for different altitudes of observation. The curves marked D_1, E_1 and F_2 refer to sea level measurements from which a transition function,

$$E_p = 2.69.10^{10} N^{0.89} \text{ eV}, \qquad (7.4)$$

has been derived from the extensive and highly detailed work of Dixon et al. (op. cit.).

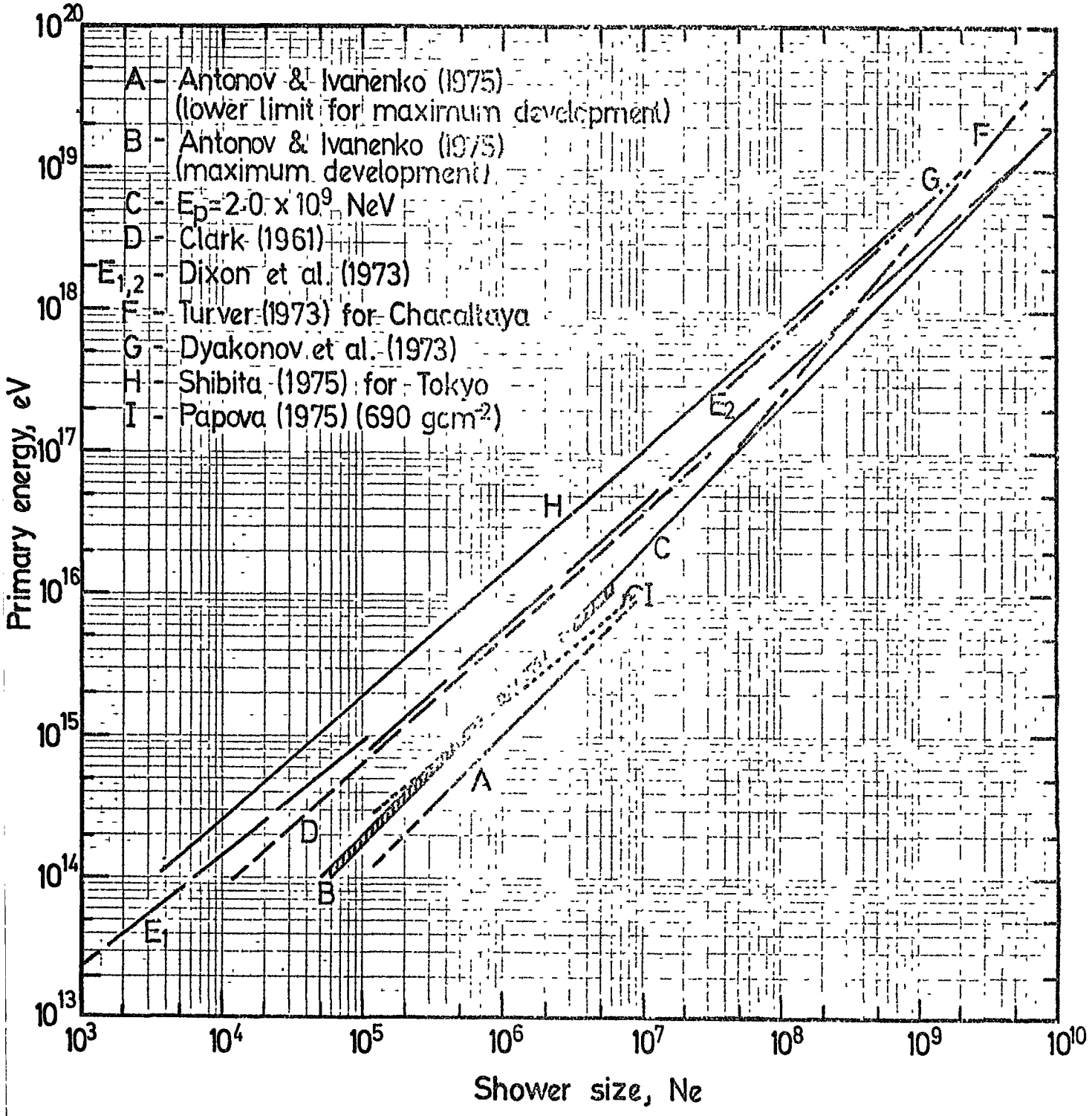

Figure 7.4. The relationship between electron shower size and primary proton energy from various authors. Curves D, E_1, E_2 refer to sea level.

7.5.1. The Shower Size Spectrum

Thus far the present array has not accumulated sufficient data for a detailed investigation of the size spectrum of air showers. The analysis of 10,315 events has yielded 1,474 Class A and Class B showers which are plotted in figure 7.5 before any correction terms have been applied. This spectrum has beer acquired using a trigger requirement of the central detector plus detectors 13,33 and 53 (figure 3.2), an energy threshold of ~10 MeV per detector (1 particle m^2) and a live time of 218.82 hours. The acceptance criteria were that the shower axes be analysed within 50m of the central detector and that the analysed zenith angles were less than, or equal to 30^o. If the intensities in figure 7.5 are multiplied by the factor f in figure 6.9 then a weighted least squares fit to these data give,

$$\text{No. of showers per 0.1 logarithmic interval bin} = (17\pm3)\left(\frac{N_{obs}}{10^6}\right)^{-(2.85\pm0.22)}$$

for this array and the above running time.

The correction to $N_{observed}$ to give the real shower size N_r is, from a least squares fit to the data of figure 6.8,

$$\left(\frac{N_{obs}}{10^6}\right) = (1.58\pm0.07)\left(\frac{N_r}{10^6}\right)^{0.91\pm0.02}$$

By combining these two equations to produce the integral shower size spectrum for real showers and including the array acceptance, the $\cos^{10.2}\theta$ zenith angle dependence and the total running time of the experiment one gets

$$n(>N_r) = (3.7\pm0.9)10^{-8}\left(\frac{N_r}{10^6}\right)^{-(2.6\pm0.2)} \; m^{-2}s^{-1}sr^{-1} \qquad (7.5)$$

$$\text{for } 8.10^5 \leqslant N_r \leqslant 310^6$$

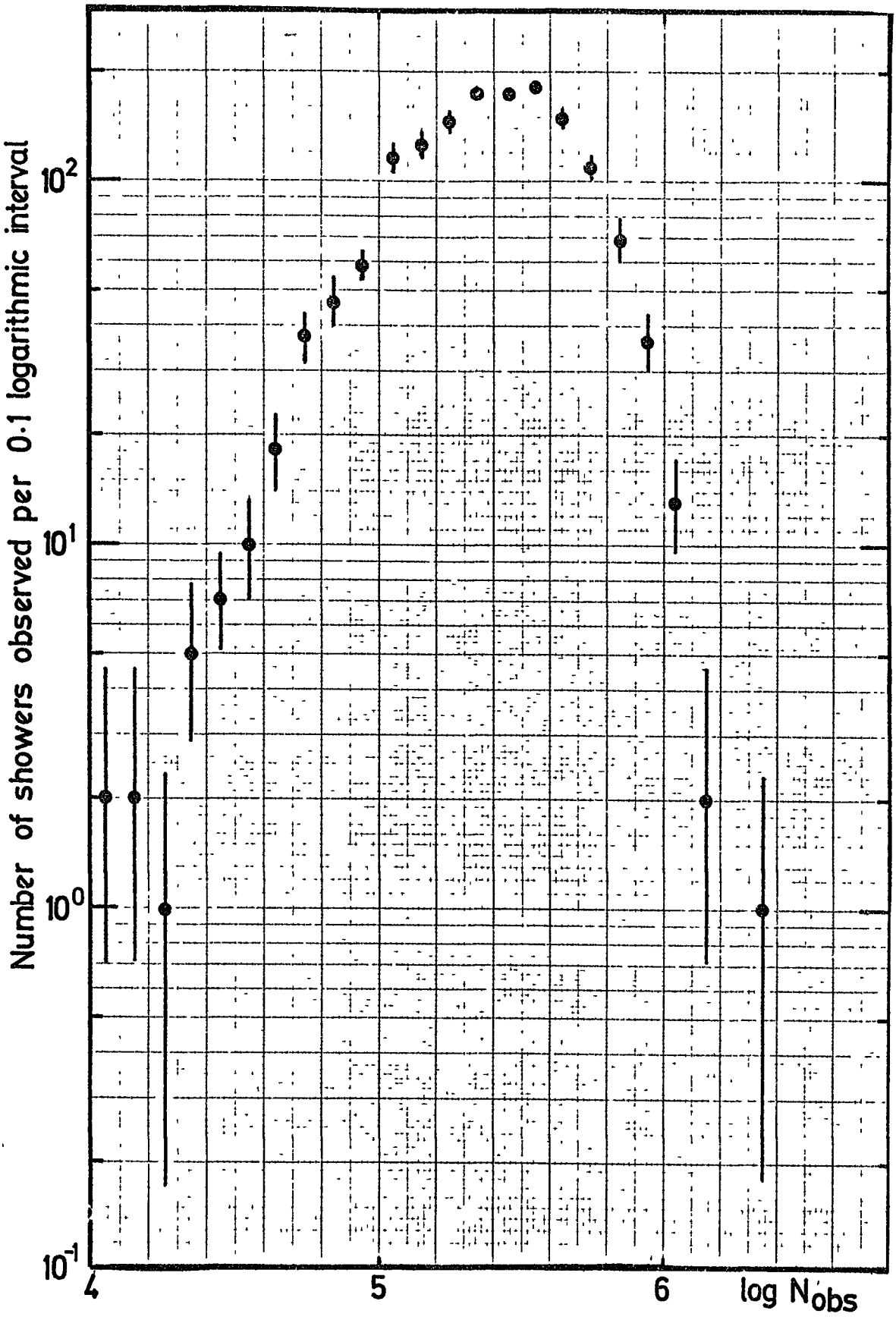

Figure 7·5. The observed shower size spectrum in a running time of 218·82 hours for showers falling within 50m of the central detector and with $\theta \leq 30°$.

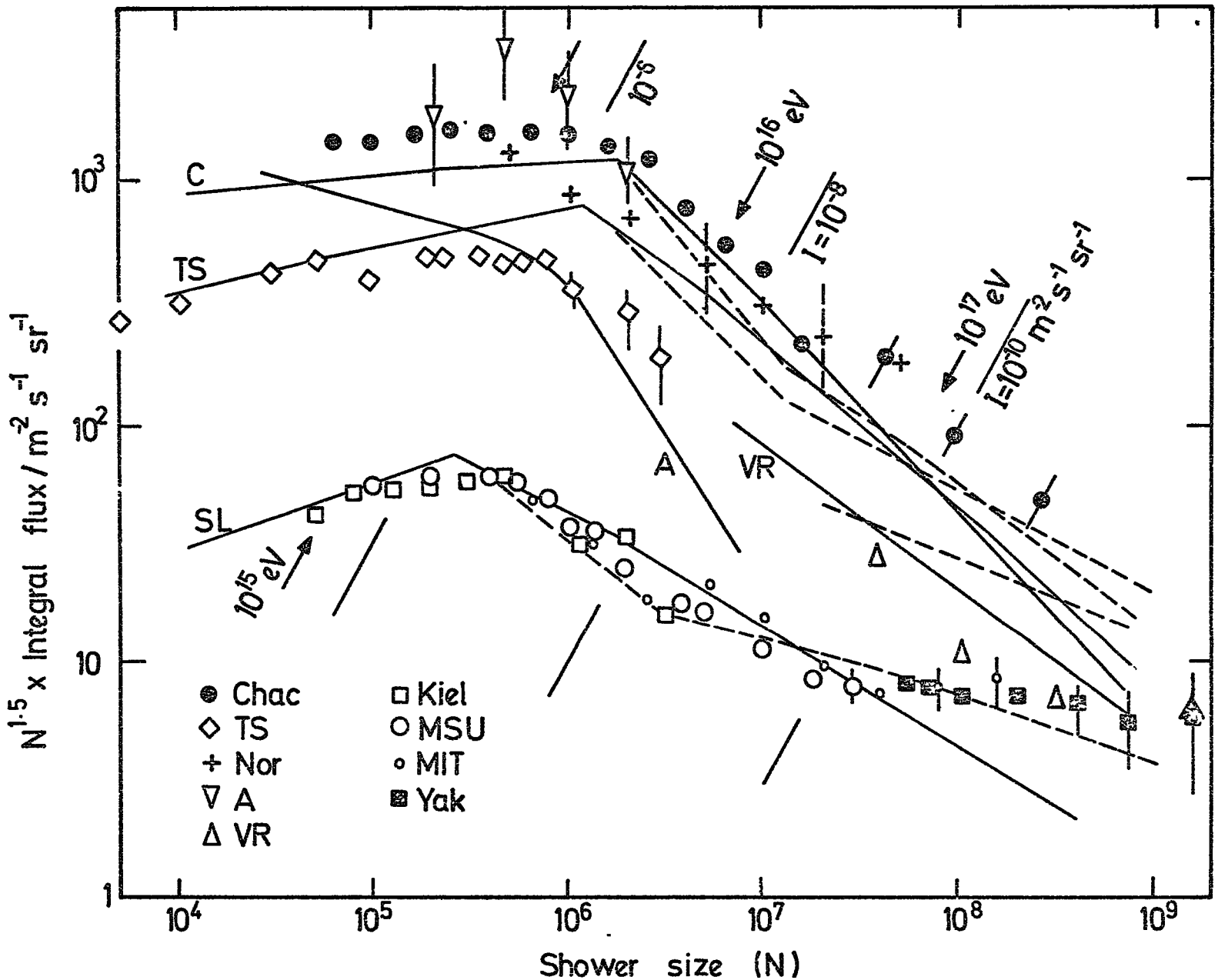

Figure 7.6. The integral shower size spectrum observed at various altitudes. The lines show the approximate fluxes to be expected according to a conventional shower model of Hillas. (from Hillas, 1975)

TABLE 7.2

Some recently reported measurements of γ_I for air showers at sea level

Size Range	γ_I	$J(>N)\left(\frac{10^6}{N}\right)^{-\gamma_I}$ $m^{-2}s^{-1}sr^{-1}$	Reference
10^4 - 10^6	1.4 ± 0.01	7.10^{-8}	Hayakawa, 1969
10^6 - 10^7	2.0 ± 0.02	5.10^{-8}	Hayakawa, 1969
10^6 - 10^8	1.90 ± 0.10	$(3.48 \pm 0.53).10^{-8}$	Hayakawa, 1969
3.10^6 - 3.10^8	1.88 ± 0.15	$2.6.10^{-8}$	Hayakawa, 1969
6.10^6 - 6.10^9	1.84 ± 0.06	$(3.58 \pm 0.28).10^{-8}$	Hayakawa, 1969
$<7.10^5$	1.3 ± 0.1	-	Ashton and Parvaresh, 1975
7.10^5 - 3.10^7	2.0	-	Ashton and Parvaresh, 1975
10^5 - 10^6	1.35	-	Khristiansen et al., 1974,(see Ashton and Parvaresh, 1975)
10^5 - 10^6	1.5 ± 0.1	-	Khristiansen et al., 1965b
10^6 - 10^7	2.0 ± 0.1	-	Khristiansen et al., 1965b
$>10^7$	1.5 ± 0.2	-	Khristiansen et al., 1965b
3.10^7 - 10^9	1.68 ± 0.05	$1.8.10^{-8}$	Kerschenholz, et al., 1973

From the spectrum review of Hillas (1975) (figure 7.6) and the results of individual groups (Table 7.2) the integral intensities at $N = 10^6$ are found to be consistent with this present result but the slope is not. This is probably due to the sparse data thus far collected and used in determining the integral shower size spectrum.

Application of equation 7.4 to equation 7.5 given the slope of the integral energy spectrum in the energy region

$$5.10^{15}\text{eV} < E_p < 2.10^{16}\text{eV}$$

as

$$\gamma_I = -2.9 \pm 0.2$$

Here again the discrepancy between Hillas' best estimate and the present result can be attributed to the paucity of data from this experiment.

7.6 Discussion and Conclusion

The data thus acquired by the present experiment and of its subsequent interpretation have shown that several modifications and in-depth investigations of the array and its response to showers, both as actually acquired and as interpreted by the analysis programmes, are needed.

It is found that the array analysis is rejecting many events that would be analysed as Class B showers due to them not having sufficient timing data to enable an arrival direction to be computed and, as a consequence, are analysed as Option 2 (Class C) showers. This is a serious problem and one that cannot be corrected for very easily during the analysis. However, the large fraction of events "lost" in this way, about 35% of all showers that arrive with zenith angles less than 30° and at all radial distances, can be significantly reduced by utilising a different shower triggering criterion in which the triggering detectors, which must possess the fast timing facility, are nearer to each other than at present. This requirement can be met by triggering with detectors C, 11, 31 and 51 (figure 3.2) but, unfortunately, the last three detectors are not yet operational. Thus it must be that many showers will be lost until these remaining detectors have been included in the array. Alternative to introducing the detectors mentioned

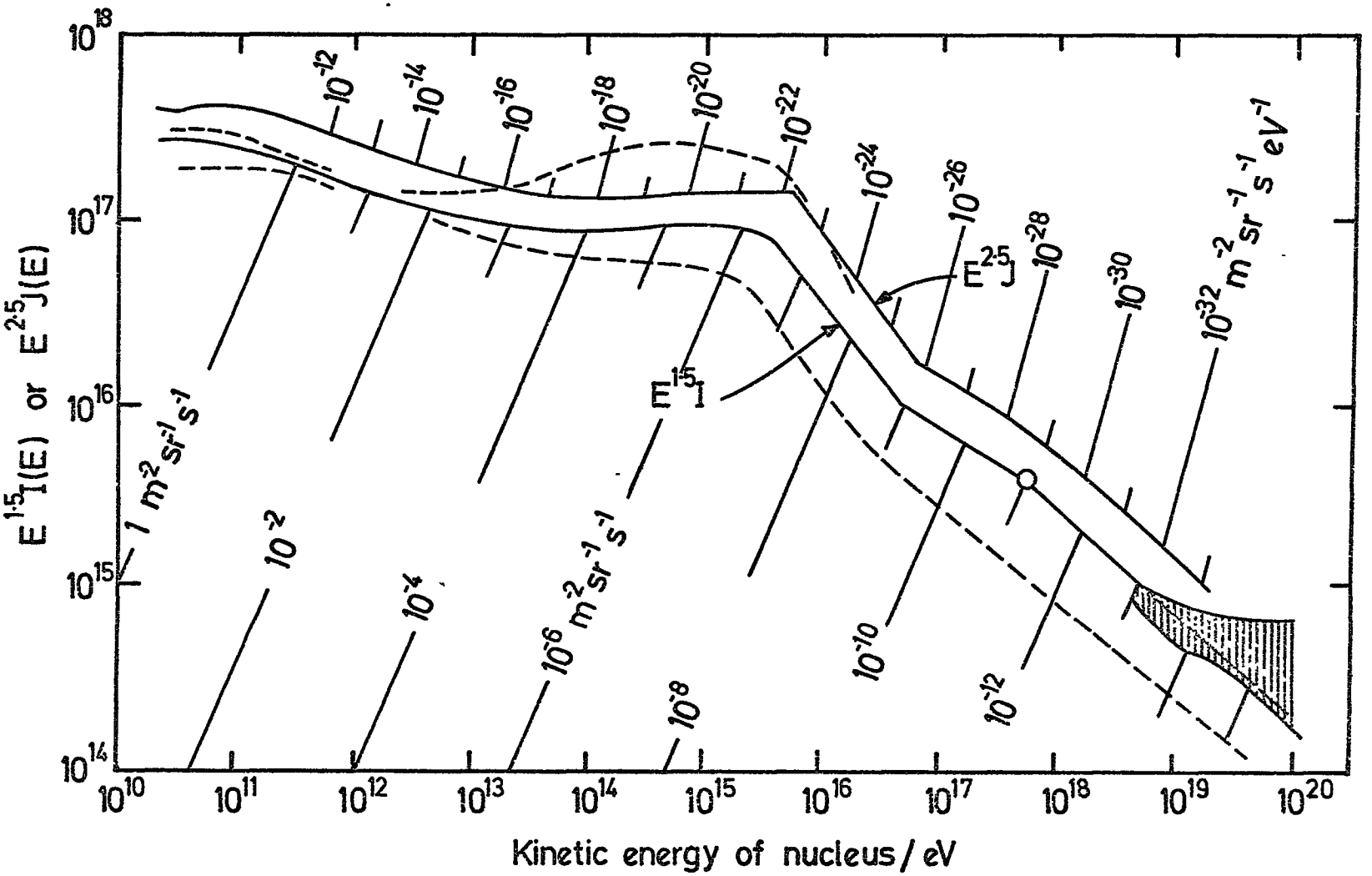

Figure 7.7. The best estimate of the energy spectrum of primary particles at high energies. The dashed curves refer to the extreme values of I which have been recently reported. (from Hillas, 1975)

above a more rigorous trigger may be demanded. Because the detectors have a fast-timing mechanism totally independent of the density measuring electronics, small particle numbers in the triggering detectors may just be sufficient to trigger the array but may be insufficient to register in the fast photomultiplier tubes. To overcome this problem the particle detection threshold could be increased, resulting in a greater detection efficiency by the fast phototube. Increasing the detector thresholds in this way reduces the number of smaller sized showers in the observed shower spectrum (see figure 3.5) and so the effect sought, of increasing the number of smaller showers with timing information, is reversed by the much reduced frequency of these showers triggering the array. Clearly it seems that it is a necessary requirement, in the case of the shower size spectrum measurements, that detectors 11, 31 and 51 be used as array triggering elements and not 13, 33 and 53 as have been used hitherto.

CHAPTER EIGHT

CONCLUSIONS AND FUTURE WORK

8.1 Summary

In the preceding chapters the description of the Durham Array, its purpose and responses have been discussed. Chapter One gave a brief introduction to the history and the general field of extensive air shower phenomena and of their interpretation in terms of broad astrophysical processes. Chapter Two took the air shower and dissected it into its various components to look at physical phenomena on a much smaller scale. The following three chapters took the form of describing the construction and operation of the array and how the data are digitised and stored automatically. The analysis and interpretation of the data are, by no means, simple tasks and topics relevant to the progress of the experiment thus far have been presented in Chapter Seven.

8.2 Present Status of the Experiment

The present status of the Durham Array is that of nearing completion, in the respect that all but three of the originally proposed plastic scintillator detectors have been deployed. The operation of the detectors (Ch.4) and of the data handling electronics (Ch.5) have been shown to be very satisfactory. The versatility built within the Durham array makes it easily extensible for up to 52 detecting elements (§5.6.4) such that much more information that is not at present acquired with each shower event can be collected using the on-line technique. The analysis programmes which were, in the major part, written by the author have been shown, by using simulated air shower data, to adequately analyse typical air shower events that are collected by the array but further work on the interpretation of these data are necessary.

8.3 Development of the Array

With the fourteen plastic scintillation detectors in the first phase of the development of the array insufficient accuracy in the various shower parameters results for those showers whose axes fall in regions where detectors are widely spaced. Within the next twelve months several $0.3m^2$ liquid scintillator detectors will be located on the Physics Department roof to alleviate this problem to a certain extent, but it is not envisaged to include more particle detectors in regions outside the department and so the present detectors there must be considered final. Extra detectors will be positioned near to the experiments in the laboratory to increase the accuracy in determining the position of the experiments with respect to the shower core - a necessary consideration since without a good estimate of this radial distance the quality of the data produced by the experiments will be reduced. The technique of delivering the pulse height data to the laboratory from the detectors in the second phase of development is inherently superior to the present technique. In this case there will be no head amplifiers at the detectors and the number of cables servicing each will thus be reduced. Charge sensitive amplifiers and E.H.T. distribution units will be located in the laboratory to increase the efficiency in checking and calibrating the detectors to which they are connected. Pulses from these detectors will be transmitted down the same cable that supplies the E.H.T. to the photomultiplier tubes (5" diameter), simplifying the data collection even more and enabling much greater flexibility in the operation and maintenance of the detectors.

8.4 Future Work

Because the array has only been operational since September 1975 there remains a great deal of work still to be done. Projects at present envisaged, or in the process of preliminary operation, include searches for tachyons, a detailed investigation of the hadron and low energy muon components

and detailed investigations of high energy single and multiple muons in air showers, using a variety of techniques with the existing flash tube chamber (§3.7) and muon spectrograph (§3.6). A continuation of this present work will increase the accuracy of the shower size spectrum and greater statistics will enable significant shower anisotropy work to be done. Alternative shower analyses are planned to increase the efficiency and accuracy of the present analysis technique.

8.5 Conclusions

The work covered and presented in this thesis has been largely that of the construction and implementation of the Durham Air Shower Array. The results that have been quoted should be taken only as those of a preliminary evaluation of the array's response and features of analysis and should by no means be considered definitive. Nevertheless, it is concluded that the array's performance is satisfactory for the investigation of extensive air shower phenomena in the range between 3.10^4 and 3.10^6 particles in size. Its on-line data handling procedures, and the variety of peripheral experiments in the cosmic ray laboratory, make the array a very useful acquisition to the research programmes currently being pursued here in Durham. It is hoped that with the use of the array much more useful and detailed work will be able to be undertaken in relation to ground based observations and in their interpretation of the structure and the nuclear processes of extensive air showers.

APPENDIX A

THE ZENITH AND AZIMUTHAL SHOWER ANGLES - AN ANALYTICAL SOLUTION FOR THREE DETECTORS

In this Appendix an analytical solution to the equations that describe a plane shower front in terms of arrival times and detector coordinates is given. This treatment considers three timing detectors, in which one detector defines the spatial and temporal origins, and from which a unique solution of the zenith and azimuthal angles are possible.

Starting from equation 6.2:

$$x_1\ell + y_1 m + z_1 n + c\left[t_1 + \left(\frac{\underline{r}_1 \cdot \underline{r}_1 - c^2 t_1^2}{2Rc}\right)\right] = 0$$

where $\ell = \sin\Theta\cos\phi$

$m = \sin\Theta\sin\phi$

$n = \cos\Theta$

$\underline{r}_1 = x_1\underline{i} + y_1\underline{j} + z_1\underline{k}$

R = radius of curvature of the shower front

x_1, y_1, z_1, t_1 = time and space coordinates

and c = velocity of light,

it can be simplified by introducing the variable T_1 where

$$T_1 = c.(t_1 + \frac{\underline{r}_1 \cdot \underline{r}_1 - c^2 t_1^2}{2Rc}) = ct_1 \text{ if } R = \infty$$

to give

$$x_1\ell + y_1 m + n_1 z + T_1 = 0$$

For the two detectors whose 'times' are referred to the detector which defines the origin of the coordinate system one can obtain the simultaneous equations

$$\begin{pmatrix} x_1 & y_1 \\ x_2 & y_2 \end{pmatrix} \cdot \begin{pmatrix} \ell \\ m \end{pmatrix} = \begin{pmatrix} -T_1 - z_1 n \\ -T_2 - z_2 n \end{pmatrix} .$$

By defining the determinant Δ to be

$$\Delta = \begin{vmatrix} x_1 & y_1 \\ x_2 & y_2 \end{vmatrix}$$

solutions for ℓ and m are

$$\frac{1}{\Delta} \cdot \begin{vmatrix} (-T_1 - z_1 n) & y_1 \\ (-T_2 - z_2 n) & y_2 \end{vmatrix} = \ell$$

and

$$\frac{1}{\Delta} \cdot \begin{vmatrix} x_1 & (-T_1 - z_1 n) \\ x_2 & (-T_2 - z_2 n) \end{vmatrix} = m.$$

These give the equations

$$\frac{1}{\Delta} \cdot \begin{vmatrix} y_1 & T_1 \\ y_2 & T_2 \end{vmatrix} + \frac{1}{\Delta} \cdot \begin{vmatrix} y_1 & z_1 \\ y_2 & z_2 \end{vmatrix} .n = \ell$$

and

$$-\frac{1}{\Delta} \cdot \begin{vmatrix} x_1 & T_1 \\ x_2 & T_2 \end{vmatrix} - \frac{1}{\Delta} \cdot \begin{vmatrix} x_1 & z_1 \\ x_2 & z_2 \end{vmatrix} .n = m$$

These relations can be further simplified by defining new variables as the coefficients of the above equations to give

$$A + Bn = \ell$$

and

$$C + Dn = m$$

Introducing the explicit expressions for ℓ, m and n one gets

$$A + B\cos\theta = \sin\theta \cos\phi$$

and

$$C + D\cos\theta = \sin\theta \sin\phi.$$

Squaring and adding gives

$$A^2 + C^2 - 1 + (2AB + 2CD)\cos\theta + (B^2 + D^2 + 1)\cos^2\theta = 0$$

whose solutions are

$$\cos\theta = \frac{-(AB + CD) \pm ((AB + CD) - (B^2 + D^2 + 1)(A^2 + C^2 - 1))^{\frac{1}{2}}}{(B^2 + D^2 + 1)}$$

and

$$\tan \phi = \frac{C + D\cos\theta}{A + B\cos\theta} .$$

APPENDIX B

THE CHI SQUARED FUNCTION AND THE PROBLEM OF SMALL PARTICLE NUMBERS

The χ^2 function is often quoted as

$$\chi^2 = \sum_{i=1}^{n} \frac{(O_i - E_i)^2}{E_i} \qquad (B.1)$$

where O_i and E_i are the observed and expected frequencies in the ith bin of a distribution. In the general case, the denominator E_i is replaced by ε_i^2, the square of the error on the expected number E_i. If the errors on E_i are purely statistical then

$$\varepsilon_i^2 = E_i \qquad (B.2)$$

and equation B.1 remains unchanged. In those cases where E_i is small ($\lesssim 10$) equation B.1 is not a satisfactory approximation to use as a measure of the goodness of fit and, for applications where poissonian statistics apply, equations B.1 and B.2 cannot be successfully employed.

True poissonian errors have been calculated by Regener (1951), to one and two standard deviation limits, and he discusses their significance in relation to small samples of cosmic ray counts. An approximation to the errors quoted by Regener can usefully be made and used in the χ^2 function using

$$\text{mean Regener error, } \bar{\varepsilon}_R = \frac{\varepsilon_R^+ + \varepsilon_R^-}{2}$$

$$\approx n^{\frac{1}{2}} + 0.5, \qquad (B.3)$$

where ε_R^+ and ε_R^- are the asymmetrical Regener errors on a measurement of n particles. This relation is accurate to better than 4% for all $n \geq 1$. For large n normal statistics apply and the mean Regener error tends to $n^{\frac{1}{2}}$ as n increases.

Additional to the statistical error in particle measurement, in an air shower detector, is an uncertainty introduced by the detector itself. In calculating the efficiencies of the air shower detecting elements (§ 3.4.2) spectra were generated for the response of an air shower detector to n particles passing through it, from an empirical distribution for one particle. The standard deviations of these distributions is given by

$$\sigma_D = 0.660.\ n^{\frac{1}{2}} \qquad \text{(B.4)}$$

for all $n \geq 1$.

The detector error, σ_D, and the statistical error, $\bar{\varepsilon}_R$, may now be combined in quadrature to give the overall error on the measured number of particles:

$$\varepsilon^2 = \bar{\varepsilon}_R^{\,2} + \sigma_D^{\,2} \qquad \text{(B.5)}$$

Substituting the equations B.3 and B.4 into B.5 gives

$$\varepsilon^2 = 1.436n + n^{\frac{1}{2}} + 0.25$$

which is the error term that has been used in the χ^2 function that is minimised in the data analysis procedures (§6.4).

For a detailed account of the χ^2 goodness of fit test see Cochran, W.G., Ann. Math. Stat., 23, (1952), 315.

REFERENCES

(P.I.C.C.R. = Proceedings of the International Conference on Cosmic Rays)

Adcock, C., Wdowczyk, J., and Wolfendale, A.W., J. Phys. A., 2, (1969), 574

Adcock, C., et al., J. Phys. A., 3, (1970), 697

Allan, H.R., et al., P.I.C.C.R. (Denver), 4, (1973), 2407

Antonov, R.A., et al., P.I.C.C.R.(Hobart), 6, (1971), 2194

Antonov, R.A., and Ivanenko, I.P., P.I.C.C.R.(Munich), 8, (1975), 2708

Aseikin, V.S., et al., P.I.C.C.R.(Munich), 8, (1975a), 2960

Aseikin, V.S., et al., P.I.C.C.R.(Munich), 8 (1975b), 2726

Ashton, F., et al., P.I.C.C.R.(Munich), 8, (1975), 2831

Ashton, F., and Parvaresh, A., P.I.C.C.R.(Munich), 8, (1975), 2719

Auger, P., et al., Revs. Mod. Phys., 11, (1939), 288

Ayre, C.A., Ph.D.. Thesis, University of Durham, (1971)

Bell, C.J., et al., J. Phys. A., 7, (1974), 990

Bennett, S., et al., J. Phys., Soc. Japan. Suppl. A III, 17, (1962), 196

Bhabha, H.J., and Heitler, W., Proc. Roy. Soc., 159, (1937), 432

Bosia, G., et al., Nuovo Cimento, 9, Series 11, (1972), 177

Bradt, H. et al., P.I.C.C.R.,(London), 2, (1965), 715

Brecher, K., and Burbridge, G.R., Astrophys. J., 174, (1972), 253

Chatterjee, B.K., et al., Can. J. Phys., 46, (1968), S136

Citron, A., see Ashton et al., 1975

Clark, G., et al., Nuovo Cimento, 8, Suppl. 2, Series 10, (1958), 623

Clark, G.W., et al., Phys. Rev., 122, (1961), 637

Clay, J., Proc. Roy. Acad. Amsterdam, 30, (1927), 1115

Coates, R.B., et al., J. Phys. A., 3, (1970), 689

Cocconi, G., Koester, L.J., and Perkins, D.H., U.R.C.L. High Energy Physics Study Seminars, 28, part 2, U.C.I.D. - 1444, (1961)

Compton, A.H., Phys. Rev., 43, (1933), 387

Cooper, D.A., Ph.D. Thesis, University of Durham, (1974)

de Beer, J.F., et al., Proc. Phys. Soc., 89, (1966), 567

de Beer, J.F., et al., J. Phys. A., 1, (1968), 72

Dennis, B.R., Ph.D. Thesis, University of Leeds, (1964)

Dake, S., et al., P.I.C.C.R.(Hobart), 3, (1971), 948

Dixon, H.E., and Turver, K.E., Proc. Roy. Soc. Lond. A., 339, (1974), 171

Dixon, H.E., et al., P.I.C.C.R.(Denver), 4, (1973), 2473

Dixon, H.E., et al., Proc. Roy. Soc. Lond., A339, (1974a), 133

Dixon, H.E., et al., Proc. Roy. Soc. Lond., A339, (1974b), 157

Dyakonov, M.N., et al., P.I.C.C.R.(Denver), 4, (1973), 2384

Earnshaw, J.C., et al., Proc. Phys. Soc., 90, (1967), 91

Efimov, N.N., et al., P.I.C.C.R.(Denver), 4, (1973), 2378

Elster, J., and Geitel, H., Physik. Z., 1, (1899), 11

Fermi, E., Phys. Rev., 75, (1949), 1169

Fermi, E., Astrophys. J., 119, (1954), 1

Feynman, R.P., Phys. Rev. Lett., 23, (1969), 1415

Fowler, G.N., and Wolfendale, A.W., Handb. Phys., (Berlin; Springer), 46/1, (1961), 272

Fowler, P.H., and Perkins, D.H., Proc. Roy. Soc. Lond., A278, (1964), 401

Froman, D.K., and Stearns, J.C., Revs. Mod. Phys., 10, (1938), 133

Gaisser, T.K., et al., P.I.C.C.R.(Denver), 4, (1973), 2652

Galbraith, W., Extensive Air Showers, (Butterworths Scientific Publications), (1958)

Galbraith, W., and Jelley, J.V., Nature, 171, (1953), 349

Garcia-Munoz, M., Mason, G.M., and Simpson, J.A., P.I.C.C.R.(Hobart), 1, (1971), 209

Gawin, J., et al., Can. J. Phys., 46, (1968), S104

Geitel, H., Physik, Z., 2, (1900), 116

Ginzburg, V.L., and Syrovatskii, S.I., The Origin of Cosmic Rays, (Pergamon Press), (1964)

Gockel, A., Physik. Z., 11, (1910), 280

Gockel, A., Physik, Z., 12, (1911), 295

Goldstein, A.A., and Price, J.F., Math. Comp., 25, (1971), 569

Greider, P.K.F., P.I.C.C.R.(Denver), 4, (1973), 2639

Greisen, K., Progr. Cosmic Ray Physics III, (North Holland Pub. Co., Amsterdam), (1956), 1

Greisen, K., Ann. Rev. Nucl. Science, 10, (1960), 63

Greisen, K., Phys. Rev. Lett., 16, (1966), 748

Hagedorn, R., Suppl. Nuovo Cimento, 3, (1965), 147

Hasegawa, H., et al., J. Phys. Soc. Japan, 17, AIII, (1962), 189

Hayakawa, S., Cosmic Ray Physics, (Monographs and texts in Physics and Astronomy, Vol. XXII, Wiley-Interscience), (1969), 467 and 468

Hazen, W.E., et al., P.I.C.C.R.(Munich), 1, (1975), 2473, (Abs.)

Hess, V.F., Physik, Z., 12, (1911), 998

Hess, V.F., Physik. Z., 13, (1912), 1084

Hess, V.F., Physik. Z., 14, (1913), 610

Hillas, A. M., Acta Phys. Hung., 29, Suppl. 3, (1970), 539

Hillas, A.M. et al., P.I.C.C.R.(Hobart), 3, (1971), 1007

Hillas, A. M., Physics Reports (Phys. Lett. C.), 20C, (1975), 61

James, F., and Roos, M., C.E.R.N. Computer 7600 Program Library, D505, D516, (1971)

Jory, F.S., Phys. Rev., 102, (1956), 1167

Julliusson, E., P.I.C.C.R.(Munich), 8, (1975), 2689

Kamata, K., and Nishimura, J., Suppl. Prog. Theor. Phys., 6, (1958), 93

Kameda, T., et al., P.I.C.C.R.(London), 2, (1965), 681

Kaneko, T., et al., P.I.C.C.R.(Munich), 8, (1975), 2747

Karakula, S., (1968), See Wdowczyk, J., (1973)

Kempa, J., Wdowczyk, J., and Wolfendale, A.W., J. Phys. A., 7, (1974), 1213

Kershenholz, I.M., et al., P.I.C.C.R.(Denver), 4, (1973), 2507

Khrenov, B.A., Izvest. Akad. Sci. U.S.S.R., 26, (1962), 5

Khristiansen, G.B., et al., P.I.C.C.R.(London), 2, (1965a), 774

Khristiansen, G.B., et al., P.I.C.C.R.(London), 2 (1965b), 799

Khristiansen, G.B., et al., P.I.C.C.R.(Hobart), 3, (1971), 1074

Kolhorster, W., (1913, 1914). See 'Introduction to Modern Physics', Richtmyer, F.K., Kennard, E.H., and Lauritsen, T., 5th Ed., McGraw-Hill, 1955)

Komori,H., P.I.C.C.R.(Munich), 8, (1975a), 2842, (Abs)

Komori, H., (1975b), Private communication.

Kozlov, V.I., et al., P.I.C.C.R.(Denver), 4, (1973), 2588

La Pointe, M., et al., Can. J. Phys., 46, (1968), S68

Le Maitre, G., and Vallarta, M.S., Phys. Rev. 43, (1933), 87

Linsley, J., et al., J. Phys.Soc.Japan, 17, Suppl. AIII, (1962), 91

Malos, J., P.I.C.C.R.(Moscow), 2, (1960), 84

Marsden, D.J., Ph.D. Thesis, University of Leeds, (1971)

Millikan, R.A., and Cameron, G.H., Phys. Rev., 28, (1926), 851

Millikan, R.A., and Cameron, G.H., (Latitude Effect) see Millikan R.A., Electrons + and - , (Chicago Univ. Press, Chicago), (1947)

Miyake, S., et al., Acta Phys. Hung. 29, Suppl. 3, (1970), 463

Murthy, G.T., et al., Can. J. Phys., 46, (1968), S153

Nishimura, J. and Kamata, K., Progr. Theor. Phys., 5, (1950), 899

Nishimura, J. and Kamata, K., Progr. Theor. Phys., 1, (1952), 185

Nishimura, J., and Kamata, K., (1958), see Kamata J., and Nishimura, K., (1958)

Orford, K. J., et al., P.I.C.C.R.(Munich), 8, (1975), 3019

Ostriker, J.P., and Gunn, J.E., Astrophys. J., 157, (1969), 1395

Pidcock, J.K., Ph.D. Thesis, University of London, (1967)

Popova , L., P.I.C.C.R.(Munich), 8, (1975), 2819

Popova, L. and Wdowczyk, J., P.I.C.C.R.(Munich), 8, (1975), 2883

Protheroe, R.J., et al., P.I.C.C.R.(Munich), 8, (1975), 3008

Regener, V.H., Phys. Rev., 84, (1951), 161

Rozhdestvensky, S.M. et al., P.I.C.C.R.(Munich), 8, (1975), 2790

Rossi, B., P.I.C.C.R.(Moscow), 2, (1960), 18

Rutherford, E., and Cooke, H.L., Phys. Rev., 16, 1st Series (1903), 183

Samorski, M., et al., P.I.C.C.R.(Hobart), 3, (1971), 959

Shapiro, M. M., and Silberberg, R., Can. J. Phys., 46, (1968), S561

Shibita, T., P.I.C.C.R.(Munich), 8, (1975), 2910

Stormer, C., see D. J. X. Montgomery, Cosmic Ray Physics (Princeton Univ. Press, Princeton, N.J.), (1949)

Strong, A.W., Wdowczyk, J., and Wolfendale, A.W., J. Phys. A., 7, (1974), 1489

Thompson, M.G., Cosmic Rays at Ground Level, (Ed. Wolfendale, A.W. The Institute of Physics, London), (1973)

Turver, K.E., Cosmic Rays at Ground Level, (Ed. Wolfendale, A.W., The Institute of Physics, London), (1973)

Torsti, J.J., Nuovo Cimento, 25B, (1975), 829

Ueda, A., and Ogita, N., Progr. Theor. Phys., 18, (1957), 209

Van Staa, R., Aschenbach, B., and Böhm, E., P.I.C.C.R.(Denver), 4, (1973), 2676

Vernov, S.N., et al., Sov. Phys. J.E.T.P., 41, (1962), 247

Vernov, S.N., et al., Izvest. Akad. Sci. U.S.S.R., 28, (1964), 1886

Vernov, S.N., et al., Can. J. Phys., 46, (1968a), S110

Vernov, S.N., et al., Izvest, Akad. Sci. U.S.S.R., 32, (1968b), 458

Vernov, S.N., et al., Acta Phys. Hung., 3, (1970), 429

Wdowczyk, J., Cosmic Rays at Ground Level, (Ed. Wolfendale, A.W., The Institute of Physics, London), (1973)

Wdowczyk, J., and Wolfendale, A.W., Nat. Phys. Sci., 236, (1972), 29

Wdowczyk, J., and Wolfendale, A.W., J. Phys. A., 6, (1973a), L48

Wdowczyk, J., and Wolfendale, A.W., P.I.C.C.R.(Denver), 3, (1973b), 2336

Wells, S.C., Ph.D. Thesis, University of Durham, (1972)

Whalley, M.R., Ph.D. Thesis, University of Durham, (1974)

Wilson, C.T.R., Proc. Cambs. Phil. Soc., 11, (1900), 32

Wilson, J.G., Progr. in Cosmic Ray Physics, III, (North Holland Pub. Co., Amsterdam), (1956)

Wolfendale, A.W., Cosmic Rays at Ground Level, (Ed. Wolfendale, A.W., The Institute of Physics, London), (1973)

ACKNOWLEDGEMENTS

The author would like to thank Professors G. D. Rochester and A. W. Wolfendale for the use of the Physics Department's excellently equipped laboratories and for their interest and encouragement with this air shower project.

The author is grateful to his supervisor, Dr. M. G. Thompson, for his help and guidance at all stages of this work. Dr. M. R. Whalley, Mr. T. R. Stewart, Mr. W. S. Rada and all members of the M.A.R.S. group are thanked for their constant help and advice. To Mr. K. Tindale go grateful thanks for his unfailing assistance in the experiment's construction and implementation. Mr. W. Leslie, Mr. H. Davison and Mr. P. Cottle are thanked for their exceptionally fine work in the construction of the detector huts, boxes and beds and Mr. P. Armstrong is also thanked for the construction of many excellent modular units. Mr. E. Lincoln and the Electronics Workshop staff are also thanked for their assistance with many electronic devices.

Grateful thanks go to Mrs. A. Gregory for the drawing of the excellent figures in this thesis and to Mrs. J. Moore for its typing.

To Miss D. M. Milner, for her support, help and encouragement the author is indebted.

Finally, the Science Research Council is thanked for the provision of a Studentship and for the facilities provided by the Northumbrian Universities Multiple Access Computer.